A Set-Point Dependent Nonlinear Model for the Neural Integrator in the Vestibulo-Ocular Reflex

Wilbur W. P. Chan

A thesis submitted to the Faculty of Graduate Studies and Research in partial fulfillment of the requirements for the degree of Doctor of Philosophy

Department of Biomedical Engineering

McGill University, Montreal

August, 2008

Abstract

The Neural Integrator (NI) in the oculomotor system is a conceptual process presumed to perform mathematical integration of eye velocity related sensory signals into motor signals controlling ocular orientation (position) in the orbit. It participates in tasks such as maintaining gaze in space during head fixed or head-free viewing of targets. The NI is classically assumed to perform ideally (large time constants) and to be identical in all tasks. This thesis explores past assumptions on the time-invariant characteristics of the NI. During passive head movement in the dark and measurements of the horizontal Vestibulo-Ocular Reflex (VOR), the dynamics of the NI were found to vary dynamically, depending on head velocity and eye positional set-points. To investigate the observed phenomenon, we incorporated a nonlinear component into an existing model for the NI and attempted to emulate the context-dependent changes in the NI dynamics. To estimate the model parameters, optimization methods were used instead of the least squared based algorithms due to the more complex formulation of the nonlinear NI model. When comparing nonlinear NI model estimates during passive VOR responses in human subjects, the nonlinear parameters were found to differ greatly between vestibular patients and the control group; furthermore, the nonlinear model predicts apparent NI dynamics that are set-point dependent for most of the subjects, even in controls. The form and optimal set-point for the NI characteristics are well correlated with the side of a lesion in patients, even after compensation. Furthermore, the non-linear NI formulation provides better fits on ocular data, than the presumed ideal integrator. The results have implications for both more sensitive detection of vestibular anomalies, and for the appropriate choice of analyses methods in the study of oculomotor physiology and reflexes.

Résumé

L'intégrateur neural (IN) dans le système oculomoteur est un processus conceptuel présumé d'effectuer l'intégration mathématique des signaux sensoriels relatifs à la vitesse de l'oeil en signaux moteurs commandant l'orientation oculaire (position de l'oeil) dans l'orbite. L'IN participe aux tâches telles que maintenir le regard dans l'espace pendant le visionnement des cibles à tête fixe ou libre. Classiquement, l'IN est supposé intégrer idéalement (avec de grandes constantes de temps) et identiquement dans toutes les tâches. Cette thèse explore les anciennes prétentions sur les caractéristiques temps-invariables de l'IN. Durant le mouvement passif de la tête dans l'obscurité et en mesurant le réflexe Vestibulo-Oculaire (RVO) horizontal, la dynamique de l'IN s'est avérée de varier dynamiquement, selon la vitesse de la tête et les points de consigne de la position de l'œil. Pour étudier le phénomène observé, nous avons incorporé un composant non linéaire à un modèle existant de l'IN et nous avons essayé d'émuler les changements contexte-dépendants dans les dynamiques de l'IN. Pour estimer les paramètres du modèle, des méthodes d'optimisation ont été employées au lieu des algorithmes basés sur le moindre carré à cause de la formulation plus complexe du modèle non linéaire de l'IN. En comparant des évaluations non linéaires du modèle pendant des RVO passives chez des sujets humains, on a trouvé que les paramètres non linéaires diffèrent considérablement entre les patients vestibulaires et le groupe de control; de plus, le modèle non linéaire prévoit les dynamiques apparentes de l'IN qui dépendent de la point de consigne pour la majorité des sujets, même chez le groupe de control. La forme et le point de consigne optimale pour les caractéristiques de l'IN sont bien corrélés avec le côté de lésion chez les patients, même après la compensation. En outre, la formulation non linéaire de l'IN correspond mieux aux données oculaires que l'intégrateur idéal présumé. Les résultats ont des implications pour une détection plus sensible des anomalies vestibulaires, ainsi que pour le choix approprié des méthodes d'analyses dans l'étude de la physiologie et réflexes oculomoteurs.

Acknowledgement

I would like to express my gratitude to my supervisor Prof. Henrietta L. Galiana for being an incredible mentor to me. I am especially thankful for her insight and patience during the preparation of this dissertation. I am also grateful for the research oriented example that she had displayed in fostering an incredible environment to work in.

I am especially thankful for Heather Smith and Dr. Athanasios Katsarkas in providing assistance in the collection of clinical data. It would be impossible to have access to the patient data without their help.

I am also grateful for Dr. Ross Wagner's aid while redesigning and building the experimental hardware. He has added a hands-on practical dimension to the research process.

The method of optimization used in this dissertation was introduced to me by Dr. Alexei Motto. I would not be able to discover the wonderful GAMS software without him. I am very thankful for his advice and assistance which were essential in the parameter estimation process in this thesis.

The oculomotor research lab has been an incredible environment in which to conduct research. I especially appreciate the many insightful discussions with Dr. Ross Wagner, Tony Kam-Thong and Elham Khojasteh-Lakelayeh, in challenging the fundamentals that we have taken for granted.

I would also like to thank my family members in their unyielding support throughout the years of the research.

Lastly and most importantly, I would like to thank my wife Carole for her unyielding support, her continuous words of encouragement, her immeasurable amount of patience and her unyielding love.

To Valerie,

And

In loving memory of Phyllis

Table of Contents

Contributions of Authors 9

1.Introduction.....10

2. Literature Review.....12

2.1 Physiology 12

2.2 Physiological Behaviour.....15

2.3 Models for the VOR 19

2.4 Model Parameter Estimation Algorithms 23

2.5 Summary.....40

3. Extended Methods 41

3.1 Experimental Data Collection.....41

3.2 Signal Processing.....43

3.3 VOR Simulation 44

3.4 Identification Procedure and Cross Validation.....45

4. Integrator function in the Oculomotor System is Dependent on Sensory Context47

4.2 Methods 49

4.3 Results.....54

4.4 Discussion.....55

3.4 References.....59

5. Modeling the Non-Linear Context Dependency of the Neural Integrator in the Vestibulo-Ocular Reflex 73

5.1 Introduction 74

5.2 Methodology 75

5.3 Simulation 84

5.4 Recordings from Real Subjects 85

5.5 Parameter Estimation and Model Selection/Validation 85

5.6 Results 88

5.7 Discussion 97

5.8 References 100

6. A Nonlinear Model of the Neural Integrator Improves Detection of Deficits in the Human VOR 105

6.1 INTRODUCTION 106

6.2 Methodology 107

6.3 Results 113

6.4 Discussion 136

6.5 APPENDIX 140

6.6 Acknowledgement 142

6.7 References 142

7. Conclusion and Future Work 146

7.1 Conclusion 146

7.2 Original Contributions 149

7.3 Future Work 150

Bibliography 153

Contributions of Authors

In all three manuscripts included in this thesis, the author (Wilbur Chan) was the lead contributor, including conducting research, designing and performing experiments, derivation of mathematical models, performing analysis and writing of the manuscripts; the coauthor (Henrietta Galiana) assumed the normal role of supervision such as providing guidance throughout the process and editorial revision of the manuscripts.

Chan, Wilbur W. P., Galiana, Henrietta L. "Integrator function in the oculomotor system is dependent on sensory context." *Journal of Neurophysiology*, 93(6): 3709-3717, 2005.

Chan, Wilbur W P, and Henrietta L Galiana. "Modeling the Non-Linear Context Dependency of the Neural Integrator in the Vestibulo-Ocular Reflex." *IEEE Transactions on Biomedical Engineering*, 55(8): 1946-55, 2008.

Chan, Wilbur W P, and Henrietta L Galiana. "Using an Asymmetric Nonlinear Model of the Neural Integrator for the Classification of Human VOR in the Clinic." In Press *IEEE Transactions on Biomedical Engineering*, 2009.

1. Introduction

The Vestibulo-Ocular Reflex (VOR) is responsible for maintaining gaze in space during head perturbations. In the horizontal VOR, head rotational movement is detected by the horizontal semi-circular canals, converted into velocity-related neuronal signals and sent to the brainstem for processing. The central processing network in the brainstem includes the Vestibular Nuclei (VN), the reticular formation (RF) in the brainstem, the superior colliculus (SC) and the Prepositus Hypoglossi (PH). This network creates an estimate of the expected eye position required to correct for the head movement and then projects this positional drive signal as part of the eye control signal to the motorneurons of the eyes. The conversion of the velocity-related signal from the semi-circular canals to the positional signal in the motorneuronal drive suggests the existence of a mathematical integrator, known as the Neural Integrator in the oculomotor literature (Robinson 1981).

The Neural Integrator (NI) has been modeled in the past as a linear low-pass filter (Robinson 1975; Raphan & Cohen 1978; Barnes 1979) presumed constant and with a large time constant (>15s, a 'leaky' integrator). However earlier experiments by (Crawford et al 1992) implied a possible change in the gaze holding properties of the NI, with initial eye eccentricity. The implications of a model for VOR modulation with target depth also predicts NI properties that would change with binocular set-points (Khojasteh & Galiana 2006). In addition, lesion experiments in the brainstem within the circuit supporting NI function also caused wide changes in its function, with the greatest effect caused by PH lesions (Cannon & Robinson 1987; Mettens et al. 1994). Similarly, intact connections between the brainstem and cerebellum are also required to preserve a strong NI with large time constant (Robinson 1989; McCrea, et al. 1987; Aksay et al. 2000).

The goal of this PhD research was to investigate the sensorimotor conditions (input/output context) that would cause variability in the NI dynamics, and to postulate a model structure that could support this variability in a physiologically significant manner. The experimental results in this study document that NI function depends both on eye

eccentricity and on concurrent head velocity levels. It is proposed that a non-linear element inside an existing loop model for the NI will accommodate for the set-point dependent characteristics of the NI dynamics. This non-linear element is placed at the level of VN premotor cells known to combine vestibular afferent information with internal efferent copies of eye position (so-called Position-Vestibular-Pause cells). Since the NI is known to be shared by all oculomotor reflexes, its context-dependency should also affect the dynamics of many reflexes in a similar manner. Thus, the modified NI model is used to estimate model parameters in VOR tests from human control subjects and peripheral vestibular patients. Comparisons of the estimates from the different subject groups imply a more sensitive detection of vestibular anomalies and a more sensitive tool for diagnosis, even after lesion compensation.

This manuscript-based thesis begins with a Literature Review of the physiology and current models of the VOR, and the tools that are used to estimate these model parameters (VOR dynamics). The third chapter presents the first published manuscript, the discovery that the dynamics of the NI are setpoint-dependent even in the dark (gaze holding), and further change with the testing conditions (head fixed vs. passive head turns). The fourth chapter presents the published manuscript with a nonlinear feedback model that emulates the observed setpoint-dependent dynamics of the NI, together with a validated algorithm to estimate the model coefficients from passive VOR responses in the dark. Finally, the fifth chapter compares the parameter estimates for this model form from different human subject groups in a manuscript submitted for publication. The thesis then concludes with a discussion linking the manuscript chapters and outlining their implications for future theoretical and clinical work on oculomotor control.

2. Literature Review

In this review, we attempt to present all the tools that are essential for this thesis. They cover areas such as the physiology of the Vestibulo-Ocular Reflex (VOR), the various existing models for the VOR, and the different parameter estimation algorithms, such as the Least Squares Method and methods of Optimization.

2.1 Physiology

Numerous anatomical sites are involved in the horizontal Vestibular Ocular Reflex (VOR), such as the Semicircular Canals, Vestibular Nuclei, Prepositus Hypoglossi, Reticular Formation, Superior Colliculus and Abducen Nuclei. A brief overview on the different sites is given below:

2.1.1 Semicircular Canals

The inner ear contains three semicircular canals oriented orthogonal to each other (horizontal, anterior and posterior). A pair of fluid-filled semi-circular canals lying on the horizontal plane detects horizontal head rotations from the induced pressure differential across the cupula, which in turn bends hair cells and triggers spikes in the vestibular nerve. The geometric and fluid properties of the canals cause the transduction of head velocity to spike frequency as a high-pass filter. Canal signals are then transmitted to the Vestibular Nuclei through the afferent vestibular nerve fibres.

$$H_C(s) = G_C \frac{T_C s}{T_C s + 1} \tag{1}$$

(Goldberg and Fernandez 1980; Wilson and Melvill Jones 1979)

2.1.2 Vestibular Nuclei

The Vestibular Nuclei (VN) consist of four major subdivisions: the superior, lateral, medial and descending VN (Buttner and Buttner-Ennever 2006). Most of the vestibular

nerves containing information on horizontal head rotation terminate in the medial VN. Disruption of the VN, such as electrical stimulation (Cohen 1974) and lesions (Uemura and Cohen 1973), leads to nystagmus during eye movement. Neurons in the VN can be classified into five general groups: Group I – vestibular only neurons which respond only to vestibular stimulation; Group II – vestibular plus saccades neurons which burst or pause in response to saccades in addition to responding to vestibular stimulation; Group III – vestibular plus position neurons which show activity changes related to both orbital eye position and vestibular stimulation; Group IV – gaze velocity neurons which encode eye velocity in space; and Group V – saccade plus position neurons which behave like ocular motorneurons and have a burst-tonic pattern during spontaneous eye movement with no sensitivity to vestibular stimulation (Buttner and Buttner-Ennever 2006). The presence of the Group III neurons in the VN provides a physiological substrate for the VOR and neural integrator models (below) in this thesis that rely on an internal estimate of the eye position in a closed loop.

2.1.3 The Reticular Formation

The reticular formation forms the central core of the brainstem. Since it has no distinct cytoarchitectural boundaries, it is subdivided according to its general location, such as the mesencephalic reticular formation, the Paramedian pontine reticular formation and the medullary reticular formation (Horn 2006). The Mesencephalic reticular formation or the rostral interstitial nucleus of the medial longitudinal fasciculus (RIMLF) contains premotor burst neurons which are essential for the generation of vertical and torsional saccades (Buttner, Buttner-Ennever and Henn 1977; Crawford and Vilis 1992). The paramedian pontine reticular formation lies between the abducens nucleus and the trochlear nucleus. It projects to motorneurons and internuclear neurons within the ipsilateral abducens nucleus, and the medial vestibular nuclei (Langer, et al. 1986) and is involved in the generation of horizontal saccades (Robinson 1972). The medullary reticular formation corresponds to the area just caudal and ventral to the abducens nucleus, and contains premotor inhibitory burst neurons for horizontal saccades (Scudder, Fuchs and Langer 1988). These inhibitory burst neurons have dendrites that enter either

the abducens or the PH (Strassman, Highstein and McCrea 1986). Studies on the firing rate of these burst cells indicate that their activity is related to concurrent eye velocity during saccades.

2.1.4 Prepositus Hypoglossi

The Prepositus Hypoglossi (PH) consists of neurons that are located between the hypoglossal nucleus and the abducen nucleus in the brain stem (McCrea and Horn 2006). It receives inputs from areas that are involved in the control of eye movements, such as the vestibular nuclei and the reticular formation (McCrea and Horn 2006). Furthermore, it receives input from areas that drive gaze to spatial targets, such as the superior colliculus and the flocculus (Grantyn and Grantyn 1982; Balaban, Schuerger and Porter 2000). Due to its heavy interconnection with anatomical sites that are responsible for the generation of the VOR, the PH plays an essential role in the VOR as well as in the neural integration process (Mettens, et al. 1994). Whether by distributed circuitry (Kaneko 1997) or acting as a sole contributor to neural integration (Cannon and Robinson 1987), the PH's involvement in the neural integration process is generally accepted. Many cells in this nucleus modulate their activity with orbital eye position, regardless of the sensory stimulus that caused the ocular response (Gonzalez-Forero et al. 2003; Cheron et al. 1986; Baker et al. 1975). Hence it is also generally accepted that the NI function in the PH is shared by all ocular reflexes.

2.1.5 Superior Colliculus

The superior colliculus (SC) is located rostral to the midbrain and plays an important role in the generation of saccadic eye movements (Moschovakis and Highstein 1994). It is involved in generating involuntary and visually-guided saccades, and plays a role in supporting visual fixation in cats (Munoz and Guitton 1991) and in monkeys (Munoz and Wurtz, 1993). Although lesion of the SC does not have any long term effect on the subject's ability to perform saccades since the Frontal Eye Field (FEF) is also involved in the task of generating saccadic eye movements, but the latency of the compensated saccadic eye movements increases substantially (Schiller et al. 1987). This suggests that

the SC provides a more direct pathway in generating saccadic eye movement. Neurons in the SC were found to synapse onto sites including the abducens nuclei, the burst neurons (BN) and Prepositus Hypoglossi (PH) in the medullary reticular formations (Guitton 1991). There exist many saccade burst generator models, such as the Scudder model (Scudder 1988) and the Galiana model (Guitton et al. 1990), but a review on these models is beyond the scope of this thesis.

2.2 Physiological Behaviour

2.2.1 Types of Eye Movements

Eye movements are usually categorized in the following types: saccades, smooth pursuit eye movements, vestibulo-ocular reflex, optokinetic reflex, vergence and gaze holding (Buttner and Buttner-Ennever 2006). Saccadic eye movements correspond to fast conjugate eye movements that reposition the eyes to new spatial targets. Visual information is suppressed during saccades for normal subjects. Smooth pursuit eye movements are exhibited during voluntary tracking of a small foveal moving target, which can be mixed with fast catch-up or corrective saccades (pursuit nystagmus). The vestibulo-ocular reflex (VOR) adjusts eye movements when the head is subjected to perturbations in space. It consists of both slow phase (compensatory) and fast phase (anticompensatory) eye movements to form the VOR nystagmus pattern.

An example of VOR nystagmus is provided in Figure 1. It is clear that the eye velocity profile during slow phases follows in mirror fashion the head velocity profile.

Optokinetic eye movements are triggered by movement of a large visual field, and consist of slow (following) segments interrupted by opposite rapid movements creating optokinetic nystagmus (OKN) (Henn et al. 1980). Subjects undergoing optokinetic stimuli often have the sensation of moving in a direction opposite to the visual flow, despite remaining stationary. Hence OKN and VOR are deemed to serve complementary roles at premotor levels (Robinson 1972, Raphan and Cohen 1978). Convergence, or vergence, eye movements correspond to the foveation of the two eyes on objects at

varying distances. Gaze holding corresponds to the fixation of the eyes on a chosen target even in the dark, though with decaying trajectories.

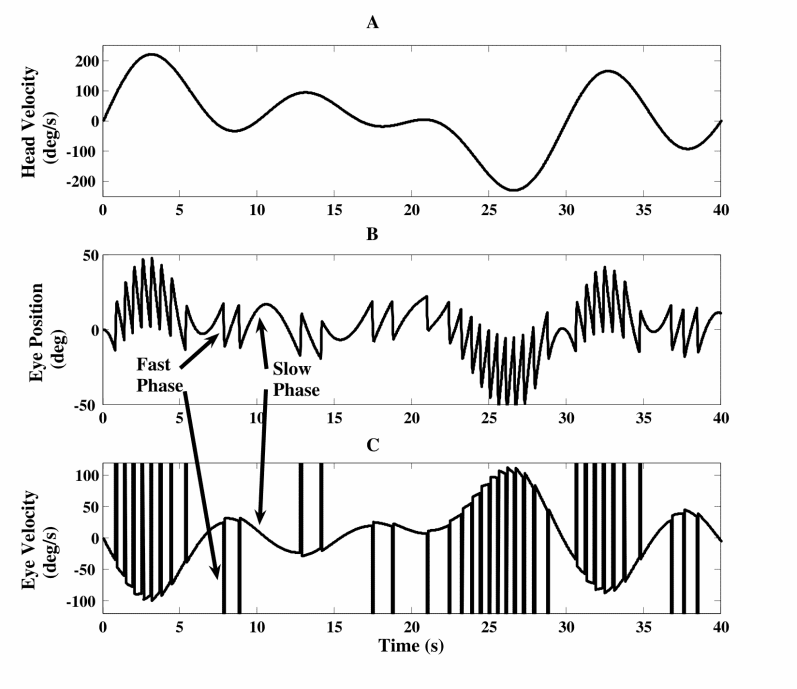

Figure 1: VOR Nystagmus: eye position (B) and eye velocity (C) when subjected to a head velocity profile (A).

The classification of eye movements according to response type and sensory trigger is typical in the literature. However, recent data in the literature emphasizes that many of these movements rely on identical brain circuits, and differ only in their sensory processes (Henn et al. 1980). Hence a simpler classification refers to rapid eye movements to redirect gaze in any reflex (saccades, VOR and OKN fast phases, fast vergence), and to slow eye movements aligning the eyes on a current goal (in VOR, OKN, pursuit and slow vergence).

2.2.2 Vestibular Deficits

The role of the Vestibulo-Ocular Reflex (VOR) is to stabilize gaze on objects during head movements. Performance of the VOR may be affected by abnormalities in any part of the

vestibular and oculomotor systems. We will go over some of the abnormalities that will be presented in this thesis and their effects on the VOR data.

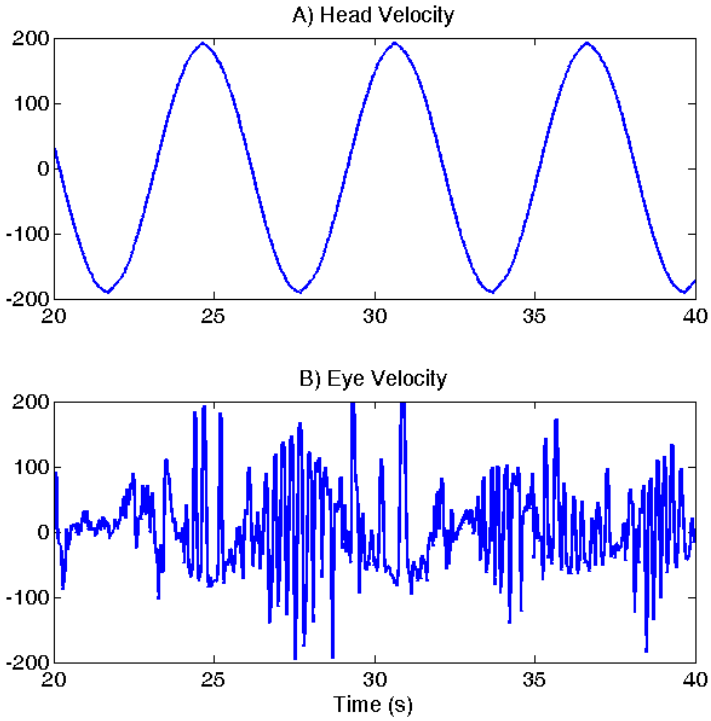

Figure 2: Example of a subject suffering from Vestibular Neuronitis on the right side, with (A) the head velocity and (B) the response eye velocity in the dark. The slow phases of the nystagmus are directed opposite to the head rotation direction. Note dereased reflex gain during rigtward head rotation (positive).

2.2.2.1 Vestibular Neuronitis

Vestibular Neuronitis (VN) is caused by a viral infection of the vestibular nerve. Symptoms of Vestibular Neuronitis (or neuritis) include vertigo, nausea, imbalance, spontaneous nystagmus and blurred vision. Subjects with Vestibular Neuronitis usually experience the acute phase of the vertiginous episodes for one to two weeks, and then recover either because of compensation or of prevalence of the auto immune system over the virus. The recurrence rate of Vestibular Neuronitis symptoms is extremely low and compensated subjects with previous Vestibular Neuronitis function as well as normal subjects in daily tasks (Heardman et al 2000), but multiple recurrences are still possible

and may be reclassified as Benign Paroxysmal Vertigo (Basser 1964) or Meniere's disease (Rasekh and Harker 1992). The infection may be localized in one vestibular apparatus and produces a suppressed VOR response during rotation to the affected side (Figure 2).

2.2.2.2 Sudden Hearing Loss

Sudden Hearing Loss consists of an acute loss of hearing and may be accompanied by symptoms similar to those of Vestibular Neuronitis, such as dizziness and nausea. It may be caused by sudden air pressure change in the ear, infection, side effect from ototoxic drugs/medications or acoustic trauma (Lazarini & Camargo 2006). Depending on the prognosis, methods of intervention may include surgery, cessation of ototoxic drugs administration, or administration of medication for the infection (Narozny et al. 2006). Its effects on the vestibular system and VOR may be similar to that of Vestibular Neuronitis and require an extended period of compensation.

The data of Vestibular Neuronitis or Sudden Hearing Loss patients that are presented in this thesis were from individuals who suffered only one vestibular episode and were recorded within a few months after the initial complaint. No labyrinthectomy was performed on any of these patients.

2.2.2.3 Meniere's disease

Patients suffering from Meniere's disease generally experience intermittent vertiginous episodes lasting for several minutes, tinnitus which is described as a sensation of ringing or fullness within the inner ear, and fluctuations in hearing (Atkinson 1961). It may be associated with endolymphatic hydrops, or the building up of pressure within the semi-circular canals (Kariya et al 2007), some patients experiencing symptoms of Meniere's disease may or may not be showing any endolymphatic hydrops, but it is the only histologic marker for Meniere's disease (Cureoglu et al 2004). Thus the diagnosis of Meniere's disease in subjects is done by eliminating other possible causes, such as Vestibular Neuronitis, strokes or a tumor in the brainstem, which may result in the same symptoms as Meniere's disease (Mills 2007). Patients initially suffering from Meniere's

disease unilaterally may progress to exhibit symptoms bilaterally with time (Kariya et al 2007). Since the occurrence and frequency of vertigo, tinnitus and hearing loss are unpredictable, many Meniere's disease patients suffering from frequent and severe episodes may opt for vestibular neurectomy (Pelletier 2002). Meniere's disease patients, when not experiencing any episodes, often exhibit a VOR that is comparable to that of normal subjects when relying on standard clinical tests.

2.3 Models for the VOR

2.3.1 Velocity Storage

The semicircular canals can be modeled by a first order high-pass filter of the form:

$$H_{VS}(s) = G_{VS}\frac{T_{VS}s}{T_{VS}s+1} \tag{2}$$

Due to the physical properties of the cupula-endolymph system, velocity-step head speed profiles appear in the primary vestibular afferents as activity declining with a time constant of 4-6s in man or monkey (Fernandez and Goldberg 1971; Gizzi and Harper 2003; Wilson and Melvill Jones 1979).

On the other hand during the rotation profile, it has been observed that the response of cells in the Vestibular Nuclei (VN) decays instead with a time constant of around 20s in human (Dai, et al. 1999). Ocular nystagmus in this protocol also follows a slow decay pattern. The slower pattern of central and behavioral decay is called velocity storage in the literature. It has been modeled by postulating a lead-lag process that cancels the canal primary time constant and replaces it with the observed central/ocular decay time constant (Robinson 1981; Raphan and Cohen 1978):

$$H_{VN}(s) = G_{VN}\frac{T_C s+1}{T_V s+1} \tag{3}$$

Where $T_V = 20\,s$ .Thus lumping this model with the canal model with an arbitrary projection gain 'g', we have:

$$H_{Vs}(s) = H_C(s)H_{VN}(s) = \frac{T_C s}{T_C s + 1}\frac{T_C s + 1}{T_{VS} s + 1} g = \frac{gT_C s}{T_{VS} s + 1} = G_{VS}\frac{T_{VS} s}{T_{VS} s + 1} \qquad (4)$$

This provides in a global sense the first order high-pass filter properties observed at VN and ocular levels during steps in head velocity.

2.3.2 Neural Integrator (NI)

Neural Integrator is the term used to describe the process of mathematical integration performed at the neuronal level. Such an NI is necessary in the oculomotor system to accommodate observed premotor and motor responses. Its exact physiological site is still under great debate, but the VN and Prepositus Hypoglossi, the Reticular Formation and the Superior Colicullus are believed to form a network that functions as an integrator (Gonzalez-Forero, et al. 2003). Appropriate construction of motor signals for eye control can either be achieved by an integrator in parallel with a feedforward path or an integrator with a feedback path. The NI itself is generally modeled as a global first order low pass filter with the form:

$$H_{NI}(s) = \frac{1}{T_{NI} s + 1} \qquad (5)$$

Where T_{NI} corresponds to the Neural Integrator time constant, usually assumed > 15s.

2.3.3 Building Motor signals

The Eye Plant is responsible for converting motorneural signals into eye movement. It consists of the eyeball and the ocular muscles that control the movement of the eye. The horizontal Eye Plant can be modeled by a first order low-pass filter (Sylvestre and Cullen 1999; Skavenski and Robinson 1973) as:

$$\frac{E(s)}{F(s)} = H_{EP}(s) = \frac{1}{T_{EP}s + 1} \tag{6}$$

Where $E(s)$ and $F(s)$ respectively denote the eye position and motoneuronal firing rate, and T_{EP} denotes the eye plant time constant of approximately 100-150 ms.

A realization of the VOR to provide adequate signals on ocular motorneurons consists of passing the head velocity signal encoded by the Velocity Storage (VS) process onto, in parallel, the postulated NI process (first order low-pass filter) and a simple feedforward gain,. The sum then simply combines at the level of the MN (Skavenski and Robinson 1973) (Figure 3A). In this case, the coefficients a and b control the weight between the two feedforward pathways, while the coefficient β denotes the gain before the NI model. The overall transfer function of this realization is:

$$H_1(s) = \frac{-\beta(bT_{NI}s + a + b)}{(T_{NI}s + 1)(T_{EP}s + 1)} = -\frac{G_{VOR}}{T_{NI}s + 1} \tag{7}$$

Where $T_{EP} = bT_{NI}/(a + b)$ and $G_{VOR} = \beta/(a + b)$.

Another realization embedding suitable NI function and eye plant compensation consists of a feedforward pathway within a feedback loop containing an internal copy of the eye position from an approximate eye plant model (Skavenski and Robinson 1973) (Figure 3B). This realization is supported by the presence of cells in the Vestibular Nuclei and PH that modulate with both eye position and head velocity (Mettens et al. 1994). The overall transfer function of this realization is:

$$H_2(s) = \frac{-\beta/(1-\gamma)}{T_{EP}/(1-\gamma)s + 1} = -\frac{G_{VOR}}{T_{NI}s + 1} \tag{8}$$

With $G_{VOR} = \beta/(1-\gamma)$ and $T_{NI} = T_{EP}/(1-\gamma)$.

For the two realizations to be equivalent, we set:

$$a + b = 1/(1-\gamma) \text{ and } T_{NI} = T_{EP}/(1-\gamma) \quad (9)$$

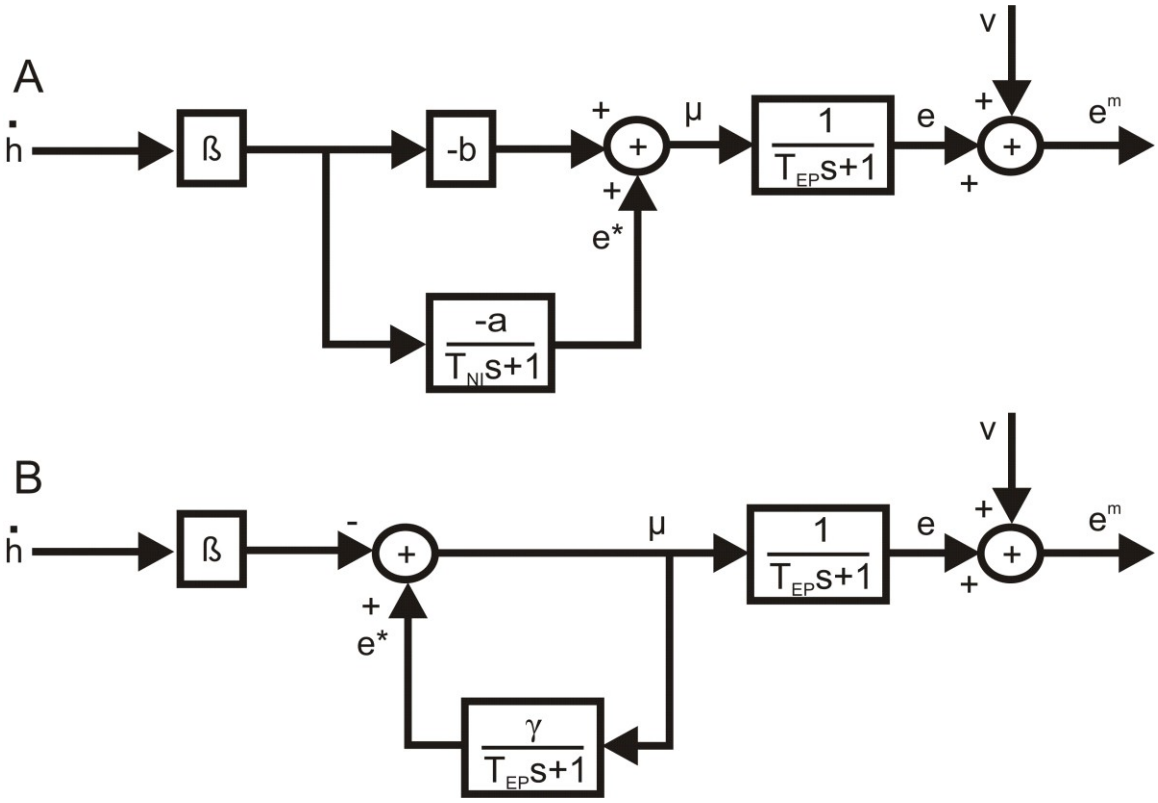

Figure 3: Different Realizations of the Neural Integrator and eye plant compensation.

The realizations that are based on the feed-forward model structure, such as the Robinson model (Figure 3A) and the models proposed by Galiana & Outerbridge (1984) and Seung et al (2000) are all based on neural-like networks and try to build from single cells the performance of a near-ideal integrator (T>10s); in contrast the feedback loop approach (Figure 3B) is relying on building a 'model' of the eye plant (linear or non-linear) with a much smaller time constant (T~200-300ms). In the linear case, all the implementations can look the same at the global level (e.g. gaze holding). However the latter points to possible execution by simpler neural networks (fewer cells as in goldfish) without loss of behavioural performance.

Thus, the dynamics of the Vestibulo-Ocular Reflex are achieved by concatenating the Velocity Storage and the Neural Integrator/MN processes together (Figure 4), yielding:

$$H_{VOR}(s) = -\frac{T_{VS}\, s}{T_{VS}\, s + 1}\,\frac{G_{NI}}{T_{NI}\, s + 1} \tag{10}$$

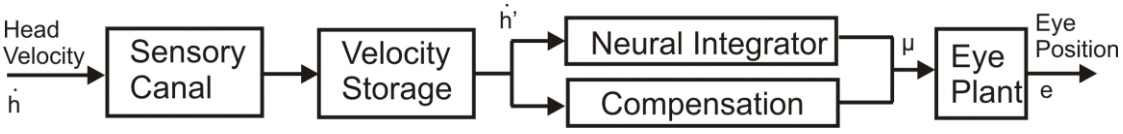

Figure 4: Block diagram of the overall VOR model structure

This is a cascade of a first order high-pass filter and a first order low-pass filter regardless of the realization used for the NI. G_{VOR} represents the gain of eye velocity with respect to head velocity for large rotation frequencies ($\omega > 1/T_{VS}\,; 1/T_{NI}$).

2.4 Model Parameter Estimation Algorithms

Regardless of the model form that may be postulated, testing a model's validity requires fitting coefficients to central or ocular data, and evaluating its predictive capability. An overview of available identification schemes is now provided.

2.4.1 Method of Least Squares

Let us first consider a linear system with the model structure given as in Figure 5 with the input given by $x(n)$, the output given by $y(n)$ and the transfer function given by $h(n)$.

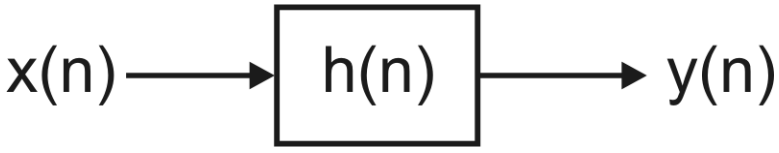

Figure 5: A system with an input stimulus and observed output

Below, *M* will denote the order of the system (number of states in discrete or continuous time) and *N* the length of the data (number of data points). The problem must first be formulated in terms of multiple segments of ocular nystagmus of the same type (e.g. slow phases for the VOR). Hence the input data X in a given segment of length N can be

defined as an N by M matrix with each of its rows containing M samples of the input data starting at n, while Y is a column vector of N samples:

$$X = \begin{bmatrix} x(n) & x(n-1) & \dots & x(n-M+1) \\ x(n-1) & x(n-2) & \dots & x(n-M) \\ \vdots & \vdots & \ddots & \vdots \\ x(n-N+1) & x(n-N) & \dots & x(n-M-N+2) \end{bmatrix} \tag{11}$$

$$Y = \begin{bmatrix} y(n) & y(n-1) & \dots & y(n-N+1) \end{bmatrix}^T \tag{12}$$

The relationship between the input and output of the system can then be expressed as:

$$Y = X\Theta + e \tag{13}$$

Where Θ corresponds to the system parameters of $h(n)$ and e corresponds to the residual caused by observation noise or model deficiencies.

$$\Theta = \begin{bmatrix} \theta_1 & \theta_2 & \dots & \theta_M \end{bmatrix}^T \tag{14}$$

By the method of least squares (Kukreja et al. 2005; Ljung & Glad 1994; Freund & Walpole 1987), the estimate of the model parameters is given by:

$$\hat{\Theta} = (X^T X)^{-1} X^T Y \tag{15}$$

While the variance-covariance matrix of the estimates is given by:

$$D(\hat{\Theta}) = \sigma^2 (X^T X)^{-1} \tag{16}$$

and σ , the variance of the output residual, can be estimated with:

$$\hat{\sigma}^2 = \frac{(Y - X\hat{\Theta})^T (Y - X\hat{\Theta})}{M - N} \tag{17}$$

In order to use the method of least squares and obtain unbiased estimates, the system has to satisfy the following criteria (Kukreja 2001; Ljung & Glad 1994):

- The input signal has to be deterministic, i.e. noiseless.
- The output residual (and observation noise) has to be zero mean and white (or uncorrelated) with respect to the input.
- The model used in the estimation process has to be correct.

In addition the input characteristics should include the expected bandwidth of the system under study. This solution presumes a linear system with long data records that allow transients (initial conditions) to play a minor role. Also it is presumed that each output is only a function of delayed inputs – moving average with exogenous input (Ljung and Glad 1994). Alternatives are needed for systems with auto-regressive components or non-linearities in the presence of observation noise and/or short data segments (as in nystagmus).

2.4.2 Extended Least Squares for NARMAX Models

Many biological systems can be represented well by cascades of static non-linearities with linear systems (e.g. Wiener or Hammerstein systems; Kukreja 2001). Let us consider a nonlinear model with the following configuration:

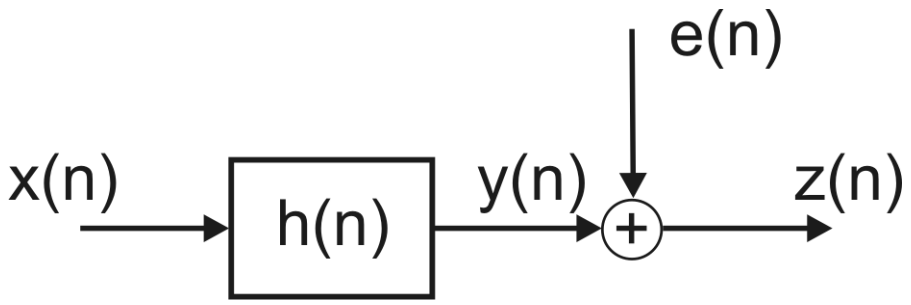

Figure 6: System with Noise

A NARMAX structure can serve to identify models with auto-regressive components and cascaded non-linearities. For example, in Figure 5, let us consider a Wiener structure with:

$$y(n) = \theta_1 x(n) + \theta_2 x(n-d_1) + \theta_3 x^2(n-d_2) + \theta_4 y(n-d_3) \tag{18}$$

And since we can only measure $z(n)$ instead of $y(n)$:

$$z(n) - e(n) = \theta_1 x(n) + \theta_2 x(n-d_1) + \theta_3 x^2(n-d_2) + \theta_4 [z(n-d_3) - e(n-d_3)] \tag{19}$$

Grouping the observed output $z(n)$ on the left hand side, we have:

$$z(n) = \theta_1 x(n) + \theta_2 x(n-d_1) + \theta_3 x^2(n-d_2) + \theta_4 z(n-d_3) + e(n) - \theta_4 e(n-d_3) \tag{20}$$

Or for N samples,

$$Z = \Psi_{zu} \Theta + r \tag{21}$$

with

$$\Psi_{zu} = \begin{bmatrix} x(n) & x(n-d_1) & x^2(n-d_2) & z(n-d_3) \\ x(n-1) & x(n-1-d_1) & x^2(n-1-d_2) & z(n-1-d_3) \\ \vdots & \vdots & \vdots & \vdots \\ x(n-N+1) & x(n-N+1-d_1) & x^2(n-N+1-d_2) & z(n-N+1-d_3) \end{bmatrix} \tag{22}$$

$$\Theta = \begin{bmatrix} \theta_1 & \theta_2 & \theta_3 & \theta_4 \end{bmatrix}^T \tag{23}$$

And the residual *r* is given by:

$$\begin{aligned} r = & \begin{bmatrix} e(n) & e(n-1) & \dots & e(n-N+1) \end{bmatrix}^T \\ & - \theta_4 \begin{bmatrix} e(n-d_3) & e(n-1-d_3) & \dots & e(n-N+1-d_3) \end{bmatrix}^T \end{aligned} \tag{24}$$

We observe that the noise term $e(n - d_3)$ in the residual is biased by the coefficient θ_4. Thus the Least Squares method cannot yield unbiased estimates of this nonlinear model. To address this problem, let us consider:

$$\hat{e} = Z - \hat{Z} \tag{25}$$

Where Z denotes the measured output and $\hat{Z}$ denotes the predicted output. $\hat{Z}$ can be calculated by iteration, where the first attempt is calculated from the method of Least Squares with:

$$\hat{Z} = \Psi_{ZU} \hat{\Theta}_{ZU} \tag{26}$$

and Ψ_{zu} and $\hat{\Theta}_{ZU}$ only contain terms that are related to the input $x(n)$ and output $z(n)$.

With the estimated residual, the system parameters can be recomputed with an extended regressor to include the coefficients for the noise model:

$$\hat{\Theta}_{zue} = (\Psi^T \Psi)^{-1} \Psi^T Z \tag{27}$$

Where $\Psi = [\Psi_{zx} \Psi_{zx\hat{e}} \Psi_{\hat{e}}]$, and Ψ_{zx} contains combinations of z and x terms only, $\Psi_{zx\hat{e}}$ contains all cross-terms between z, x and $\hat{e}$, and $\Psi_{\hat{e}}$ contains polynomials of $\hat{e}$ only. Thus the procedure is:

1. Calculate the estimates $\hat{\Theta}_{zx}$ for all combined terms of z and x only with the method of Least Squares.
2. Calculate the residual estimate $\hat{e}$ from $\hat{Z} = \Psi_{zx} \hat{\Theta}_{zx}$.
3. Formulate $\Psi = [\Psi_{zx} \Psi_{zx\hat{e}} \Psi_{\hat{e}}]$ and calculate $\hat{\Theta}_{zue} = (\Psi^T \Psi)^{-1} \Psi^T Z$.
4. Calculate the residual estimate $\hat{e}$ from $\hat{Z} = \Psi_{zx\hat{e}} \hat{\Theta}_{zx\hat{e}}$.
5. Repeat 3 and 4 until convergence.

The Method of Extended Least Squares requires that all the noise and residual terms be included in the model, hence the complexity of the model increases rapidly as the model's order of nonlinearity increases (Kukreja 2001). Furthermore, the Method of Extended Least Squares requires the model ouput to be expressible explicitly as a function of inputs and *past* outputs, i.e. in the form:

$$y(n) = f\left(y(n-1),..., y(n-m_y), x(n),..., x(n-m_y), e(n-1),..., e(n-m_e)\right) \quad (28)$$

For models whose output cannot be explicitly expressed due to non-linearities, such as:

$$y(n) = f\left(y(n), y(n-1),..., y(n-m_y), x(n),..., x(n-m_y), e(n-1),..., e(n-m_e)\right) \quad (29)$$

alternatives to Least Squares are required to estimate the system parameters. Optimization tools are such an option.

2.4.3 Methods of Optimization

The goal of optimization is to search for a set of parameters that minimizes (or maximizes) an objective function while satisfying certain constraints. Let us formulate it as:

$$\min_{\theta} V(\theta) \quad (30)$$

Subject to

$$g(\Theta) = 0 \quad (31)$$

with $\Theta = [\theta_1 \quad \theta_2 \quad \ldots \quad \theta_n]^T$ denoting the n parameters to be estimated, $V(\Theta)$ denoting the objective (or cost) function and $g(\Theta)$ denoting the constraints on the parameter set Θ.

An example of an optimization problem would be to find the set of parameters to minimize an error function, such as the mean-squared error:

$$V(\theta) = \frac{1}{N}\sum \left(y_m(n) - \hat{y}(n)\right)^2 \tag{32}$$

Where N denotes the data length, $y_m(n)$ the measured output at instance n and $\hat{y}(n)$ the predicted output from the model at instance n .

While the system equation for the model is included in the constraint:

$$\begin{aligned} & g(\Theta) = y(n) \\ & - f\left(y(n), y(n-1),..., y(n-m_y), x(n),..., x(n-m_y), e(n-1),..., e(n-m_e), \Theta\right) = 0 \end{aligned} \tag{33}$$

Thus the output from the system $y(n)$ is not required to be expressed explicitly in the system equation.

We will present an overview of several optimization methods that are widely used and compare their advantages and merits.

2.4.3.1 Linear Optimization

For linear optimization, both the objective function and the constraint are linear. We can reformulate them as:

$$\min_{\theta} \; z = C^T \Theta \tag{34}$$

Subject to

$$A\Theta \le B, \tag{35}$$

$$\Theta \ge 0 \tag{36}$$

Where

$$C = \begin{bmatrix} c_1 & c_2 & \dots & c_n \end{bmatrix}^T \tag{37}$$

$$\Theta = \begin{bmatrix} \theta_1 & \theta_2 & \dots & \theta_n \end{bmatrix}^T \tag{38}$$

$$A = \begin{bmatrix} a_{11} & a_{21} & \dots & a_{n1} \\ a_{12} & a_{22} & \dots & a_{n2} \\ \vdots & \vdots & \ddots & \vdots \\ a_{1m} & a_{2m} & \dots & a_{nm} \end{bmatrix} \tag{39}$$

$$B = \begin{bmatrix} b_1 & b_2 & \dots & b_m \end{bmatrix}^T \tag{40}$$

Where $C \in n \times 1$, $\Theta \in n \times 1$, $A \in m \times n$ and $B \in m \times 1$.

Then for the i th row in the matrix A, we have:

$$a_{1i}\theta_1 + a_{2i}\theta_2 + \dots + a_{ni}\theta_n - \theta_{si} = 0 \tag{41}$$

Where

$$\theta_{si} \geq 0 \tag{42}$$

Therefore we can rewrite the constraint as:

$$\left[\begin{array}{c|ccc} 1 & -C^T & 0 \\ \hline 0 & A & I \end{array}\right] \begin{bmatrix} z \\ \Theta \\ \Theta_s \end{bmatrix} = \begin{bmatrix} 0 \\ B \end{bmatrix} \tag{43}$$

With $\Theta \geq 0$ and $\Theta_s \geq 0$, and I the $m \times m$ identity matrix

$$\Theta_s = \begin{bmatrix} \theta_{s1} & \theta_{s2} & \dots & \theta_{sm} \end{bmatrix} \tag{44}$$

With this formulation, we can now present the Conjugate Gradient Method or the Direct Search Method to solve the linear optimization problem.

2.4.3.2 Conjugate Gradient Method

The Conjugate Gradient Method is another linear optimization method that uses an iterative approach to search for the optimal solution. Let us consider the following problem (Hestenes & Stiefel 1952):

$$\min_{\theta} \; Ax = b \tag{45}$$

Where A is an n-by-n symmetric positive-definite matrix.

Then the Conjugate Gradient Method consists of the following algorithm:

1. We define the residual for the initial step as: $r_0 = b - Ax_0$, where x_0 is the initial point of the solution, and the direction of descent is defined as: $p_0 = r_0$, with $k = 0$.

2. We then have: $\alpha_k = \frac{r_k^T r_k}{p_k^T A p_k}$, $x_{k+1} = x_k + \alpha_k p_k$ and $r_{k+1} = r_k + \alpha_k A p_k$. If r_{k+1} is 'small', we have x_{k+1} as our optimal solution, otherwise,

3. We perform the following updates: $r_k = \frac{r_{k+1}^T r_{k+1}}{r_k^T r_k}$, $p_{k+1} = r_{k+1} + \beta_k p_k$ and $k = k + 1$, and go back to step 2.

The Conjugate Gradient method is suited to be used on sparse systems that are too large for the direct search methods, which will be presented in the next section.

2.4.3.3 Direct Search Methods

The benefit of direct search methods is that they search for the optimal solution without calculating derivatives (Powell 1998). Instead, direct search methods define an area around a point, and search for a direction to improve the objective function.

Simplex Method:

One of the most widely used Direct Search Method is the Simplex method. Given an optimization problem with n number of parameters, the underlying idea of Direct Search Method is to iteratively move a polytope of dimension $n+1$, one vertex at a time, around on the objective function such that the new vertex would have an improved yield from the objective function (Han and Michael 2006), (Nelder and Mead 1965). Mathematically, we can denote the set of vertices of the polytope as $(v_0, v_1, \ldots, v_n)$ with $V(v_0) \le V(v_1) \le \ldots \le V(v_n)$ where $V(\cdot)$ is the objective function. To move the polytope towards the optimum, the worse vertex, in this case v_n, will have to be replaced by a new vertex. Four operations can be used to search for the new vertex: reflection, expansion, contraction and shrinkage. To express the operations mathematically, we respectively assign the multipliers α, β, γ and δ to reflection, expansion, contraction and shrinkage. Note that $\alpha > 0$, $\beta > 1$, $0 < \gamma < 1$ and $0 < \delta < 1$. We define the centroid of the polytope as

$$\bar{v} = \frac{1}{n}\sum_{i=0}^{n-1} v_i \tag{46}$$

and the reflection, expansion, outside contraction, inside contraction and shrink procedures are respectively defined as:

$$v_r = \bar{v} + \alpha(\bar{v} - v_n) \tag{47}$$

$$v_e = \bar{v} + \beta(\bar{v} - v_n) \tag{48}$$

$$v_{oc} = \bar{v} + \gamma(\bar{v} - v_n) \tag{49}$$

$$v_{ic} = \bar{v} - \alpha(\bar{v} - v_n) \tag{50}$$

$$v_i = \bar{v} + \delta(\bar{v} - v_n) \tag{51}$$

Thus the steps for the Simplex Method are:

1. Search for the v_n that yields the worse value from the objective function,
2. Evaluate $V(v_r)$. If $V(v_0) \le V(v_r) < V(v_n)$, replace v_n with v_r,
3. If $V(v_r) < V(v_0)$, compute $V(v_e)$. If $V(v_e) < V(v_r)$, replace v_n with v_e; otherwise, replace v_n with v_r,
4. If $V(v_{n-1}) \le V(v_r) < V(v_n)$, compute $V(v_{oc})$. If $V(v_{oc}) < V(v_r)$, replace v_n with v_{oc},
5. If $V(v_r) \ge V(v_n)$, compute $V(v_{ic})$. If $V(v_{ic}) < V(v_n)$, replace v_n with v_{ic}, otherwise,
6. We shrink the polytope for $1 \le i \le n$.

Grid-Based Method:

Another realization of the direct search methods is the grid-based methods. The idea behind the grid-based methods is that a grid is formed over the feasible region, with one of the points on the grid selected as the current solution. Then the optimal solution is found by searching through the directions of the coordinate system (Carlyle, Montgomery and Runger 2000). An overview of the algorithm is as follow:

1. Select an initial point, $\theta^1 = (\theta^1_{x1} \quad \theta^1_{x2} \quad \dots \quad \theta^1_{xn})$, where $x1, x2, \dots, xn$ corresponds to the n dimension for the objective function.
2. Evaluate $V(\theta^1)$.
3. Define a minimum step length γ_0. Then define a certain step parameters for each coordinate: $\gamma_{x1}, \gamma_{x2}, \dots, \gamma_{xn}$.
4. Evaluate $V(\theta^1_{x1+\gamma_{x1}}, \theta^1_{x2}, \dots, \theta^1_{xn})$, if $< V(\theta^1)$, replace the current point θ^1 by $\theta^1_{x1+\gamma_{x1}}, \theta^1_{x2}, \dots, \theta^1_{xn}$; otherwise, evaluate $V(\theta^1_{x1-\gamma_{x1}}, \theta^1_{x2}, \dots, \theta^1_{xn})$, if $< V(\theta^1)$, replace the current point θ^1 by $\theta^1_{x1-\gamma_{x1}}, \theta^1_{x2}, \dots, \theta^1_{xn}$.

5. Repeat step 4 for θ_n^1 with the step parameter γ_{xn}, denote the new current point as θ^2.

6. If $\theta^1 \neq \theta^2$, repeat step 4 to 6 with θ^2 as the new value, otherwise:

7. Divide all γ's by 2. If $\gamma > \gamma_0$, go back to step 4 with the new γ, otherwise, stop the process.

2.4.3.4 Nonlinear Optimization Methods

The disadvantage of direct search algorithms is that they do not necessarily converge to the global minimum. The Linear optimization methods are only capable of solving problems with a linear cost function in the form $V(\theta) = c^T\theta$, but if the mean-squared error is used as the cost function (Eq. (32)), nonlinear optimization methods will need to be used.

Let us reconsider an optimization problem posed as follow:

$$\min_{\theta} V(\theta) \tag{52}$$

Subject to

$$\begin{aligned} g(\theta) &= 0 \\ h(\theta) &\geq 0 \end{aligned} \tag{53}$$

When the objective function $V(\theta)$ does not possess a linear form, i.e. it cannot be expressed with the form $V(\theta) = c^T\theta$, nonlinear optimization methods will need to be used. In the next section, we present the Generalized Reduced Gradient algorithm on which most of the nonlinear optimization solvers are based.

2.4.3.5 Generalized Reduced Gradient Method

The Generalized Reduced Gradient (GRG) method handles optimization problems in which both the objective function and the constraints are nonlinear. The following outlines a summary of the algorithm, for further reference, please refer to (Abadie and Carpentier 1968).

1. The problem starts off with:

$$\max_{x} \; f(x) \tag{54}$$

Subject to:

$$g(x) = 0, A \le X \le B \tag{55}$$

Where $x \in R^N$, and x is bounded by A and B.

All constraints, including inequalities, can be expressed as in equation (55) by introducing non-negative slack variables.

2. With the inclusion of the slack variables, we assume that there exist a solution X^0 and it can be separated into two parts, such that

$$X^0 = \left(x^0, y^0\right) \tag{56}$$

Where $x^0 \in R^n$, $y^0 \in R^m$, with $n = N - m$.

Then the boundaries can be separated as $A = (a, a')$ and $B = (b, b')$ such that $a' < y^0 < b'$ and $(\partial g / \partial y)_{x=x^0} = 0$ is nonsingular.

Then the problem can be restated as:

$$\max \; f(x, y) \tag{57}$$

Subject to

$$g(x, y) = 0\,, \tag{58}$$

$$a \le x \le b\,, \tag{59}$$

$$a' \le y \le y' \tag{60}$$

At the optimal point (x^0, y^0), the Kunh-Tucker conditions (Kuhn & Tucker 1951), as well as the necessary conditions for a solution, state that there exists $u \in R_m$ and $v \in R_n$ (with R_n denoting the dual space to R^n) such that:

$$v_i \begin{cases} \le 0, x_i^0 = a_i \\ \ge 0, x_i^0 = b_i \\ = 0, a_i < x_i^0 < b_i \end{cases}, \tag{61}$$

Then,

$$\frac{\partial f}{\partial x^0} - u\frac{\partial g}{\partial x^0} = v \tag{62}$$

$$\frac{\partial f}{\partial y^0} - u\frac{\partial g}{\partial y^0} = 0 \tag{63}$$

Thus,

$$u = \frac{\partial f}{\partial y^0}\left(\frac{\partial g}{\partial y^0}\right)^{-1} \tag{64}$$

$$v = \frac{\partial f}{\partial x^0} - \frac{\partial f}{\partial y^0}\left(\frac{\partial g}{\partial y^0}\right)^{-1}\frac{\partial g}{\partial x^0} \tag{65}$$

If the computed v satisfies equation (61), then X^0 is a stationary point, i.e. optimal solution. Otherwise, we update x as:

$$h_i \begin{cases} 0, x_i^0 = a_i \ \& \ v_i < 0; or: x_i^0 = b_i \ \& \ v_i > 0 \\ v_i, otherwise \end{cases} \tag{66}$$

Then we define a continuous curve Γ around the neighborhood of (x^0, y^0) by:

$$x = x^0 + \theta h, \theta \geq 0 \tag{67}$$

$$y = y(\theta), y(0) = y^0 \tag{68}$$

$$g(x^0 + \theta h, y(\theta)) = 0 \tag{69}$$

The tangent L to Γ at (x^0, y^0) is then given by:

$$x = x^0 + \theta h, \theta \geq 0 \tag{70}$$

$$y = y^0 + \theta k \tag{71}$$

$$\frac{\partial g}{\partial x^0} h + \frac{\partial g}{\partial y^0} k = 0 \tag{72}$$

The following formula is easily checked:

$$\frac{d}{d\theta} f\left(x^0 + \theta h, y(\theta)\right) = \frac{d}{d\theta} f\left(x^0 + \theta h, y^0 + \theta k\right) = \theta |h|^2 \tag{73}$$

Where $|h| = \sqrt{\sum_i (h_i)^2}$.

3. A value of X , $\tilde{X}' = (x', \tilde{y}')$ will be chosen.

$$\alpha \le x^0 + \theta h \le \beta \tag{74}$$

$$\alpha' \le y^0 + \theta k \le \beta' \tag{75}$$

With $0 \le \theta \le \bar{\theta}$

Determine θ_1 as $\max\ f(x^0 + \theta h, y^0 + \theta k)$ where $0 \le \theta \le \bar{\theta}$ from which $\tilde{X}^1 = (x^1, \tilde{y}^1)$ is computed as

$$x^1 = x^0 + \theta_1 h \tag{76}$$

$$\tilde{y}^1 = y^0 + \theta_1 k \tag{77}$$

Since $\tilde{X}^1$ may not belong to V, we need to deduce a point $X^1 = (x^1, y^1) \in V$ by $g(x^1, y) = 0$.

Using Newton's method (Deuflhard 2004), starting with $\tilde{y}^1$, the current iteration for Newton's method is given by:

$$\Delta y^t = -\left(\frac{\partial g}{\partial y}\right)^{-1} g(x^1, \tilde{y}^t) \tag{78}$$

$$\tilde{y}^{t+1} = \tilde{y}^t + \Delta y^t \tag{79}$$

Where $(\partial g / \partial y)^{-1}$ should be computed at $(x^1, \tilde{y}^t)$.

Assuming convergence of $X^1 \in V \cap P$, there will be two possible ends:

a. $\alpha' \le y^1 \le \beta'$, then repeat on X^1 what has been done on X^0

b. $y_r' = \alpha_r'$ or β_r', then y_r must become x while some x_s becomes y to replace y_r. This implies that a change of basis is required.

4. Newton's method may be unsuccessful in:

    a. Failing to converge;

    b. For some iterate $\tilde{y}^t$, we have $f(x^1, \tilde{y}^t) < f(x^0, y^0)$;

    c. For some iterate $\tilde{y}^{t+1}$, the point $(x^1, \tilde{y}^{t+1})$ is outside the parallelotope P.

    In cases a and b, we reduce θ_1 and repeat the Newton's method. In case c, let $(x^1, \tilde{y}^t) \in P$, then the segment joining $(x^1, \tilde{y}^t)$ to $(x^1, \tilde{y}^{t+1})$ intersects the boundary of P at a point $(x^1, \breve{y}^{t+1})$ such that $\breve{y}_r^{t+1} = \alpha_r'$ or β_r' for some r. Then we make a change of basis and continue with the new splitting.

5. Instead of computing $(\partial g / \partial y)^{-1}$, we can use $\left(\partial g / \partial y^0\right)^{-1}$ as:

$$\left(\frac{\partial g}{\partial y}\right)^{-1} \cong \left(\frac{\partial g}{\partial y^0}\right)^{-1} - \left(\frac{\partial g}{\partial y^0}\right)^{-1}\left(\frac{\partial g}{\partial y} - \frac{\partial g}{\partial y^0}\right)\left(\frac{\partial g}{\partial y^0}\right)^{-1} \tag{80}$$

That is: $\left(\frac{\partial g}{\partial y}\right)^{-1} \cong 2\left(\frac{\partial g}{\partial y^0}\right)^{-1} - \left(\frac{\partial g}{\partial y^0}\right)^{-1}\frac{\partial g}{\partial y}\left(\frac{\partial g}{\partial y^0}\right)^{-1}$

There exist other types of nonlinear optimization methods such as the Branch and Bound method and the Sequential Quadratic Programming (Lazarini & Camargo 2006), but their use are not applicable in this thesis.

2.4.3.6 Selection of Optimization Methods for this Thesis

The cost function presented in this thesis consists of minimizing the mean squared error of the prediction from the model, as given by Eq.(32). The formulation is thus a nonlinear formulation. Therefore only the nonlinear optimization methods, such as the Generalized Reduced Gradient, are applicable in our case.

2.5 Summary

All data acquisition and processing procedures presented in the results chapters were performed in the Matlab environment (Mathworks, Newark, Mass.). The mathematical optimization process was performed in the General Algebraic Modeling System (GAMS, Washington, DC) environment, with its nonlinear optimization toolboxes such as CONOPT and MINOS, which are based on the Generalized Reduced Gradient method (Drud 1985). The results of such optimization methods applied to the VOR identification steps will be presented in chapters 5 and 6.

Chapter 4 presents experimental data to substantiate the presence of dynamic non-linearities in the NI process that supports the VOR. This leads to the need to postulate a new model or realization for the VOR/NI system (Chapter 5), and finally to fitting this model to control and patient VOR data (Chapter 6). Implications in clinical diagnosis of acute lesions and detection of compensated patients follow.

3. Extended Methods

This chapter was put in place to give a more detailed description of the experimental setup and the protocols used in the ocular recordings in this thesis.

3.1 Experimental Data Collection

All ocular recordings were acquired with Electrooculography (EOG). Bilateral horizontal electrodes recording were averaged out to yield conjugate eye recordings. The experimental setup was shown in Figure 7. The electrodes were connected to a pre-amplifier stage to provide high impedance that matches the high impedance on the skin surface. The amplified EOG signals were sent through the slip-rings at the base of the rotary chair and passed through an 8th order Bessel anti-aliasing filter set at 40Hz, which is well above the bandwidth of ocular nystagmus (30Hz). The signals were then downloaded onto an A/D board (National Instrument DI-5024) with a sampling frequency of 500Hz for off-line analysis.

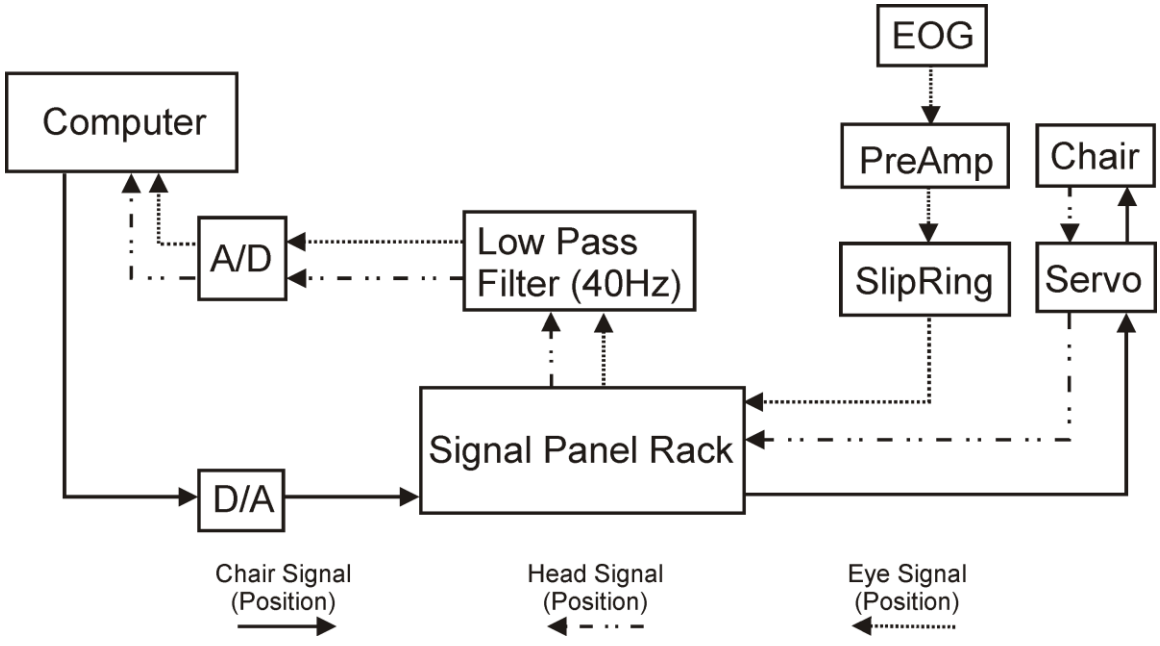

Figure 7: Experimental setup of the rotary chair

Both the gaze holding protocol described in Chapter 4 and the horizontal rotational protocols mentioned in Chapters 4, 5 and 6 are described below:

All human subjects have signed a consent form outlining the recording procedure before the recording sessions (Ethics certificate provided as an appendix). After the surface electrodes were placed on the skin on both sides of each eye, the subject was seated in the dark for 20 minutes for the ocular potential to stabilize to its level in the dark. The subject was then secured on the rotary chair with his/her head restrained with the head rest. The EOG was then calibrated by having the subject fixate flashed targets with known horizontal deviations from the center. The same calibration procedure was carried out at the end of the recording session to ensure the EOG maintaining the same voltage differences with respect to the same set of eye deviations.

The gaze holding protocol was used to measure the gaze shift in space without any head movement in the dark. While performing mental arithmetic, the subject fixates onto a flash target with random deviation from the center projected on the screen in front of the subject. Each flash target would appear for 5 seconds and disappear for 30 seconds. The drift of the subject's eye position was then recorded. To dissociate drifting of the eye position from drifting caused by the change of the EOG baseline, a flash target was occasionally projected at the front center of the subject. The corresponding EOG levels at the 'zero' light was then used to detrend the EOG signal (Figure 8) during data analysis.

For the rotational protocols, the subjects were rotated with a signal that consists of the sum of three sinusoids or with a single sinusoid. It was verified that a stimulating signal consisting of a sum of sinusoids provides more robust system parameter estimates (Smith et al 2005). The sinusoids were chosen at 0.03Hz, 0.1Hz and 0.17Hz, having non-overlapping harmonics to dissociate their nonlinear effects from each other. Furthermore, the bandwidth of the stimulus was chosen in the frequency range that would activate ocular nystagmus in the subjects, yielding output with bandwidth spanning from 0.03Hz up to 20Hz. The bandwidth of the output includes the generally accepted range of the Neural Integrator time constant of 10-15s (pole locating at 0.07Hz-0.1Hz). The input

chair profile from an optical position sensor, and the output eye position were sampled at 500Hz, well above the 40Hz cut-off frequency of the anti-aliasing filter.

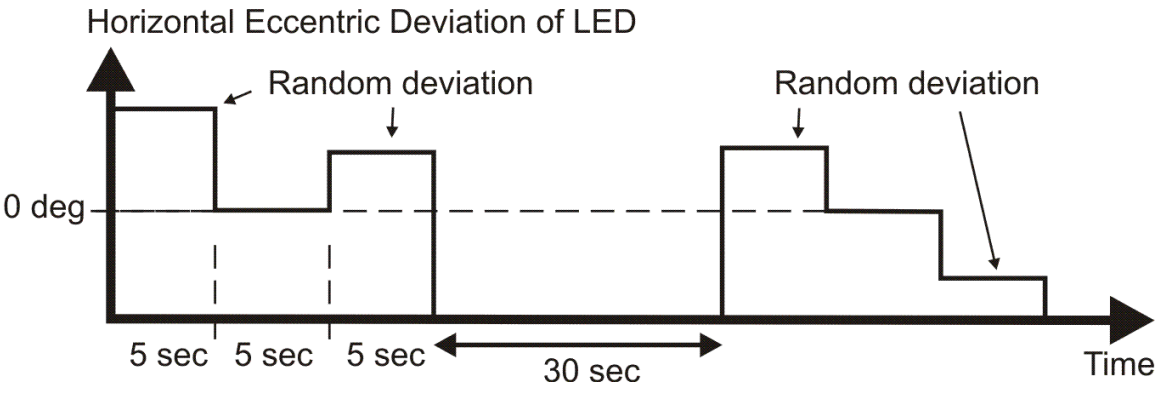

Figure 8: Deviation of the flash target during the stationary protocol

3.2 Signal Processing

This section outlines the steps of offline signal processing on the recorded data before they were used in the analysis procedure.

As mentioned in the previous section, the random flash target during the stationary protocol was occasionally projected right in front of the subject to allow later detrending of any drift of the EOG potential. During the stage of signal processing, a linear interpolation was performed on the EOG potential at the different instances of the 'zero' light presentation. The raw EOG data was then de-trended by this measured shift in null-point, and digitally filtered with an 8^{th} order Bessel filter of 40Hz to minimize noise levels.

As for the chair signal during the rotational protocol, it is also filtered through an 8^{th} order Bessel anti-aliasing filter set at 40Hz.

Since this thesis only performs analysis on slow phase eye movements, a classification method, which was developed by Rey & Galiana (1993) and modified by Radinsky (2004), between fast and slow phase eye movement was used to perform the task. Subsequent analysis of eye recordings was then restricted to those segments flagged as

belonging to fixation intervals or slow phases of nystagmus. To avoid biases introduced by filtering effects near transitions between slow and fast phases, classified slow phase intervals were narrowed at each end by half the filter width used in discrete filtering (see above) before performing any model fits.

3.3 VOR Simulation

In Chapter 5 and 6, simulated VOR data are generated by models consisting of three basic structures: linear, Hammerstein nonlinear and dynamically nonlinear models. The detailed explanation on the corresponding models will be given in chapter 5 & 6, while the block diagrams and the list of parameters of the models used in the simulation are presented in this section. The simulation was carried out with the basic structure given in Figure 4. In detail, the sensory stage and the velocity stage were lumped together into a high-pass filter given by

$$H_{VS}(s) = \frac{T_{VS}\, s}{T_{VS}\, s + 1} \tag{81}$$

And the neural integrator/eye plant compensation stages were modeled by the feedback model given in Figure 3B. Therefore, for the simplest linear VOR model, the following parameters were required in the simulation:

- T_{VS} - time constant corresponding to the sensory/velocity storage stage
- β - gain of the VOR model
- γ - ratio between the gain of the feedback eye position estimate and the output eye positon estimate
- T_{EP} - time constant of the eye plant dynamics

Note that there is no specific time constant corresponding to the neural integrator, instead the mathematical integration is achieved from the effects of the feedback loop, as outlined in section 2.3.

Furthermore, for the nonlinear VOR model with the Hammerstein structure that will be described in chapter 5, a static 3rd order polynomial is placed between the velocity storage stage and the NI/compensator stage, with the following expression:

$$g(k) = p_3 k^3 + p_2 k^2 + k \tag{82}$$

Where k corresponds to the input to the nonlinearity.

For the dynamic nonlinear model that will be proposed in Chapter 5, a symmetric static nonlinearity is placed in the feedforward pathway within the feedback loop, with the form

$$f(i) = \frac{b^2 i}{b^2 + i^2} \tag{83}$$

Where b corresponds to a controlling parameter of the nonlinearity. As for the asymmetric case presented in chapter 6, a third order polynomial was used instead:

$$f(i) = a + i + ci^2 + di^3 \tag{84}$$

3.4 Identification Procedure and Cross Validation

This section outlines the procedure used in the model parameter estimation and validation of the parameter estimates on the data set. All slow phase segments eye position were concatenated into a vector with flags outlining the initial point of each slow phase segment. In the sections requiring the selection of correct model structures from the data sets (Chapter 5 & 6), each data set was divided into two sections of equal length: the first half of the data set was used in the parameter estimation process and the second half was used to cross-validate the estimates by calculating the difference, or residual, between the predicted data from the model parameter estimates and the data set. Once the residual in

the cross-validation is zero-mean and near the EOG noise (±1deg), it is presumed from the central-limit theorem that the associated model form and coefficients is the optimal one for the data, and the MSE was sufficient for the correct model form selection. The AIC was only used if two postulated model forms had similar MSE but different complexity.

Since the basic model structures presented in this thesis were in the continuous time domain and the data were sampled in the discrete time domain, the method of bilinear transform was used to convert the transfer functions between the two domains.

$$s = \frac{2\left(1 - z^{-1}\right)}{T_{samp}\left(1 + z^{-1}\right)} \tag{85}$$

Where s corresponds to the variable in the Laplace domain (continuous-time), z corresponds to the variable in the Z-domain (discrete-time) and T_{samp} corresponds to the sampling rate.

4. Integrator function in the Oculomotor System is Dependent on Sensory Context

W.W.P. Chan and H.L. Galiana

This chapter was used with permission from the **Journal of Neurophysiology** and can be found with the following citation:

W.W.P. Chan and H.L. Galiana **Integrator Function in the Oculomotor System Is Dependent on Sensory Context** *J Neurophysiol* 93(6): 3709-17, 2005.

Abstract

The oculomotor integrator is usually defined by the characteristics of decay in gaze after saccades to flashed targets or after spontaneous gaze shifts in the dark. This property is then presumed fixed and accessed by other ocular reflexes, such as the vestibulo-ocular reflex (VOR) or pursuit, in order to shape motoneural signals. An alternate view of this integrator proposes that it relies on a distributed network, which should change its properties with sensory-motor context. Here we demonstrate in ten normal subjects, that the function of integration can vary in an individual with the imposed test. The value of the time constant for the decay of gaze holding in the dark can be significantly different from the effective integration time constant estimated from VOR responses. Hence analytical tools for the study of dynamics in ocular reflexes must allow for non-ideal and labile integrator function. The mechanisms underlying such labile integration remain to be explored, and may be different in various ocular reflexes (e.g. visual vs vestibular).

Keywords: VOR, oculomotor integrator, gaze holding

4.1 Introduction

The oculomotor system has long been represented as relying on sensory processes which then converge on a shared 'oculomotor integrator'. Many publications have addressed the issue of estimating the time constant of this gaze-holding integrator (T_g), as most recently illustrated in Goldman et al (2002). A common presumption is that this gaze holding capability is a localized (anatomically) process whose function is *invariant* and necessary for the appropriate formation of motoneural drives to the ocular muscles. That is, the oculomotor integrator is presumed to rely on a filtering process with very large time constants (>20 s, Cannon & Robinson, 1987; Mettens et al 1994). This integrator is then presumed to interact with other systems to produce proper reflexes such as the Vestibular Ocular Reflex (VOR). While it is accepted that the VOR can change its dynamics (gain, time constant) with vergence context (Paige et al, 1998), the gaze integrator is always presumed to be fixed and with large time constant unless lesioned (Cannon & Robinson, 1987; Cheron et al 1986; Cheron & Godaux, 1987; Goldman et al, 2002, Mettens et al 1994). In an alternate representation of the oculomotor system and the VOR, Galiana et al have proposed that the process of integration could rely instead on a distributed process (Galiana, 1991; Khojasteh & Galiana, 2003), recently supported by Aksay et al (2003). Because of central non-linearities, the connectivity of this distributed process should change with sensory-motor context, and hence this hypothesis predicts that the oculomotor integrator should have a time constant that is variable with test conditions (dark/light, fixed/free head…). Figure 9 summarizes the different views of central integration in the oculomotor system (see Methods).

Here we report on the first direct test of oculomotor integration performance in normal human subjects. The ocular responses to three conditions are examined: the decay of fixation in the dark to flashed targets at various eccentricities, the responses during slow phases of the VOR to passive harmonic rotation with one sinusoid, or a sum of two uncorrelated sinusoids. The VOR produces compensatory eye movements during the slow phases of induced nystagmus with head perturbations. The reflex pathways are known to converge on an oculomotor integration process, located in the VN-Prepositus

Hypoglossi (PH) complex used by all horizontal ocular reflexes, including the maintenance of gaze direction in the dark after fixation of a flashed target (Cannon et al 1987, Mettens et al 1994, Robinson 1968).In a previous paper (Green & Galiana 1998), we demonstrated that sharing of the integrator would be facilitated by sensory projections on different points on the network. Hence we selected a comparison of integrator function with and without head motion to test the validity of our hypothesis: integration function should vary with recruited sensory pathways. We have already demonstrated in a model study that integrator function could be labile with binocular context (orbital positions) given non-linearities in vestibular neural responses during the VOR (Khojasteh & Galiana 2003b): this suggests a mechanism for the prior observations of Crawford et al (1993), showing that gaze direction decays with different time constants depending on eye eccentricity. Preliminary results supporting labile integration have appeared elsewhere in abstract form (Chan et al, 2004).

4.2 Methods

Data Acquisition

Ten human volunteers with no known vestibular dysfunction participated in the experiment. All subjects signed a consent form, describing the protocol approved by the Institutional Review Board of McGill's Faculty of Medicine. The experimental procedure has been described in detail elsewhere (e.g. see Galiana et al 1995). In brief, to avoid invasive procedures, horizontal conjugate eye movements were measured by Electro-oculography (EOG) with an accuracy of $\pm 1.5^{o}$ estimated in the calibration data. Passive head rotations around a vertical axis were performed en-block using a servo-controlled chair with either a single sinusoid (1/6 Hz, peak 150deg/s) or a sum of two sine waves (0.03Hz and 0.1Hz, peak 120 deg/s). The intent here is to also test for possible changes in reflex dynamics with changes in input bandwidth. EOG and turntable signals were filtered to 40 Hz with an 8-pole Besel filter and stored on a PC at 500Hz for later analysis.

After a 20 min. rest period in the dark to stabilize the EOG electrodes, the recording procedure in the dark included: calibration with a laser target over +/- 50 deg range to quantify any bias and recording sensitivity (^{o}/V), recording of eye movement with rotational stimuli (VOR, no target), recording of self-paced fixations intermingled between flashed targets (gaze, no rotation) and a final re-calibration. Pauses between tests were used to ensure the disappearance of any residual effects from the previous test. The dark-fixation trials were designed with imbedded catch-trials (flashed targets) to control for the well-known drift properties of EOG (Wolfgang 1973). First a horizontal target was presented randomly on a circular screen within 50 deg from the mid-point for 5 s and back to centre for 5 s; and then a new target was *flashed* at another random location and the subject was allowed to perform spontaneous saccades over 60s. This sequence was repeated 4 times, and allowed calibration of the EOG throughout the gaze holding trials, particularly for any changes in zero offset. In our experience, the *amplitude* calibration (volts to saccade *size* in deg) does not change over our trials. Trends in the zero offset during catch trials were used to detrend the EOG gaze holding trials, and did not exceed 5-10^{o} over the whole procedure. (i.e.~0.04^{o}/s over the gaze trials)

Data Analysis

The raw data sampled at 500Hz was first digitally filtered to 20Hz before down-sampling to 100Hz for analysis. Slow phase segments of the eye movements were then selected from records in each test, with a minimum duration of 0.2s to allow for the estimation of large time constants in the presence of noise. The selection was based on the classification routines developed by Galiana & colleagues (Rey et al 1993, Radinsky et al 2004), which propose a simple reduced model for the relationship between stimulus and eye response and accept as slow phase only those segments that are behaving within a range of the model. This often appears as selection based on an eye velocity criteria, but in general allows classification for any stimulus trajectory and robustly rejects low-velocity saccades.

To quantify the dynamics of eye responses, we rely on a global schematic generally accepted in oculomotor control for the conjugate slow phases of the VOR

(Figure 9): angular head velocity ($\dot{H}$) is the stimulus and angular eye position (E) is the response, assuming the eye plant is well-enough described as a simple low-pass filter with time constant T and gain K. In Figure 9A the classical approach uses a first stage typically called 'velocity storage' (VS) (Raphan et al 1985, Robinson 1968) to describe the centrally derived vestibular signal, followed by direct and neural integrator (NI) parallel pathways to compensate for eye plant dynamics – it implies a near-perfect integrator in all eye reflexes. Figure 9B describes an alternative (Galiana 1991, Guitton et al 1990) that achieves the same integration and eye plant compensation with a single feedback loop through a model of the eye plant – here integrator function depends on loop gains through non-linear vestibular cells (VN) (Khojasteh et al 2003a, b). Both approaches can be lumped into equivalent dynamic processes (Figure 9C), where now we also include potential initial conditions on eye position E^o at the beginning of slow phase segments. Algorithms were developed in Matlab to estimate the value of the integrator time constant (T_g in Figure 9C) in each protocol:

1. For gaze holding in the dark: on a stationary chair, the input head velocity in Figure 9 is set to zero and two approaches were compared to evaluate integrator function. The first used a previously published equation (Becker & Klein 1973, Goldman et al.2002), where the integrator time constant can be extracted from the slope of an eye velocity vs eye position plot (Figure 9) with $T_g = -E_p / E_v$, in seconds. The second method relied on a subset of our NARMAX estimation method (Rey & Galiana, 1993; Smith et al. 2002; Kukreja et al, 2005; see Figure 10). In fact, the Rey & Galiana (1993) algorithm is a more general superset of that proposed by Becker and Klein (1973), later re-validated by Goldman et al (2002). The relationship in Figure 9C is mapped into the discrete domain for all pooled slow-phase segments: $E_{n+1} = aE_n \quad or \quad E_{n+1} = aE_n + b$

n {*n=1…N, the number of slow-phase data points*} refers to the sample number in a given slow-phase segment, and b allows for a non-zero null point in some subjects. For sampling interval T_{samp}, $T_g = -T_{samp} / \ln(a)$, in seconds. Since the eye position measurements (E^m) are the real eye position including the residual: $E^m = E + r$, with

assumed white noise ‘r’. As a result, the regression problem in the equations above, in terms of E^m (the data) becomes

$$E^m_{n+1} - r_{n+1} = aE^m_n + (r_{n+1} - ar_n)\text{, or} \qquad E^m_{n+1} = aE^m_n + b + (r_{n+1} - ar_n)$$

This is a linear ARMA problem: after substitution for the noisy eye position observations in the equations, there is a moving-average over the innovations (noise) but no exogenous input (such as head velocity). The estimates are found by extended least squares over all the slow-phase segments and do not require differentiation. Note that both methods are less accurate (larger standard deviations) when the time constants are large and/or when noise increases. As a result, it becomes more and more difficult to numerically resolve changes in the slopes as time constants get large in either method.

2. *For VOR in the dark*: both dynamic processes in Figure 9C must be taken into account. Analysis of VOR data was performed with our ARMAX method with an iterative regression approach to simultaneously estimate the optimal gain and time constant for the VS stage (T_v), and the time constant of the NI stage (T_g). As above, the dynamics of the VOR in Figure 9C can be mapped to the discrete domain with:

$$E_{n+1} = aE_n + b + c\dot{H}'_n$$

where $\dot{H}'_n$ denotes the internal estimate of head velocity from the VS stage into the NI stage, and {*a, b,* and *c}* denote the coefficients for the one step delay of *E*, the bias, and the head velocity input into the regressor, respectively. Again, substituting for the measured data, the regression problem in the VOR becomes:

$$E^m_{n+1} = aE^m_n + b + c\dot{H}'_n + (r_{n+1} - ar_n)\,.$$

This is an ARMAX problem, where the exogenous input $\dot{H}'_n$ must also be determined from the known head velocity profile. We relied on an iterative search where potential T_v over a range from 1 to 50 s were used to generate candidate $\dot{H}'_n$ profiles by simulation

of the VS stage in Figure 9, prior to applying each regression. The regression optimally finds the parameters in each case using all samples and then also estimates the optimal initial condition E^0 for individual slow-phase segments. This last step caused a change in the optimal time constants of no more than 5%, and was only necessary to provide accurate simulations in the selection of VS time constants, especially when T_g is less than a few seconds. The optimal $\{T_v,T_g\}$ pair was selected as the one that generated the best QF in the validation (see below). This algorithm has been extensively tested on simulated data and shown to converge correctly (Smith et al 2002, Kukreja et al. 2005). It has the advantage of being applicable to any head velocity profile.

3. Validation of models and statistical tests: A Simulink (Matlab) model of Figure 9C generated predicted eye position profiles in each VOR protocol, using the parameters estimated from the data, the measured head velocity profile and the optimal initial condition at the beginning of each slow phase (e.g. Figure 11). The quality of fit (QF) for estimated models was calculated from

$$QF = 100\left\{1 - \left[\sum \left(z_{fit} - z_{meas}\right)^2 \Big/ \sum z_{meas}{}^2\right]\right\}\%$$

where z_{fit} is the predicted trajectory (model simulation) and z_{meas} is the measured response. QF served to select the cases that minimized the modeling error with the best {Tv,Tg} combination for VOR tests.

In order to estimate the confidence interval of time constant estimates in both gaze holding and VOR protocols, a t-test was first performed on the regression coefficients (θ). In general, the regression problem can be written as: $Y = R\theta$, where Y is a vector of observations (E_{n+1} above), R is the matrix of input/output observations (regressor *without* initial conditions) that multiplies the vector of desired coefficients (θ of dimension k) (a,b,c.. above) . The regression algorithm provides a solution $\hat{\theta}$ which is used to generate the prediction $\hat{Y} = R\hat{\theta}$. The residual vector, or errors in prediction, is defined as $\varepsilon = Y - \hat{Y}$, with standard deviation $\hat{\sigma}$. From this, we expect the coefficient estimates to

belong to a Normal distribution with mean $\hat{\theta}$, and with confidence intervals defined by the t-statistic for the i^{th} estimate as

$$t = [\hat{\theta}_i - \theta_i] \quad / \quad \hat{\sigma}\sqrt{\frac{N\left|c_{ii}\right|}{N-k-1}}$$

where c_{ii} is the ith diagonal element of $(R'R)^{-1}$, N is the number of data points, and k is the number of estimated coefficients. The confidence interval so computed at the 99% level for each parameter was then converted into the range of associated time constants (T), according to the function postulated in each method {e.g. 1/a or $-T_{samp}/\ln(a)$ }. This approach relies on the fact that the cumulative probability of a coefficient interval must equal the probability of the associated range after a non-linear mapping.

4.3 Results

Gaze holding in the dark: Figure 10 provides a sample of the spontaneous saccades and post-saccadic drift for subject JN48. Like two other subjects, he had a rather small gaze holding time constant in the dark (9.1s). All other subjects had larger time constants reaching even 100s in one case, as would be expected from the classical view of an ideal oculomotor integrator (Figure 12A). Integrator time constants evaluated with either the Goldman or the ARMA method were equivalent (no statistically significant differences, Figure 12B). Despite the presence of noise on the EOG records, the standard deviations for integrator estimates are reasonable and allow statistical tests against the VOR results below.

Integration function in the VOR: Figure 11 illustrates part of the VOR response for subject DC06 during rotation with a sum of sines. Using the time constant estimates from the ARMAX method, the fits for the VOR responses in both eye position and velocity are excellent. The integrator time constants (T_g) in the single sine and sum of sinusoids protocol were found to be respectively 2.6s and 17.4s. Yet, the estimated integrator time constant during gaze holding was much larger for this subject, at T_g=31s for the Goldman method and 33s for the ARMA method (no significant difference,

p<.005). Integrator function during VOR tests is summarized for all subjects in Figure 12A and in Table 1 to Table 4. This was typical for almost all subjects: weaker integration during rotation than during gaze shifts in the dark. A large gaze holding time constant is not necessarily associated with a strong integrator function during rotation tests, when examining estimates for a *given* subject (Figure 12C). Although T_g estimated in the VOR can vary between subjects from 1s to ~20s, the mean across all subjects in the single sinusoid protocol is 4.5s, while the mean for the sum of two sinusoids is 8.2s. This can be compared to the mean for the stationary protocol (gaze holding in the dark) at 31s for the Goldman method and 33s for the ARMA method. Therefore the averages across subjects for the VOR protocols are lower than the generally accepted range for the oculomotor integrator during gaze holding (20-30s). This trend is also observed within the estimates for a *given* subject. The integration time constant during rotation is systematically reduced from that during gaze holding in the dark for almost all subjects (* in Figure 12A, p<0.005). Thus it appears that the functional level of oculomotor integration (T_g) varies with sensory context.

To further support these changes in different protocols, rotational data in the low eye-velocity range ($|\dot{E}|$<15deg/s) were selected to generate T_g estimates at eye speeds comparable to the gaze holding protocol; similarly, integrator estimates from VOR data at these low speeds were compared to those extracted only from high-speed segments ($|\dot{E}|$>25deg/s). Figure 12D illustrates the results in the three scenarios: in the eight subjects that posses a significant change in T_g from stationary protocol to rotational protocol, all but one subject retain the same trend in T_g deficits (decrease) in the VOR, whether eye velocities are small or large. There is a trend for stronger decreases in integrator time constant with larger eye speeds, which will be covered in the Discussion.

4.4 Discussion

Classically, the oculomotor integrator is assumed to be a very effective filter with a large time constant in all ocular reflexes. It was first hypothesized by Robinson as a global concept in order to transform velocity signals from sensors into position signals

for the eye plant. As a result, many analysis procedures to study ocular reflexes rely on this presumption of near-ideal integration in premotor ocular circuits: – for example, eye velocity is assumed to allow unmasking of sensory stimuli, since differentiation of eye position cancels the effect of an ideal central integrator. This study illustrates in 10 normal subjects that the general presumption of ideal integration can be totally unfounded. The results here support a distributed integrator process with very labile properties, which will have significant impact on the analysis of ocular reflex dynamics, for both neuroscientists and clinicians.

The accuracy of estimates: The estimated 'integrator' time constant in our subjects varies in a context-dependent manner. The time constant is significantly larger in the stationary protocols when compared to rotational protocols (Figure 12B). The changes in T_g during rotation tests might be ascribed to inaccurate algorithms which converge on biased values. However, we have tested the ARMAX algorithm extensively with simulations over a broad range of $\{T_v, T_g\}$ combinations, and found it robust and unbiased even in the presence of the noise levels associated with EOG. Furthermore, estimates of dark gaze-holding from the Goldman et al approach are not significantly different from those obtained with the ARMA method (Figure 12D). Though one might be tempted to argue that the ARMAX algorithm for the VOR mistakenly assigned large time constants to the vestibular system and smaller ones to integration, this is not possible: in addition to our prior tests with simulated data, we use the validation of model predictions compared to experimental data to verify the high quality (QF) of fits – if one reverses the time constant estimates, the result is a very poor fit for the VOR data. Hence, the measured changes in the oculomotor integrator with test conditions are not likely due to our analysis algorithms. In fact, there is also an indication of differences in integrator time constants in the article by Goldman et al (2002, their Figure 11) with search coil data, when comparing fixations to VOR, but it was not discussed at that time. The main difference between the Goldman method and the ARMA method described here is that the Goldman method does not include an estimate for the filtered noise term (MA) that is generated by the differentiation process of eye position. This can introduce biased estimates unless the noise level on eye records is extremely low.

Finally, one might argue that the changes in estimated integration could be due to failure of the model used in regression. For example, Goldman et al, in commenting on their estimation technique, add the cautionary note that it should only be applied at low head velocities, to avoid corruption by head velocity signals in a pathway parallel to the integrator. This is because they rely on the characteristics of eye velocity. In our method, we simply assume that the premotor pathways serve to cancel eye-plant dynamics in whatever form they may take (Figure 9C) and so the only restriction for valid estimates is that the model be valid for any head velocity profile- i.e. that the eye plant is well compensated in all conditions, and that the assumption of a linear model (Figure 9C) is valid. First, according to Sylvestre and Cullen (1999), there is no reason to believe major changes are needed in eye plant compensation in these protocols: the r/k ratios in their Figure 14 remain between 100-200ms (dominant time constant for the eye plant) for eye velocities up to and beyond 200 deg/s. Second, our analysis supports changes in the integrator time constant that not only depend on the protocol (e.g. gaze holding vs VOR), but also appear to be sensitive to other variables such as eye speed. This is clearly a non-linear property so that the model in Figure 9C is not sufficient, and some estimates will be biased. However, changes in the 'integrator' time constant must be real given the huge and statistically significant differences observed here, even after restricting eye velocity ranges where a linear model should hold. The results are not likely due to simple model failure.

Mechanisms for labile integration: Changes in T_g with protocols, and even with different subsets in the same protocol, are perfectly compatible with the concept of a distributed oculomotor integrator whose filtering properties will vary with recruitment of feedback or recurrent pathways. Activating vestibular processes in the dark can affect the recruitment level of brainstem loops around the vestibular nuclei, and the operating point of non-linear vestibular cells. In Figure 9B for example, with the assumed shape of the non-linearity, one would expect changes in the gain and time constant of the behavioral VOR with set point due to either sensory level $\dot{H}'$ or eye eccentricity E^* (Khojasteh & Galiana 2003b). This hypothesis has recently been tested successfully by Wu Zhou using acoustic clicks during head rotation (Personal Communication, manuscript submitted

2004). Similarly, a protocol in the light will add a visual loop around the brainstem filter(s) and again change the overall global performance of the 'integrator' process. Since visual signals such as slip also converge on premotor loops, one would expect the effective integration to vary with all sensory contexts and with motor context (vergence/version set-points). More experiments will be required to explore all the factors affecting integration in both normal subjects and patients.

Implications for the estimation of sensory dynamics: Traditional estimates of vestibular time constants from eye velocity trajectories in the VOR can be seriously biased (Galiana, 1991). Unless the integrator is near ideal, the estimated T_v (Figure 9) will actually be an average of the concurrent vestibular and integration function. In the ten subjects studied here for example, the average vestibular time constant T_v was found to be about 35s. This is larger than the traditionally accepted VOR time constants of about 20s, but it is compatible with the expected underestimation of vestibular time constants in the presence of degraded integration (T_g ~5.7s). The argument of biased sensory estimates would hold true for any ocular reflex since the 'integrator' is also shared by the pursuit, optokinetic, saccadic, etc systems. One might be tempted to conclude that the VOR is deficient in subjects with a small integrator time constant during rotation (near 1s in one subject), but this would be false. The global VOR performance at the behavioral level remained perfectly equivalent in all these normal subjects, in terms of the slip levels during slow phases in the dark. It is possible to achieve appropriate reflex dynamics at the behavioral level with different combinations of sensory and integrator dynamics, especially with the help of nystagmus.

In summary, the results here point to a need to fully investigate this phenomenon in a much larger group of both normal subjects and patients. More importantly, we cannot continue to use analytical methods in the study of ocular reflexes that rely on the *assumption* of a near-ideal integrator. More general statistical approaches must be applied to at least allow for the *possibility* of dynamic changes in the integrator with context. The first step will require a model framework that incorporates potential *non-linear* equations

for the integration stage (Figure 9B) in the regression problems, using NARMAX approaches (Kukreja et al 2005).

Grants:

Supported by the Canadian Institutes for Health Research

3.4 References

Aksay E., R. Baker, H.S. Seung, D. Tank, Correlated discharge among cell pairs within the oculomotor horizontal velocity-position integrator, *J. Neurosci. 23(34)*: 10852-10858, 2003.

Becker W., Klein H. M., Accuracy of saccadic eye movements and maintenance of eccentric eye positions in the dark. *Vision Res.* 13: 1021-1034, 1973.

Cannon S. C., Robinson D. A. Loss of the Neural Integrator of the Oculomotor System from Brain Stem Lesions in Monkey. *J Neurophysiol*. 57: 1383-1409, 1987.

Chan W.W.P. , H.L.H. Smith and H.L. Galiana, Gaze holding and implications for the evaluation of VOR dynamics, *14th Annual Meeting on Neural Control of Movement*, Sitges, Spain, March 28-April3, 2004.

Cheron G., Godaux E. Disabling of the oculomotor neural integrator by kainic acid injections in the prepositus-vestibular complex of the cat. *J Physiol.* 394: 267-290, 1987.

Cheron G., Godaux E., Laune J.M., Vanderkelen B. Lesions in the cat prepositus complex: effects on the vestibulo-ocular complex of the cat. *J Physiol.* 372: 75-94, 1986.

Crawford J.D., Vilis T., Modularity and parallel processing in the oculomotor integrator, *Exp. Brain Res. 96*: 443-456, 1993.

Galiana H.L., A nystagmus strategy to linearize the vestibule-ocular reflex, IEEE Trans. Biomed. Eng. 38: 532-543, 1991.

Galiana H.L., H.L. Smith & A. Katsarkas, Comparison of linear vs non-linear methods for analyzing the VOR, Acta Otolaryngol (Stockh) 115: 585-596, 1995.

Goldman M. S., Kaneko C. R. S., Major G., Aksay E., Tank D. W., Seung H. S. Linear Regression of Eye Velocity on Eye Position and Head Velocity Suggests a Common Oculomotor Neural Integrator. *J Neurophysiol.* 88: 659-665, 2002.

Green A., Galiana H.L. Hypothesis for Shared Central Processing of Canal and Otolith Signals. *J Neurophysiol.* Rapid Communication, 2222-2228, 1998.

Guitton D., Munoz D. P., Galiana H.L., Gaze Control in the Cat: Studies and Modeling of the Coupling Between Orienting Eye and Head Movements in Different Behavioral Tasks. *J Neurophysiol.* 64: 509-531, 1990.

Khojasteh E., Modeling Fixation-Distance-Related Modulations in the Vestibulo-Ocular Reflex (VOR), Master Thesis, McGill University, 2003a.

Khojasteh E. & H.L. Galiana, Context-dependence of the binocular VOR; an emerging property of brainstem circuit topology, *Proc. 25th Annual International Conference of the IEEE EMBS*, Cancun Mexico, Sept. 17th-21st , Vol. 2, pp. 1738-1741, 2003b.

Kukreja S., Galiana H.L., Kearney R.E., A Least-Squares Parameter Estimation Algorithm for Switched Hammerstein Systems with applications to the VOR , paper TBME-040-2003, accepted Aug 2004, *IEEE Trans. Biomed. Eng,* in press for March 2005

Mettens P., Godaux E., Cheron G., Galiana H.L. Effect of muscimol microinjections into the prepositus hypoglossi and the medial vestibular nuclei on cat eye movements. *J Neurophysiol*. 72: 785-802, 1994.

Paige G. D., Telford L., Seidman S. H., Barnes G. R. Human Vestibuloocular Reflex and Its Interactions With Vision and Fixation Distance During Linear and Angular Head Movement. *J Neurophysiol.* 80: 2391-2404, 1998.

Radinsky I., Galiana H.L. Improved algorithm for classification of ocular nystagmus, *Proc. 26th Annual International Conference of the IEEE EMBS,* San Francisco USA, Sept. 1-4, 2004.

Raphan T., Cohen B. Velocity storage and the ocular response to multidimensional vestibular stimuli, in Adaptive Mechanisms in Gaze Control – Fasts and Theories, eds. Berthoz and Melvill Jones, Elsevier/New York, 123-143, 1985.

Rey C.G., Galiana H.L. Transient analysis of vestibular nystagmus. *Biol Cybern* 69: 395-405, 1993.

Robinson D.A. Eye movement control in primates. *Science* 161: 1219-1224, 1968.

Schneider E., Glasauer S., Dieterich M. Central processing of human ocular torsion analyzed by galvanic vestibular stimulation. *Neuroreport* 11: 1559-1563, 2000.

Shelhamer M., Robinson D. A., Tan H. S. Context-specific adaptation of the gain of the vestibulo-ocular reflex in humans. *J Vestibular Research* 2: 89-96, 1992.

Smith H. L. H., Chan W. W. P., Galiana H. L. Transient Analysis of Non-Linear VOR Nystagmus – Clinical Implications. *Proc. 24th Annual International Conference of the IEEE EMBS*, Houston Texas, 2002, Vol. 3, pp. 2137-2138.

Sylvestre P.A., Cullen K.E., Quantitative Analysis of Abducens Neuron Discharge Dynamics During Saccadic and Slow Eye Movements, *J. Neurophysiol. 82*: 2612-2632, 1999.

Table 1: Goldman Method: Gaze Holding Time Constant in the dark

99% Confidence Interval						
Subject Code	Estimated variance of residual (σ^2)	θ (-1/T)	C_{ii}	T min	T	T max
nv67	1.2128	-0.11312	2.54E-5	7.85	8.84	10.12
dc06	0.28635	-0.03208	5.91E-6	28.22	31.17	34.80
nv20	7.3576	-0.07106	3.74E-7	13.27	14.07	14.97
mr41	0.076603	-0.00804	9.59E-6	97.60	124.42	171.54
mr81	1.0538	-0.01926	6.92E-6	38.15	51.93	81.30
mr82	1.1341	-0.19246	7.70E-5	4.62	5.20	5.94
mr83	0.80772	-0.09626	6.08E-5	8.75	10.39	12.79
jn08	3.1819	-0.01173	7.34E-7	63.81	85.22	128.27
jn48	13.042	-0.12769	3.19E-7	7.52	7.83	8.17
jl61	5.3567	-0.04307	2.10E-7	21.84	23.22	24.79

Table 2: ARMA Method: Gaze Holding Time Constant in the dark

99% Confidence Interval						
Subject Code	Estimated variance of residual (σ^2)	Θ exp(-Tsamp/T)	C_{ii}	T min (sec)	T (sec)	T max (sec)
nv67	6.41E-6	0.99945	2.07E-9	17.70	18.18	18.68
dc06	2.19E-5	0.9997	5.63E-9	28.97	33.33	39.24
nv20	0.000401	0.9993	2.49E-10	13.50	14.28	15.17
mr41	1.65E-6	0.9999	8.73E-8	86.59	100	118.31
mr81	1.05E-5	0.99985	6.89E-9	54.16	66.67	86.67
mr82	6.04E-6	0.99925	3.23E-8	12.39	13.33	14.43
mr83	9.88E-6	0.999	6.03E-8	9.09	10.00	11.10
jn08	2.55E-5	0.99985	7.78E-10	59.48	66.67	75.83
jn48	7.72E-5	0.9989	3.17E-10	8.93	9.09	9.26
jl61	5.18E-5	0.99955	2.08E-10	21.58	22.22	22.90

Table 3: ARMAX Method: Integrator time constant, Head rotation at 0.167Hz

99% Confidence Interval						
Subject Code	Estimated variance of residual (σ^2)	Θ exp(-Tsamp/T)	C_{ii}	T min (sec)	T (sec)	T max (sec)
nv67	1.1867	0.998812	1.63E-9	5.69	8.40	16.08
dc06	0.57402	0.996206	1.50E-8	2.00	2.63	3.84
nv20	1.6926	0.985775	6.63E-9	0.637	0.698	0.772
mr41	0.72036	0.999459	9.17E-10	11.46	18.47	47.50
mr81	1.5134	0.993685	5.82E-9	1.33	1.58	1.95
mr82	1.0404	0.997239	2.15E-8	2.13	3.62	11.95
mr83	1.1086	0.994994	2.11E-9	1.77	1.99	2.28
jn08	0.072248	0.997396	1.15E-7	2.64	3.84	6.98
jn48	0.18896	0.993567	6.64E-8	1.27	1.55	2.00
jl61	0.096324	0.995893	7.17E-8	1.93	2.43	3.29

Table 4: ARMAX Method: Integrator time constant, Head rotation with sum of sinusoids at 0.03Hz and 0.1Hz

99% Confidence Interval						
Subject Code	Estimated variance of residual (σ^2)	Θ exp(-Tsamp/T)	C_{ii}	T min (sec)	T (sec)	T max (sec)
nv67	0.006527	0.999427	9.78E-9	14.79	17.45	21.27
dc06	0.00605	0.99881	6.46E-8	1.61	1.68	1.76
nv20	0.004914	0.994452	3.73E-8	1.74	1.80	1.86
mr41	0.007112	0.996725	2.64E-8	2.89	3.05	3.22
mr81	0.014481	0.997623	6.53E-8	3.60	4.20	5.04
mr82	0.024783	0.998708	6.08E-9	6.89	7.74	8.81
mr83	0.031865	0.997556	1.18E-7	3.09	4.09	6.04
jn08	0.00299	0.999436	4.77E-8	13.92	17.71	24.34
jn48	0.006658	0.996265	2.81E-7	2.33	2.67	3.14
jl61	0.003386	0.998434	2.60E-8	5.92	6.38	6.91

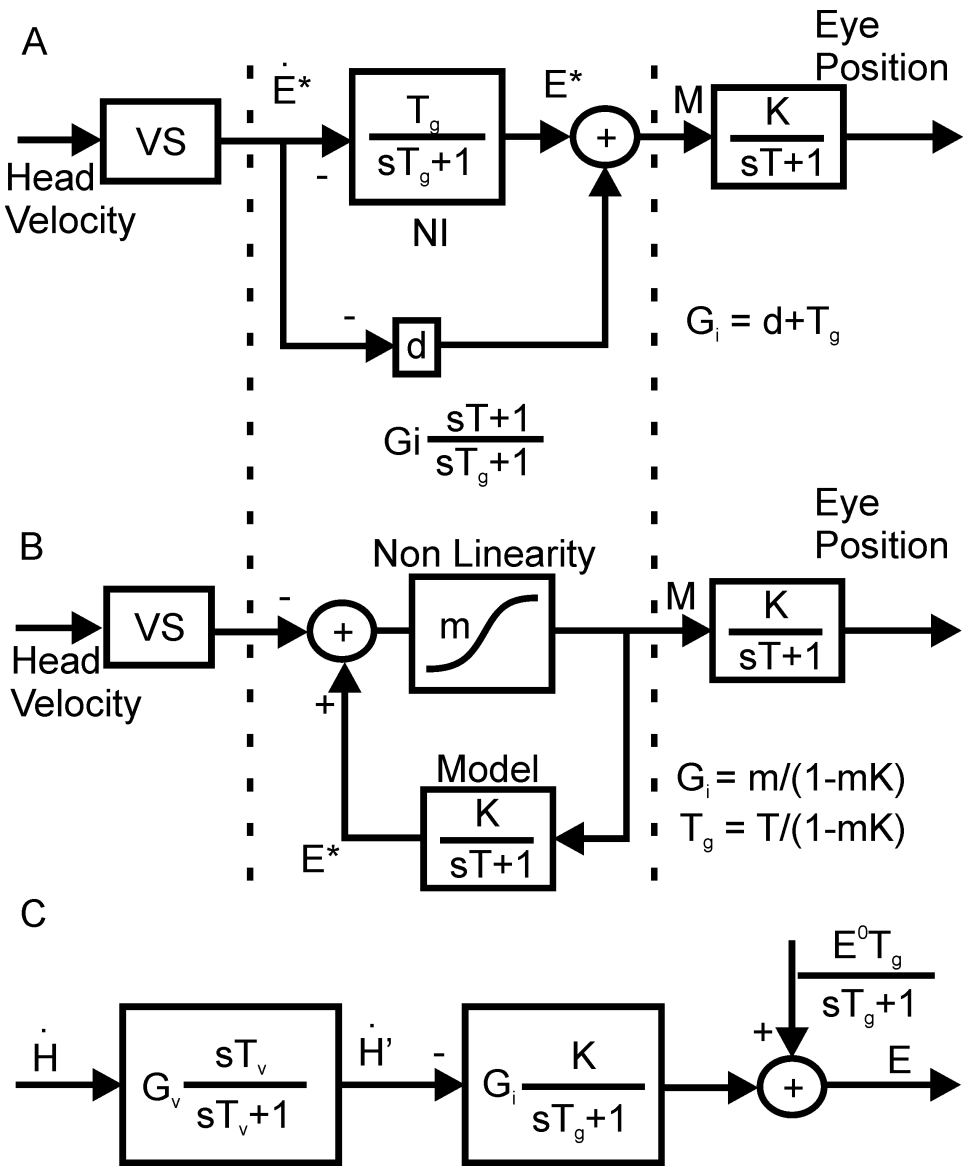

Figure 9: Block diagram representations of the VOR (input head velocity $\dot{H}$ and response eye position (E)) using velocity storage (VS) cascaded with a central integrator (NI). A) **Classical approach with parallel pathways through a near-ideal integrator (large T_g) to compensate for eye plant dynamics,** B) **Integrator is distributed in a feedback system that simultaneously compensates for eye plant dynamics, and the premotor cell has a non-linear sensitivity 'm'. Both approaches provide an equivalent mid-stage transfer function $G_i(Ts+1)/(T_gs+1)$ before projecting to the eye plant, here a simple low-pass filter with time constant T.** C) **Merging the last two stages, the two approaches are equivalent to a 2-stage cascade with VS =** $G_v(sT_v)/(sT_v+1)$**, a high-pass system with high-frequency gain of G_v and an integrator stage $G_iK/(sT_g+1)$. The initial condition**

contribution on a slow phase segment can be described by $E^0 T_g \left/ \left(sT_g + 1 \right) \right.$ **, a decaying exponential in time. In form** A: $G_i = d + T_g$ **, and** T_g **is presumed fixed; In form** B: $G_i = m/(1 - mK)$ **and** $T_g = T/(1 - mK)$ **, where** ***m*** **varies with set point. The simpler form in** C) **is used in the data analysis, to estimate global VS and 'integrator' time constants from experimental data, and to simulate predicted trajectories.**

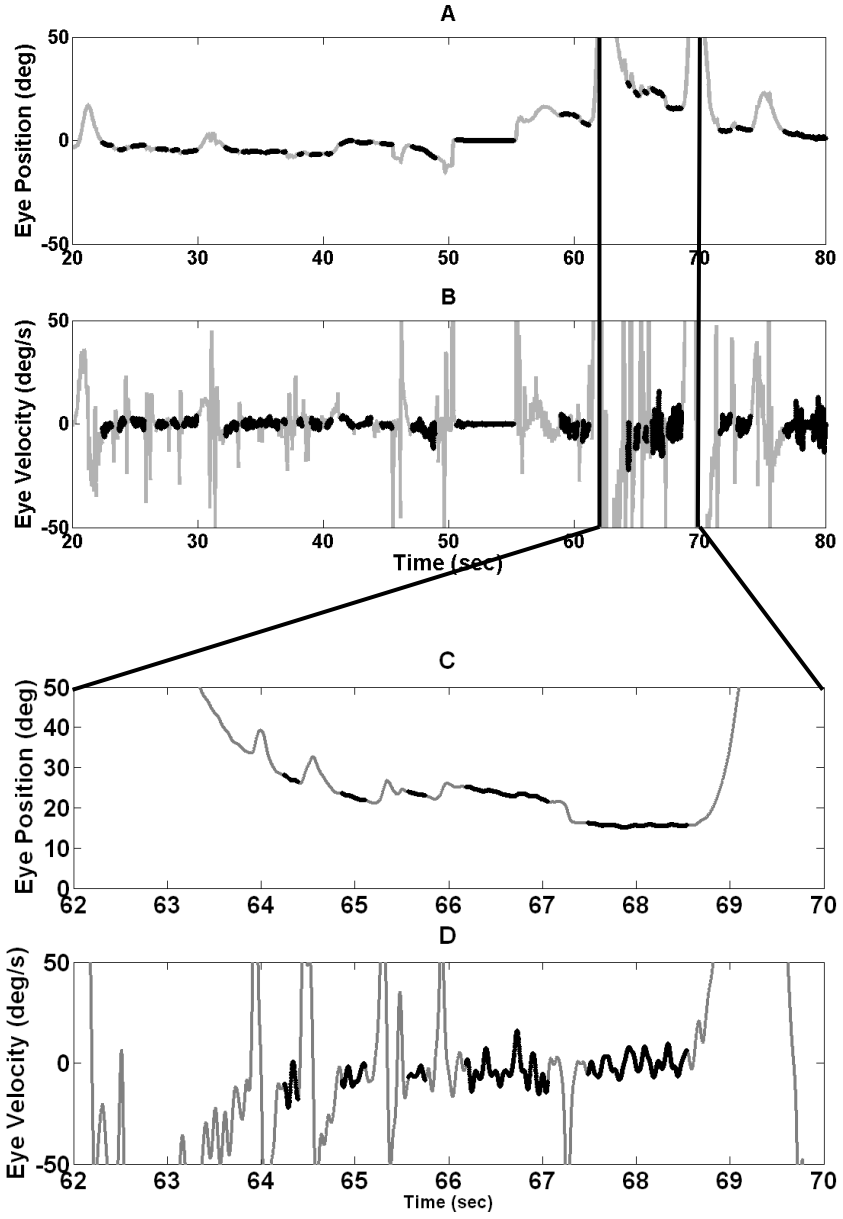

Figure 10: Eye position (A) **and eye velocity** (B) **of JN48 in an extract of gaze holding tests. C and D zoom in on a shorter time interval in eye position and eye velocity, respectively. Subject JN48 with estimated T_g=7.8s (99% confidence interval 7.5 s – 8.2 s) with the Goldman method vs. T_g= 9.09s (99% confidence interval 9.07s - 9.11s) with the ARMA method (see Methods). There is no statistically significant difference between these estimates (p<0.01) but the ARMA method has a much smaller confidence interval (more robust).**

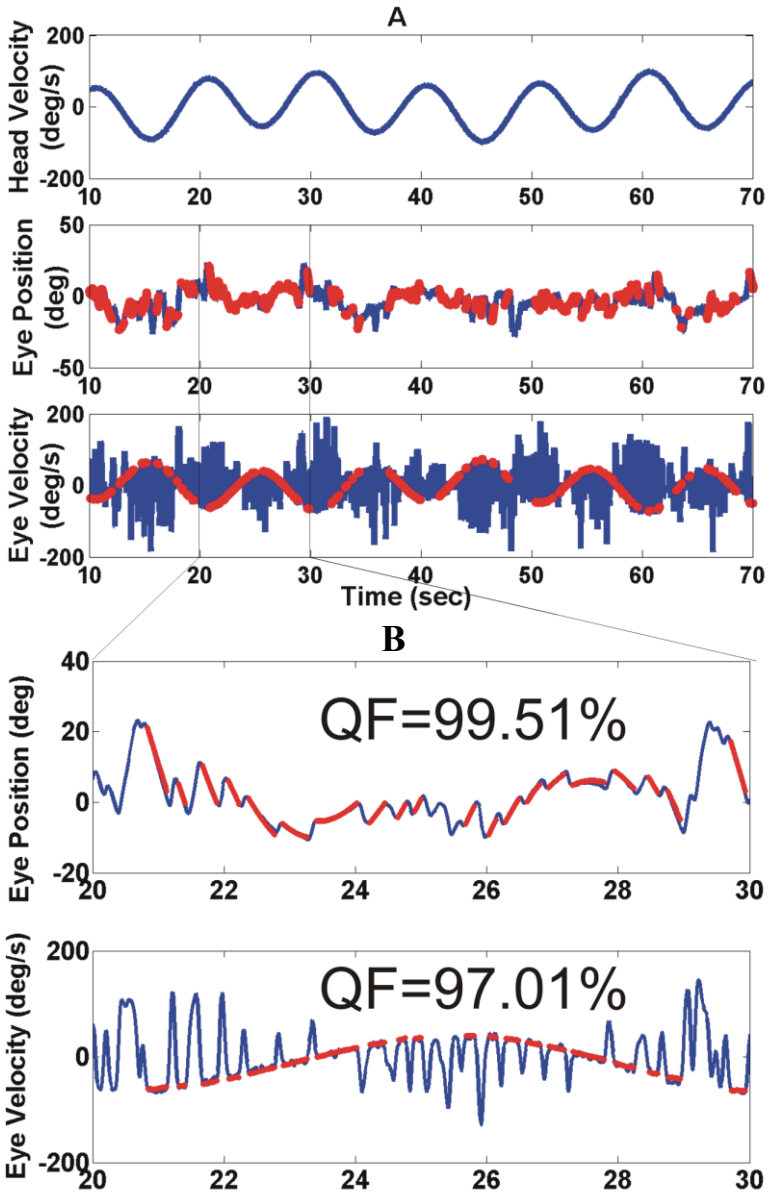

Figure 11: Passive VOR in the dark for Subject DC06. A - Head velocity, eye position and eye velocity for a rotation protocol with a sum of two sinusoids (± 20 deg/s at 0.03Hz and ± 80 deg/s at 0.1Hz) (blue) and predicted slow phase segments (red). B – Zooms in on a time section. Using ARMAX, the time constants for gaze holding and vestibular processes were found to be: T_g = 7.7s, T_v =40s; compare to the T_g of ~30s in gaze holding. The associated predicted (model) eye responses are provided superimposed, with associated QF of 99.5% (position) and 97% (velocity).

A) Oculomotor Integration Time Constants with different stimuli (99% Confidence Interval)

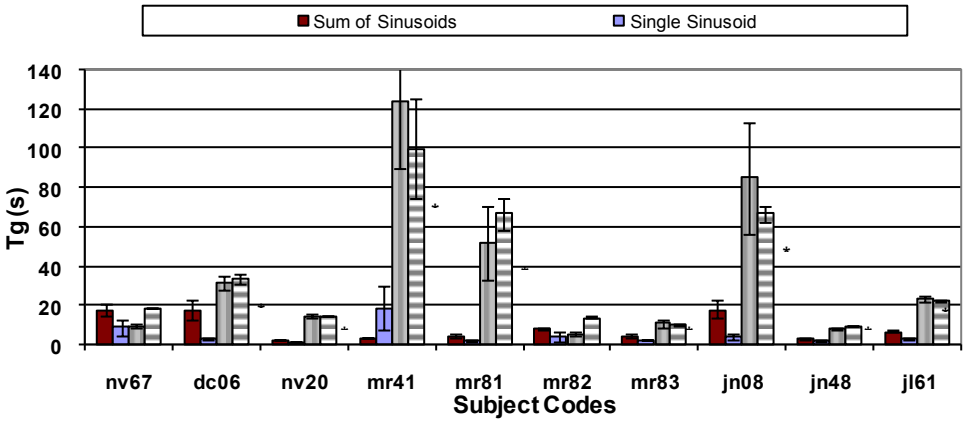

B) Stationary Tg in the dark estimated with two methods

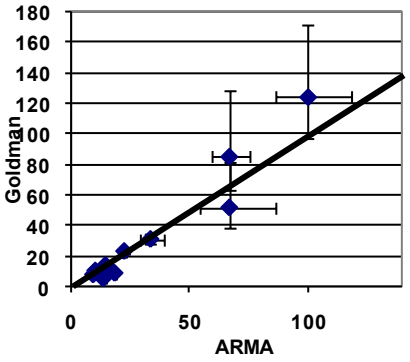

C) Rotational Tg (ARMAX) Vs Stationary Tg (ARMA)

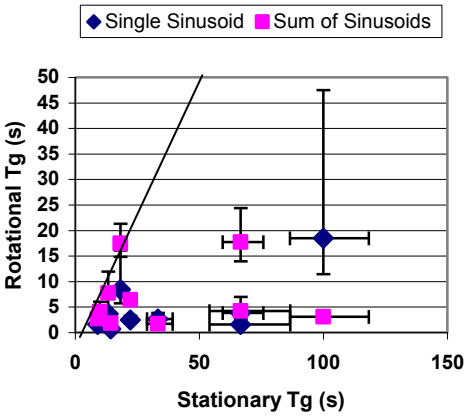

D) Oculomotor Integration Time Constants from Stationary and Sum of Sinusoids Protocol

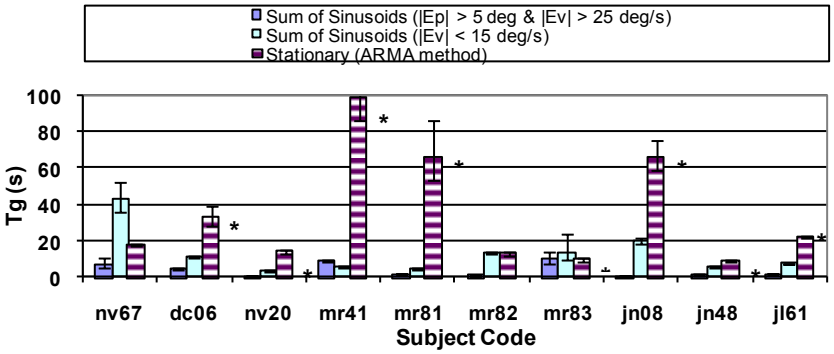

Figure 12: Estimates of 'integrator' time constants, with bars for the 99% confidence intervals on each estimate. A) **Bar Chart of 'Integrator' Time Constants from 10 normal subjects, including 2 methods for the estimation during gaze holding in the dark; * marks subjects where gaze holding integration is significantly different from that estimated during *both* rotation tests ($p<0.005$); B) Plot of gaze holding time constants in the dark, relating estimates from Goldman et al method (2002) to our ARMA method (Kukreja et al 2005). Note that there is a near one-to-one relationship between the estimates with no statistically significant difference. As expected, estimate uncertainty increases with larger time constants.** C) **Plot of time constant (T_g) of the oculomotor integrator during rotations versus that estimated during gaze holding, using the ARMA(X) method in all cases. Except for a clear reduction during rotation there is no evident relationship between the estimates. The line represents the unit slope expected if there were no change.** D) **Bar Chart of 'Integrator' Time Constants from the same 10 subjects, when the VOR data are segregated into two groups of low or high velocity (see text). The trend of decreasing 'integrator' time constants is still observed from stationary protocol to rotatory protocol.**

The previous chapter demonstrates the variability of the neural integrator time constant with respect to the set-points of the head velocity and eye position. To accommodate for the change in the apparent dynamics of the Neural Integrator, we propose a nonlinear component in the Neural Integrator model to modify it into a 'dynamically' nonlinear model. The next paper presents the derivation of such a model. Furthermore, the method of optimization is used to calculate estimates of the model parameters since the Extended Least Squared based method is inadequate in performing such a task.

5. Modeling the Non-Linear Context Dependency of the Neural Integrator in the Vestibulo-Ocular Reflex

Wilbur W. P. Chan, Henrietta L. Galiana

This chapter was re-used with permission from the **IEEE Transaction on Biomedical Engineering** and can be found with the following citation:

W.W.P. Chan, H.L. Galiana. **Modeling the nonlinear context dependency of the neural integrator in the vestibuloocular reflex**. *IEEE Trans Biomed Eng* 55(8): 1946-55, 2008.

Abstract - A Neural Integrator (NI) is presumed to exist in the oculomotor system to assist in numerous tasks such as maintaining gaze on imaginary targets in the dark. It is shared by all ocular reflexes including the Vestibulo-Ocular Reflex (VOR). It has been widely accepted that the NI acts as a `perfect' integrator even in the dark with time constants as large as 50s. However, the NI time constant is often less than ideal and its value can also be dependent on context (Chan and Galiana 2005). In this paper, a nonlinear feedback model is postulated to model the context-dependent properties of the NI. Algorithms are first developed and validated to fit both linear and nonlinear NI models to experimental data in the presence of ocular nystagmus. Preliminary results indicate that even normal subjects can have a nonlinear VOR and NI.

Keywords - Motor systems (biological), Neural Integrator, Vestibulo-Ocular Reflex.

5.1 Introduction

An internal estimate of eye position is required to perform tasks such as gaze fixation on remembered targets in the dark, and is presumed to reflect the holding properties of a central neural integrator (NI) with a large time constant. In addition, during rotations about a vertical axis, the horizontal vestibulo-ocular reflex (VOR) only receives signals related to angular head velocity during natural movements sensed by the semicircular canals. Yet during the slow compensatory phases of vestibular nystagmus, the eyes (low-pass filters of neural drive) follow a trajectory opposite to head position, rather than being related to head velocity (Robinson 1975). Hence the function of a neural integrator (NI) is also required in the VOR system to process head velocity signals into appropriate motor commands to the eyes. It is generally accepted that this network is shared during all eye movements (Guitton, Munoz and Galiana 1990) with near ideal performance that can be impaired by lesions, for example, to the region of the medial vestibular and Prepositus hypoglossi nuclei (Cannon and Robinson 1987) (Mettens, et al. 1994). The exponential decay of eye position during attempted fixation in the dark is typically used to describe the NI performance under the presumption that this value is invariant in all reflexes. However, the time constant of this decay was recently shown to be less than `perfect' and to depend on context (Chan and Galiana 2005): the ‘apparent' NI time constant was found to be larger when the eye position is close to zero (straight ahead relative to the head), while larger eye deviations lead to a lower `apparent' time constant. Furthermore, it is known that firing activities from premotor cells in the Vestibular Nuclei (VN) modulate with both head velocity and eye position (McConville, Tomlinson and Na 1996). These characteristics are the basis of a new model that can account for the context dependent nature of the `apparent' time constant of the NI and the presence of head velocity and eye position signals in the VN. The remaining sections of this paper are organized as follows: Section II presents the model used to describe the context dependent nature of the ‘apparent' time constant. Section III compares the performance of the nonlinear feedback model against a linear feedback model. Section IV presents the conclusions.

5.2 Methodology

In all the realizations presented below, the structures are first presented in the Laplace domain, and then mapped to the discrete domain using the Bilinear transform. The intent is to develop alternative representations that can be fitted to sampled experimental data using optimization techniques that minimize the mean-squared error of the fit. The models are fitted only to slow-phase segments of the VOR, assuming a time-invariant transfer function with respect to the controlled input (head velocity). However, because of the switched nature of nystagmus (Figure 13), and the short duration of slow-phase segments, it is also necessary to find optimal initial conditions for each segment, while searching for a shared global transfer function (details below).

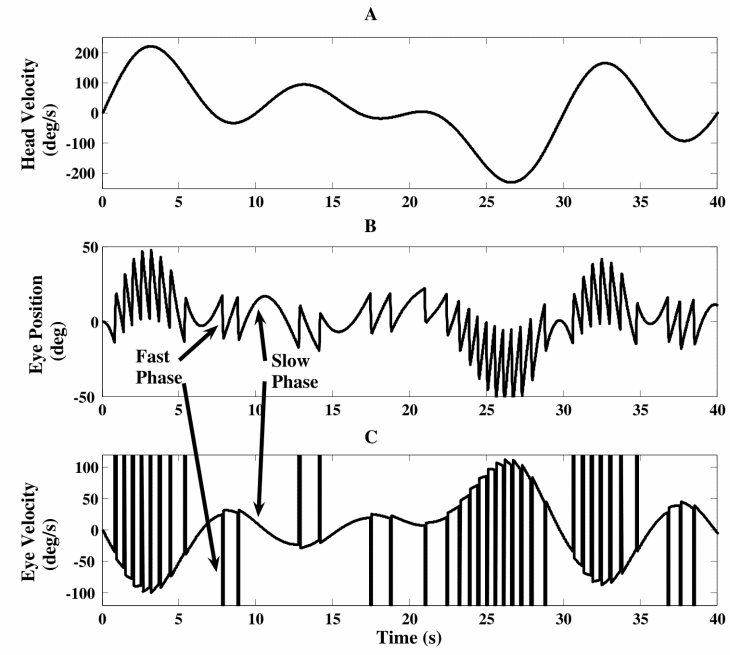

Figure 13: A simulation of the passive Vestibulo-Ocular Reflex (VOR) responses in the dark. Arrows denote segments of fast and slow phases in eye position (B) and eye velocity (C) when subjected to head rotation (A).

5.2.1 Possible Formulations for the NI Network

5.2.1.1 Formulation of the Linear Model

The Neural Integrator (NI) is classically modeled as a linear low-pass filter (Cannon and Robinson 1987). Two realizations of the linear model will be presented in this section: a feedforward model developed by Robinson (Robinson 1975) (Figure 14A) and a feedback model (see Appendix of Guitton et. al. (Guitton, Munoz and Galiana 1990)}, Figure 14B). The eyeplant dynamics D(s), and the internal estimate of eyeplant dynamics D*(s) for the feedback case (Figure 14B), are approximated by first order low pass filters (Robinson 1981).

$$D(s) = \frac{G}{Ts + 1}; D^*(s) = \frac{A}{Ts + 1} \tag{86}$$

where T denotes the eyeplant time constant, G denotes the gain of the eyeplant while A denotes the gain of the internal eyeplant model.

Experimentally, neural signals in the Vestibular Nuclei (VN) and the Prepositus Hypoglossi (PH) have been reported to be correlated with eye position (Robinson 1981) (Angelaki, Green and Dickman 2001) (Gonzalez-Forero, et al. 2003). In the model realizations, this is represented by e* (Figure 14). The realizations of the function for the linear NI process (parts A and B) are equivalent. For example, in form A after substitution of (Eq.(86)),

$$\begin{aligned}
\frac{E(s)}{\dot{H}(s)} &= \frac{-\beta G}{Ts + 1}\left(b + \frac{a}{T's + 1}\right) \\
&= \frac{-\beta G}{Ts + 1}\left(\frac{bT's + b + a}{T's + 1}\right) \\
&= \frac{-\beta G}{Ts + 1}\left[\frac{1}{b + a}\left(\frac{bT's}{b + a} + 1\right)\right]\left(\frac{1}{T's + 1}\right) \\
&\equiv \frac{G'}{T's + 1}
\end{aligned} \tag{87}$$

Where b and a are chosen such that we achieve a large time constant and cancellation of eye plant dynamics, i.e.

$$G' = -\frac{\beta G}{b+a}; T' = \frac{T(b+a)}{b} \tag{88}$$

E(s) denotes the eye position in the s-domain, $\dot{H}(s)$ is the canal filtered head velocity, β is the gain acting on the input head velocity before the summing junction, a is the gain in the NI path, b is the feedforward gain, and T' is the feedforward model's NI time constant (i.e. the time constant of decay of ocular initial conditions).

Similarly, in Figure 14B, the overall transfer function after substitution of (Eq. (86)) is given by

$$\frac{E(s)}{\dot{H}(s)} = -\frac{-\beta G}{Ts + 1 - A} \equiv \frac{G'}{T's + 1} \tag{89}$$

Where

$$G' = -\frac{\beta G}{1 - A}; T' = \frac{T}{1 - A} \tag{90}$$

Both forms provide an internal estimate of eye position (for example in form B, e*= (A/G) e) and both forms provide cancelation of eye plant dynamics. Since they are equivalent, we focus only on algorithm implementation with form B, which provides a better platform for inclusion of potential nonlinearities, besides including premotor cells with mixed sensory-motor signals.

By using the Bilinear Transformation on (Eq. (90)) and a sampling interval τ, the eye position for the linear NI model in the discrete domain then becomes

$$e_n = \xi_1 e_{n-1} + \xi_2 \left(\dot{h}_n + \dot{h}_{n-1}\right) \tag{91}$$

with the following substitutions:

$$\xi_1 = \frac{2T' - \tau}{2T' + \tau}; \xi_2 = \frac{G'\tau}{2T' + \tau} \tag{92}$$

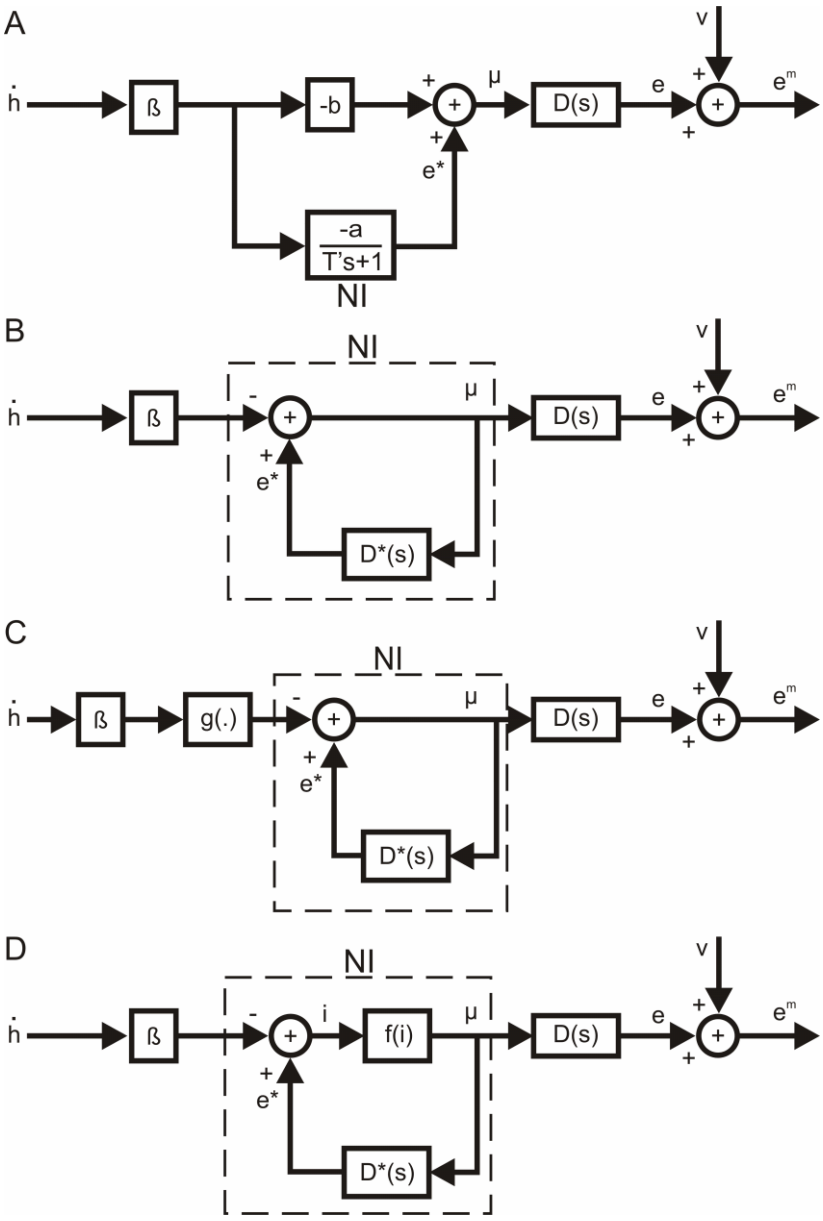

Figure 14: Block diagram of alternate Neural Integrator (NI) models: A) The feedforward linear model, B) feedback linear model, C) Hammerstein model, D) Dynamic Nonlinear model. h(dot) denotes the head velocity from the canal, e^m as the measured eye position, v the added noise, e the true eye position; β the gain before any NI block, D(s) the eyeplant dynamics and D*(s) the internal eyeplant model dynamics.

Thus the analog coefficients can be recovered from

$$G' = -\frac{2\xi_2}{\xi_1 - A}; T' = \frac{\tau(\xi_1 + 1)}{2(\xi_1 - 1)} \tag{93}$$

From this formulation, we can perform the optimization with respect to the coefficients ξ_1 and ξ_2. Constraints to the parameter search include stable dynamics and appropriate reflex direction in simulations and human subjects: Thus G'<0, T'>0. Therefore ξ_1 has to be between 0 and 1 and ξ_2 has to be negative.

An appropriate objective function for the linear model is:

$$\min_{\xi_1, \xi_2} \sum_{n \in N_1} \left\| \varepsilon(\xi_1, \xi_2) \right\|^2 \tag{94}$$

subject to $0 < \xi_1 < 1$ and $\xi_2 < 0$. N_1 denotes the slow phase eye velocity in the data set, and

$$\varepsilon(\xi_1, \xi_2) \equiv e_n^m - e_n \tag{95}$$

with e^m_n denoting the measured (noisy) eye position.

5.2.2.2 Formulation of the Hammerstein Model

The static nonlinear model is formulated as a Hammerstein model by adding a nonlinearity g(.) before the linear NI process that would represent sensory properties (Figure 14C). The eyeplant dynamics D(s) and D*(s) are the same. Since a cubic is sufficient to represent the asymmetric behavior seen in patients (Galiana, Smith and Katsarkas 1995), g(.) can be represented by a third order polynomial:

$$g(k) = p_3 k^3 + p_2 k^2 + k \tag{96}$$

The nonlinearity is located in front of the feedback loop, so the apparent time constant of the model remains constant. By substituting this nonlinearity in the numerator of (Eq. (90)), and converting to the discrete domain

$$e_n = \phi_1 e_{n-1} + \phi_2 \left(\dot{h}^3{}_n + \dot{h}^3{}_{n-1} \right) + \phi_3 \left(\dot{h}^2{}_n + \dot{h}^2{}_{n-1} \right) + \phi_4 \left(\dot{h}_n + \dot{h}_{n-1} \right) \qquad (97)$$

Where

$$\begin{aligned} \phi_1 &= \frac{2T' - \tau}{2T' + \tau}; \phi_2 = \frac{p_3 G' \tau}{2T' + \tau} \\ \phi_3 &= \frac{p_2 G' \tau}{2T' + \tau}; \phi_4 = \frac{G' \tau}{2T' + \tau} \end{aligned} \qquad (98)$$

The constraints on G' and T' are the same as in the linear model (Eq. (91)). Thus the constraints on φ_1 and φ_4 are the same as those on ξ_1 and ξ_2; there are no constraints on φ_2 and φ_3. The objective function for the Hammerstein model becomes

$$\min_{\phi_1, \phi_2, \phi_3, \phi_4} \sum_{n \in N_1} \left\| \varepsilon \left(\phi_1, \phi_2, \phi_3, \phi_4 \right) \right\|^2 \qquad (99)$$

subject to $0 < \varphi_1 < 1$ and $\varphi_4 < 0$, and

$$\varepsilon \left(\phi_1, \phi_2, \phi_3, \phi_4 \right) \equiv e_n^m - e_n \qquad (100)$$

5.2.2.3 Formulation of the Dynamic Nonlinear Model

To accommodate possible changes in the NI time constant at different eye positions, a nonlinear feedback model is proposed as an alternative to describe the NI characteristics (Figure 14D). We place a nonlinearity on the feed-forward pathway in the loop to yield an `apparent' time constant that is context dependent. Note that the input to the nonlinearity is the difference between eye position and head velocity multiplied by scale factors to represent signals combined in the VN (variable i in Figure 14D). We select a nonlinear curve that disassociates peak gain from nonlinear range to minimize free

parameters while preserving the well known nonlinear characteristics of neural cells whose firing rate sensitivity often varies with set point (Idoux, et al. 2006). An example is the 'Versiera' curve (Shikin 1995):

$$f(i) = \frac{b^2 i}{b^2 + i^2} \tag{101}$$

where f(.) and i respectively denote the output and input of the nonlinearity, and b controls the width of the pass-band in Figure 14E. The eyeplant dynamics D(s) and D*(s) in (Eq. (86)) become in sampled domain:

$$\begin{aligned} D(z) &= \frac{G\tau\left(1 + z^{-1}\right)}{(\tau - 2T)z^{-1} + (2T + \tau)} \\ D^*(z) &= \frac{A\tau\left(1 + z^{-1}\right)}{(\tau - 2T)z^{-1} + (2T + \tau)} \end{aligned} \tag{102}$$

The discrete nonlinear model, with its states at instance n, is then defined by:

$$\begin{aligned} i_n &= e^*_n - \beta \dot{h}'_n \\ \mu_n &= \frac{b^2 i_n}{b^2 + i_n^2} \\ e^*_n &= \frac{2T - \tau}{2T + \tau} e^*_{n-1} + \frac{A\tau}{2T + \tau}(\mu_n + \mu_{n-1}) \\ e_n &= \frac{2T - \tau}{2T + \tau} e_{n-1} + \frac{G\tau}{2T + \tau}(\mu_n + \mu_{n-1}) \end{aligned} \tag{103}$$

To relate input to output with minimal degrees of freedom, we combine the above equations to obtain:

$$e_n = \frac{2T - \tau}{2T + \tau} e_{n-1} + \frac{\alpha K^2 \tau}{2T + \tau}\left(\frac{\gamma e_n - \dot{h}_n}{K^2 + \left(\gamma e_n - \dot{h}_n\right)^2} + \frac{\gamma e_{n-1} - \dot{h}_{n-1}}{K^2 + \left(\gamma e_{n-1} - \dot{h}_{n-1}\right)^2} \right) \tag{104}$$

where $\alpha = G\beta$, $K = b/\beta$ and $\gamma = A/(G\beta)$.

Thus we are down to four free parameters, α, K, γ and T, to describe the nonlinear NI process. As a general guide, α can be interpreted as the gain controlling parameter, K as the parameter controlling the belt (or the roll-off) of the nonlinear curve, γ as the parameter for the feedback gain, and T the dynamics for the eyeplant time constant. Denoting r as the instantaneous gain of f(i)/i, this determines the set-point in a small-signal model of the system, where the apparent overall gain and local time constant are given by:

$$T_{NI} = \frac{T}{1 - r\alpha\gamma} > 0; G_{VOR} = \frac{T_{\alpha}}{1 - r\alpha\gamma} \tag{105}$$

Which restricts r > (1-T)/αγ.

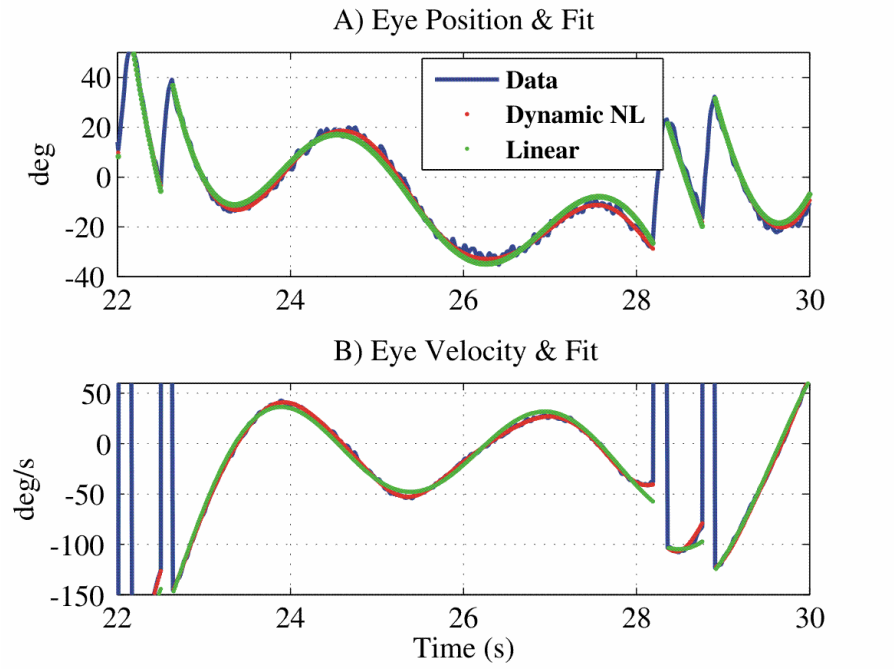

Figure 15: Example of model predictions from a linear fit (Figure 14B) and dynamic nonlinear fit (Figure 14D) to noisy simulated data of the nonlinear family (Data set 3 (Table 7)). The linear predictions (green curves, MSE=4.74, AIC=9754) are worse than the correct nonlinear model structure (red curves, MSE=1.89,AIC=3903), as expected (see Table 7)

In other words, with α, γ > 0, 0 < T < 1. This time constant restriction is consistent with reported experimental results on eye plant dynamics (T< 200 ms) (Robinson 1981). Given the original analog system, all the parameters are greater than zero.

The objective function is then defined as

$$\min_{\alpha,K,\gamma,T} \sum_{n\in N_1} \left\| \varepsilon_n(\alpha, K, \gamma, T) \right\|^2 \tag{106}$$

Subject to α, K, γ > 0 and 0 < T < 1, and the residual becomes

$$\varepsilon_n(\alpha, K, \gamma, T) \equiv e_n^m - e_n \tag{107}$$

5.2.2.4 Initial Conditions due to Switching

Eye movements in the VOR consist of two modes of operation, with the slow phase eye movement generally opposite to the head motion while the fast phase eye movement is in the same direction as the head movement (Figure 13). This phenomenon can be modeled by switching between two system dynamics. This paper only deals with the modeling of the slow phase dynamics and thus fast phase models are not discussed in the previous sections. Whenever switching occurs, the initial condition at the beginning of each slow phase segment needs to be included in the model in the optimization process. We create a variable named e^0_j which represents the initial condition in the jth segment of slow phase.

$$\begin{aligned} &e_j^0 = e_{1j}, \text{ for the } 1^{st} \text{ point in the jth slow phase segment} \\ &e_j^0 = 0, \text{ otherwise} \end{aligned} \tag{108}$$

Since this is measured noisy data, and transients are important, we introduce a new coefficient δ_j to allow estimation of the true initial condition as part of the optimization process. Hence, in the jth slow phase segment, the discrete model equation as a function of the input to D(s) becomes (valid for all forms in Figure 14).

$$e_{nj} = \frac{2T - \tau}{2T + \tau} e_{(n-1)j} + \frac{G\tau}{2T + \tau}\left(\mu_{nj} + \mu_{(n-1)j}\right) + \delta_j e_j^0 \qquad (109)$$

The δ_j are treated as weights applied to the first noisy data point (segment initial condition) in the modeling of each segment's second data point, while the other coefficients are shared by all data entries across all slow-phase segments. Estimating the initial conditions on each segment is a necessary step in finding unbiased system coefficients and in producing optimal predictions for validations described below. In summary, all discrete models to be compared during data fitting are described by the following equations for the jth segment

$$e_{nj} = DM_k + \delta_j e_j^0 \qquad (110)$$

where DM_k represents the right-hand side of Eq. (91), Eq. (91) or Eq. (104), according to the selected discrete model type. This formulation is repeated for all segments in the data set. Clearly only the first equation in each segment includes the effect of its initial condition. Subsequent points in each segment follow the original mentioned equations Eq. (91), Eq. (91) or Eq. (104).

5.3 Simulation

Simulations in Matlab Simulink (MathWorks, Natick, MA, USA) of all the model forms presented in the previous sections are used to validate model identification algorithms. All simulations were carried out at 500Hz, sufficient for the dynamics studied here. We used a switching strategy previously published (Galiana 1991) for each of the feedback representations in (Figure 14B, C & D). When noise was added to the output of simulations, the Signal to Noise Ratio was defined as:

$$SNR = 10 \log_{10} \frac{\sum e_n^2}{\sum \varepsilon^2} \qquad (111)$$

where e_n denotes the eye position and ε denotes the noise added at the output. Normally distributed noise was low-pass filtered to 40Hz with an eighth order Bessel filter and added to the output signal of the model (i.e. eye position) to approximate experimental conditions during clinical data acquisition.

5.4 Recordings from Real Subjects

Vestibulo-Ocular Reflex (VOR) data was recorded from four human subjects with no known VOR dysfunction. The data was acquired by electrooculography (EOG) after appropriate electrode stabilization and calibration (Galiana, Smith and Katsarkas 1995). These data were used in preliminary tests of the model type that might best suit normal subjects. All subjects signed a consent form outlining the protocol which was approved by the Institutional Review Board of McGill's Faculty of Medicine. They were asked to sit in total darkness for a 20-min period to stabilize the EOG electrodes. Calibration extended over ±50deg range and included viewing a central target (0 degree) immediately before and after each rotational protocol. This allows defining not only sensitivity but also correction for drift on the electrodes. See (Galiana, Smith and Katsarkas 1995) for more details.

5.5 Parameter Estimation and Model Selection/Validation

Optimal parameter estimation was carried out with both a previously developed algorithm coded in Matlab (MathWorks, Natick, MA, USA) and the General Algebraic Modeling System (GAMS) (Washington, DC, USA). Our previous Matlab code is based on a sequential optimization process; it assumes Linear or Non-linear Autoregressive Moving Average Exogenous (ARMAX or NARMAX) structures and uses the Modified Extended Least Square (MELS) method developed by Kukreja et al (Kukreja, Kearney and Galiana 2005) to solve for the parameters. As such it can only be applied on structures described by Figure 14A, B & C. It cannot be applied to dynamic non-linear descriptions (Figure 14D). The MELS method first estimates system parameters with ELS and then, based on these, finds estimates of initial conditions in each segment, inside an iterative search. The GAMS code, on the other hand, is formulated to perform

parameter searches (including initial conditions for each slow phase segment) globally and simultaneously. The CONOPT solver is more general and was used to perform the optimization on all proposed models. For a detailed description of the algorithm, please refer to (Carlyle, Montgomery and Runger 2000), (Abadie and Carpentier 1969).

5.5.1 Validation of parameter estimates with the correct model

Since MELS is not applicable to the nonlinear cases (Figure 14D), initial comparison of the new GAMS-based approach against MELS was carried out on results from linear models only. Identification used half the data set to find the optimal system parameters, together with optimal segment initial conditions. Prediction and model validation used the reserved second half of the data set, and was based solely on the stimulus data sequence (head velocity) and the global identified parameter set (infinite horizon); this allows a better distinction between alternate models than simple one-step prediction. Normal residuals of minimal variance were obtained by starting each segment at an optimal initial point, as required for trajectories that contain a transient component.

Standard deviations on estimated system parameters were obtained in two ways. One approach relied on a Monte Carlo method, with 20 runs at the selected SNR with different noise seeds to compute the expected value and standard deviation for each parameter. A second approach derived the sensitivity functions for each parameter analytically, from the applied cost function and the standard deviation of the residuals (see (Ljung and Glad 1994), chapter 9 for details). The latter approach gives us an advantage in which one experimental data set is sufficient to define both the expected value and standard deviation of model coefficients.

5.5.2 Validation of appropriate model selection

We define Akaike's Information Criteria (AIC) (Akaike 1974) and Mean Squared Error (MSE) as:

$$AIC = \left(1 + \frac{2d}{N}\right)\sum \left(y_i - \hat{y}_i\right)^2 \tag{112}$$

$$MSE = \frac{1}{N}\sum \left(y_i - \hat{y}_i\right)^2 \tag{113}$$

where y corresponds to either the noisy simulated eye position in the simulation case or the measured eye position in the trials with real subjects, $\hat{y}$ corresponds to the prediction of y from the identified model, N is the sample length and d denotes the order of the model (number of estimated coefficients). Only the number of system coefficients defined the order of the model (2 for the linear model and a value of 4 for the Hammerstein and Dynamic Nonlinear models), since the initial conditions were not common to the data sets used for identification and validation.

Table 5: Comparison of Parameters estimated in the MELS and CONOPT environment (standard deviation in brackets)

Values used in Simulation with Linear Model					
β	T	G	A	ξ_1	$\xi_2 (\times 10^{-3})$
0.1	0.3	0.6	0.95	0.9940	-3.589
Noiseless				ξ_1	$\xi_2 (\times 10^{-3})$
MELS				0.9940 (±0.00030)	-3.5892 (±0.0012)
CONOPT				0.9940 (±0.00019)	-3.5892 (±0.0081)
SNR = 10dB				ξ_1	$\xi_2 (\times 10^{-3})$
MELS				0.9920 (±0.0013)	-3.532 (±0.09)
CONOPT, 1 run				0.9938 (±0.00011)	-3.579 (±0.028)
CONOPT, 20 runs				0.9937 (±0.00020)	-3.580 (±0.040)

Table 6: Estimated Parameters, Dynamic Nonlinear case

Scenario (SNR = 10)	α	K	γ	T
True Value	0.188s	200	0.94	0.3s
CONOPT estimates	$\hat{\alpha}$	$\hat{K}$	$\hat{\gamma}$	$\hat{T}$
Mean of 20 Realizations	0.23s	227	0.95	0.37s
Std of 20 Realizations	0.025	33	1.6e-5	0.041
Estimates from one Realization	0.21s	207	0.953	0.35s
Std from one Realization	0.021	31	2.3e-5	0.039

Focusing on the GAMS-based method, MSE and AIC indicators are used to compare the accuracy and complexity measures using the three alternate estimators defined for the Linear (Eq. (94)), Hammerstein (Eq. (99)) and Dynamic Nonlinear (Eq. (106)) models. All three are applied to each data set extracted from simulations of these model types, to test appropriate model selection. Similarly MSE and AIC are also used in the selection of the model type best describing each of the four experimental subjects for preliminary tests of the new non-linear model's general applicability.

5.6 Results

5.6.1 Parameter Estimation and Validation with Simulated Data

5.6.1.1 Linear Estimators

To validate the performance of the CONOPT-based algorithm, we simulated a data set with the Linear model described in section 4.2.1.1 (Figure 14B) and estimated its parameters with both MELS and CONOPT. We used an eye plant time constant of 0.3s (Angelaki, Green and Dickman 2001) (Robinson 1981) (Kaneko 1997) and a feedforward gain (G') of -0.6 (Minor, et al. 1999) (Collewijn, Martins and Steinman 1983) reflecting

the properties of the typical VOR in the dark. Their corresponding discrete coefficients ξ_1 and ξ_2 are summarized in Table 5. The estimates are provided for different levels of Signal to Noise Ratio (SNR), using up to 20 runs (different seeds) at the same SNR. The CONOPT estimator remains robust and unbiased even at high noise levels, while the results from MELS are more likely to become biased, as expected. Hence, in the following validation tests, we focus only on the CONOPT-based approach to model identification and selection.

5.6.1.2 Nonlinear Estimator

We document the asymptotic property of CONOPT during parameter estimation of the most difficult case: the Dynamic Nonlinear model for the NI process. This case cannot even be addressed by the MELS approach.

Table 6 contains the true values of the parameter set used in simulation and their corresponding estimates for the model in Figure 14D. 20 different noise sequences were generated and added to the simulated data to generate 20 realizations of data with a Signal-to-Noise ratio (SNR) of 10, a noise level that exceeds that seen in our experimental data. The mean and the standard deviations of the estimates from the 20 realizations are included in the table. The estimates from one realization are also included together with the standard deviation derived analytically from sensitivity functions and the standard deviation of the residual (see Appendix). The similarity between numerically derived std's (20 runs) and the analytically derived results support the accuracy of the CONOPT solver, since none of the standard deviations exceed 10% of the estimate.

The purpose of the nonlinear model is to support possible changes in the Neural Integrator apparent time constant, T_{NI}, with context. In the current representation, T_{NI} is at its highest when the input to the nonlinearity, i_n, is closest to the origin, and decreases as i_n deviates from zero. The simulated data set had a maximum T_{NI} of 5s. With the estimated parameters in a given context, the predicted apparent time constant and VOR gain are given by Eq. (105), or

$$\hat{T}_{NI} = -\frac{\hat{T}}{1-\hat{\alpha}\hat{\gamma}f(i)/i}; \hat{G}_{VOR} = \frac{\hat{\alpha}}{1-\hat{\alpha}\hat{\gamma}f(i)/i} \quad (114)$$

The expected T_{NI} in this test could thus vary from 4.4s to 1.23s (Figure 16A& B), depending on the context (combined head velocity and eye position).

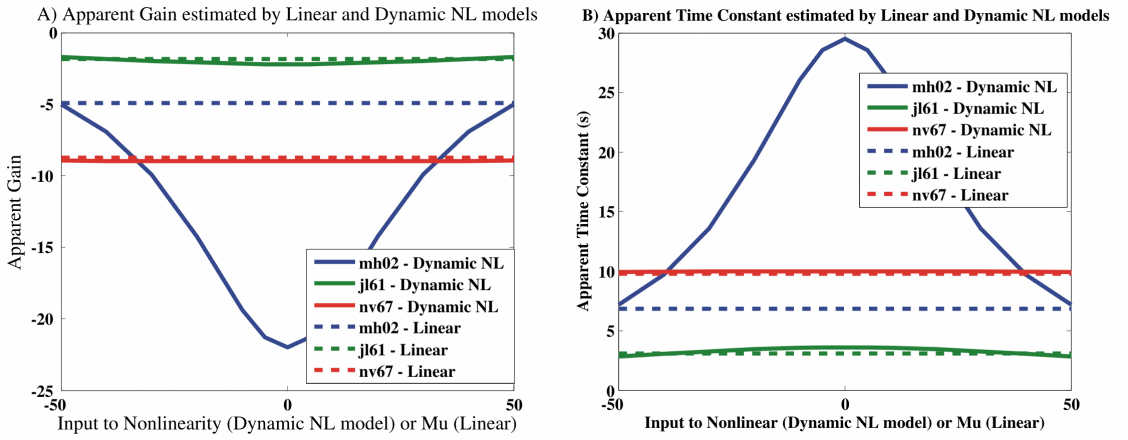

Figure 16: Predicted variability in apparent VOR gain (A) and time constants (B) from linear and non-linear models applied to three experimental subjects. One observes that subjects nv67 (red) could be classified as 'linear' in his behavior, jl61 (green) is mildly non-linear while mh02 (blue) is very non-linear. Where the subjects are nearly-linear, the model predictions are very consistent.

5.6.2 Cross-validation of the Linear, Hammerstein and Dynamic Nonlinear models

Here the validation consists in demonstrating the robustness of the estimators in terms of proper selection of the best model structure for a given data set. To this end, simulated data were generated using the Linear, Hammerstein and Dynamic Nonlinear models introduced in section 4.2.1 with SNR of 10 (Table 7).

The goal for the nonlinear feedback model is to define a nonlinear curve that accounts for the change in the dynamics in the feedback loop. Thus the exact mathematical representation of the nonlinearity is not as important as the dynamic behavior that it is supposed to represent since the nonlinearity only approximates the context-dependent behavior in subjects. The nonlinearity in (Eq. (101)) was chosen for the convenience that

its roll-off is simply controlled by one parameter b independent of its peak value. Figure 15 contains the simulated and predicted data for the context-dependent case. To verify the robustness of our algorithm, we also generated a fourth data set with another nonlinear function of similar shape, while preserving the overall structure of Figure 13D. Here the nonlinear sensitivity was chosen to be

$$f_{alt}(i) = \frac{ai}{\cosh\left(i / 2\eta\right)} \tag{115}$$

where a and η corresponds to the coefficients of the nonlinearity.

Table 7: Estimated Parameters on Simulated Data (standard deviation in brackets), * denotes selected model

Parameters used in data simulation				
Data Set 1 – Linear Model (2 parameters)	$\xi_1 = 0.99960$		$\xi_2 = 6.259 \times 10^{-4}$	
Data Set 2 – Hammerstein Model (4 parameters)	$\phi_1 = 0.99960$	$\phi_2 = -1.612 \times 10^{-9}$	$\phi_3 = 6.259 \times 10^{-8}$	$\phi_4 = -6.259 \times 10^{-4}$
Data Set 3 – Dynamic Nonlinear Model (4 parameters)	$\alpha = 0.18$	$K = 100$	$\gamma = 0.94$	$T_{ep} = 0.3$
Data Set 4 – Dynamic NL Model with NL in Eq. (115)	$\alpha = 0.188$	$\eta = 50$	$\gamma = 0.94$	$T_{ep} = 0.3$

Parameters Estimated by the Linear Model					
Set	$\hat{\xi}_1$	$\hat{\xi}_2 (\times 10^{-4})$		AIC	MSE
*1	0.99967 (±1.97e-4)	6.418 (±0.297)		4248	2.12
2	0.99971 (±9.78e-5)	7.522 (±0.774)		4614	2.23
3	0.99904 (±1.76e-4)	5.447 (±2.30)		9754	4.74
4	0.99921 (±1.98e-4)	5.671 (±2.57)		4397	2.16
Parameters Estimated by the Hammerstein Model					
Set	$\hat{\phi}_1$	$\hat{\phi}_2 (\times 10^{-10})$	$\hat{\phi}_3 (\times 10^{-8})$	$\hat{\phi}_3 (\times 10^{-4})$	AIC	MSE
1	0.99959 (±3.96e-4)	-4.882 (±0.219)	10.81 (±0.995)	-6.475 (±0.407)	4609	2.30
*2	0.99964 (±1.30e-4)	-17.68 (±1.09)	6.47 (±0.994)	-6.788 (±0.290)	4500	2.18
3	0.99904 (±2.26e-4)	-0.7059 (±0.230)	0.9394 (±0.349)	-5.430 (±2.50)	10011	4.85
4	0.99924 (±3.18e-4)	-2.313 (±0.276)	3.983 (±0.987)	-5.642 (±0.295)	4232	2.08
Parameters Estimated by the Dynamic Nonlinear Model						
Set	$\hat{\alpha}$	$\hat{K}$	$\hat{\gamma}$	$\hat{T}_{ep}$	AIC	MSE
1	0.170 (±0.013)	500 (±23)	0.95 (±0.0023)	26 (±0.90)	5284	2.63
2	0.400 (±0.023)	359 (±17)	0.90 (±0.0012)	64 (±0.62)	6105	2.95
*3	0.190 (±0.032)	101 (±9)	0.94 (±0.011)	30 (±0.50)	3903	0.89
*4	0.200 (±0.0081)	118 (±6)	0.95 (±0.0023)	32 (±0.47)	3947	1.94

The values of MSE and AIC are both at their lowest when the model structure of the estimator matches the model structure used in the simulations. Hence, as denoted by * in Table 7, the correct model is selected in each case, based on these criteria. This confirms that the algorithm is performing correctly, because the data belonged to one of the tested model forms.

Although the formulation of the model nonlinearity did not match that used to generate data set 4, the Dynamic Nonlinear estimator has the lowest AIC of all estimators, and the estimated nonlinearity follows the same trend as the nonlinear curve used in the simulation (Figure 17). This confirms the robustness of the Dynamic Nonlinear model for general nonlinearities of similar shape. In addition, all the estimated coefficients in the selected models have 95% confidence intervals that include the true values.

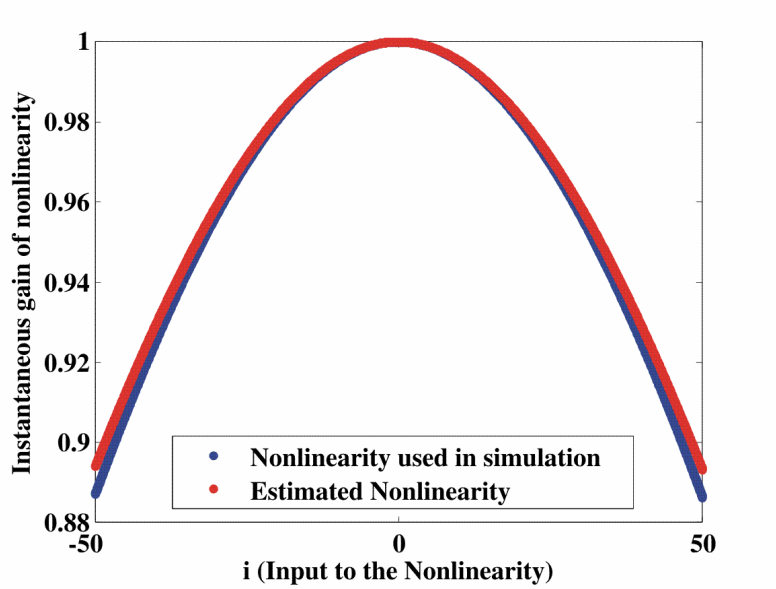

Figure 17: Convergence to the correct non-linear shape in dynamic non-linear models (Figure 14D). The simulated non-linearity used an inverted cosh function (Eq. (115), blue curve), while the estimation relied on fitting a Versiera function (red). The matches are excellent in both cases.

5.6.3 Parameter Estimation on data from Human Subjects

Now that the robustness of the estimators against misidentification of the model structure is verified, the three model estimators are applied to data recorded from human subjects

during VOR tests. The Linear, Hammerstein and the Dynamic Nonlinear estimators were all used to find the model with optimal prediction quality based on MSE and AIC, in four normal subjects with no history of vestibular deficits. Standard deviations on the estimated parameter sets were calculated with the analytical approach outlined in section 4.5.1. All four subjects are best described by the Dynamic Nonlinear estimator (see Figure 18 for an example of the fit on one of the subjects). The instantaneous G_{NI} and T_{NI} of mh02, jl61 and nv67 are shown in Figure 16A&B. The absolute values of G_{NI} and T_{NI} are at their maximums when the input i to the nonlinearity is at the origin, and decay as i moves away from the origin. For subject jl61 and nv67, the values of G_{NI} and T_{NI} estimated by the Dynamic Nonlinear model remain almost constant throughout the range of i. In these cases, the nonlinearity f(i) in the Dynamic Nonlinear model simply consists of a gain, therefore the linear model may be sufficient enough to describe the two data sets. Thus the Dynamic Nonlinear model can be used to fit all the data sets while the estimates and shape of the non-linearity can be used to classify the data sets.

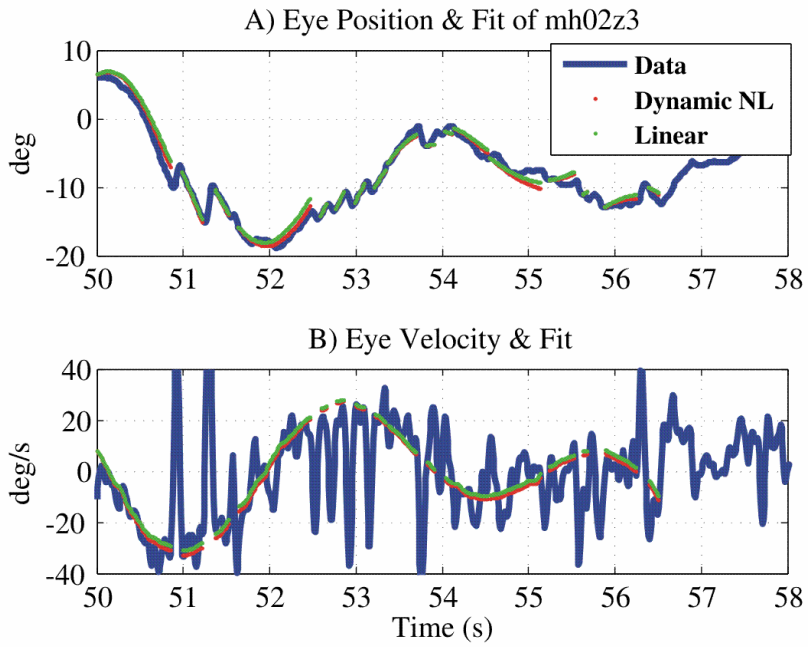

Figure 18: Example of model predictions on human experimental data. Subject mh02 is best fit by the Dynamic non-linear model (MSE=0.75, AIC=1644, red curves) when compared to linear model predictions (MSE=0.86, AIC=1883, green curves). The differences are most visible at the ends of segments with large eye deviations, as expected from a context-dependent non-linearity.

Table 8: Estimated parameters on human VOR data (standard deviation in brackets), * denotes selected model.

Parameters Estimated by the Linear Model					
Subject	$T_c(s)$	$\hat{\xi}_1$	$\hat{\xi}_2(\times 10^{-4})$	AIC	MSE
mh02	20	0.999617 (±0.00021)	7.475 (±0.593)	1883	0.86
Jl61	20	0.999946 (±0.00016)	6.032 (±0.489)	1432	0.81
jn08	50	0.999919 (±0.00014)	37.74 (±4.44)	1616	1.32
nv67	50	0.999831 (±0.00021)	8.643 (±1.27)	1729	0.79

Parameters Estimated by the Hammerstein Model							
Subject	$T_c(s)$	$\hat{\phi}_1$	$\hat{\phi}_2(\times 10^{-5})$	$\hat{\phi}_3(\times 10^{-4})$	$\hat{\phi}_4(\times 10^{-2})$	AIC	MSE
mh02	10	0.9802 (±0.0059)	-2.475 (±0.032)	-8.069 (±0.39)	-4.950 (±0.69)	56523	25.85
Jl61	20	0.9820 (±0.0014)	-2.047 (±0.055)	3.279 (±0.11)	-4.685 (±0.42)	32291	18.22
jn08	50	0.9861 (±0.0048)	-0.6096 (±0.030)	-5.958 (±0.079)	-45.83 (±3.5)	1630	1.33
nv67	50	0.9976 (±0.0010)	-4.444 (±0.063)	17.07 (±2.7)	-57.87 (±1.9)	59387	26.96

Parameters Estimated by the Dynamic Nonlinear Model							
Subject	$T_c(s)$	$\hat{\alpha}$	$\hat{K}$	$\hat{\gamma}$	$\hat{T}_{ep}$	AIC	MSE
mh02	15	0.44 (±0.047)	192 (±3.4)	0.979 (±0.005)	0.59 (±0.046)	1646	0.75
Jl61	20	0.22 (±0.013)	284 (±1.2)	0.90 (±0.002)	0.36 (±0.024)	1200	0.68
jn08	50	0.34 (±0.057)	2557 (±3.2)	0.98 (±0.001)	0.8 (±0.014)	1261	1.03
nv67	50	0.18 (±0.018)	4326 (±13)	0.98 (±0.001)	0.2 (±0.025)	1644	0.75

We performed a small signal analysis with the linear estimator on a data set best described by the Dynamic Nonlinear model. We segregated the data set into nine segments, with the corresponding segregation from -250deg/s to -25deg/s, -25deg/s to 25deg/s and 25deg/s to 250deg/s for the head velocity; and from -50deg to -15deg, -15deg to 15deg and 15deg to 50deg for eye position. The estimated parameters and the apparent T' and G' in each subset are given in Table 9. We observe that mh02 exhibits changes in both apparent T' and G'. Furthermore, we observe the diagonal terms of the $\hat{T}'$ and $\hat{G}'$ 'matrices' contain higher values compared to the non-diagonal terms (Table 9). These characteristics are compatible with the optimal model type selected with global identification, but would only be expressed by plots of expected T_{NI} and VOR gain from fits of the most complex model (see below), given sufficiently high rotation speeds.

Table 9: Values from Small Signal Analysis on subject mh02 (± standard deviation)

Eye Pos. (deg)	-50 to -15	-15 to 15	15 to 50	-50 to -15	-15 to 15	15 to 50
Head Vel. (deg/s)	$\hat{\xi}_1$			$\hat{\xi}_2 (\times 10^{-4})$		
-250 to -25	0.999808 (±0.000012)	0.999145 (±0.000048)	0.999149 (±0.000034)	-8.259 (±1.3)	-7.307 (±1.8)	-6.906 (±0.6)
-25 to 25	0.999010 (±0.000026)	0.999952 (±0.000031)	0.999600 (±0.000024)	-6.119 (±1.6)	-7.726 (±2.3)	-5.895 (±1.1)
25 to 250	0.998493 (±0.000067)	0.999589 (±0.000021)	0.999907 (±0.000054)	-10.37 (±1.2)	-7.664 (±3.1)	-13.42 (±1.0)
	$\hat{T}'$			$\hat{G}'$		
-250 to -25	19.65	2.338	2.349	-16.23	-1.709	-1.623
-25 to 25	2.019	41.95	5.002	-1.236	-32.41	-2.948
25 to 250	1.326	4.870	21.46	-1.376	-3.733	-28.79

5.7 Discussion

This paper proposes an alternative to the currently accepted function of 'neural integration' (NI) in the oculomotor system. The NI is generally believed to be an ideal mathematical integrator that converts sensory and premotor velocity signals into efference copies of eye position. Yet it is now known that the dynamic characteristics of this NI can be very labile with context and are not predicted from simple fixation decay in the dark (Zhou, et al. 2007) (Chan and Galiana 2005). For this reason, linear and non-linear alternatives to the representation of the NI in ocular reflexes are compared, algorithms for their robust identification are validated and then the algorithms are applied to preliminary experimental data to show their relevance. Indeed even normal subjects

with no sign of vestibular dysfunction can exhibit non-linear NI characteristics. Hence, alternatives to ideal NI processes should always be considered in identifying ocular reflex dynamics, so that the best representation is detected for any subject.

Here only three representations were examined to illustrate the methodology, which includes handling transients in the responses during ocular nystagmus. Our previous identification algorithm (MELS) was compared to the GAMS-based CONOPT solver for the linear case to demonstrate that the approach with simultaneous optimization over initial conditions and parameters is more robust than the sequential/iterative MELS approach. The results on simulated data were found to be unbiased from the true values within 95% confidence intervals and validate the use of these optimization methods in identifying nonlinear NI models. Hence, whether using GAMS or another software environment (e.g. Matlab), we recommend the use of non-linear optimization approaches that prune the number of free coefficients to provide stable and unbiased results.

It is interesting to note that the Dynamic Non-linear representation was always adequate and very close to the 'best' case in fitting experimental data from MSE and AIC criteria. It seems to represent a valid superset, whose properties can be examined later for 'linear' or 'non-linear' dominance with plots such as Figure 16A&B for sensitivity with context. We need not at this time apply all possible model types - it is sufficient to identify the parameters for the most complex type.

The uniqueness of optimal solutions - Global vs Local Minima

So far, the most complex representation uses non-linear feedback in the NI process, to allow for cases where both the dynamics and the reflex sensitivity can change with sensorimotor context. Such non-linear representations potentially have multiple minima especially in the presence of noise, while CONOPT, the optimization method used in the validation tests, is a local optimization method (Drud 1985). Hence the results with CONOPT were also compared to those of global solvers also available in GAMS, including BARON, LGO and MSNLP (Pinter 1996). A global solver starts the optimization procedure with parameters at diverse initial values in the allowed range(s) to

prevent convergence to local minima. It was found that all global solvers tested converged to the same optimal values for the parameter set- containing the true values with 95% confidence. Thus the optimization algorithms are demonstrated to be robust in our application. However this test should be repeated whenever the structure of a proposed non-linear model is changed.

Symmetric vs Asymmetric Non-linearities - Extending model classes

Previous identification work on the VOR of patients with sensory lesions point to the presence of biases and asymmetries in the reflex gain, evaluated with Hammerstein representations (Jenkins, Cohen and Kimball 2000) (Crane, Tian and Demer 2000). The current representations in Figure 14 are all symmetric and bias-free. Extensions to the non-linear forms in the dynamic NL structure (Figure 14D) will be required to allow analysis of patient data. A bias can be integrated into all three models of the Neural Integrator by simply adding a bias term to Eq. (91), Eq. (91) or Eq. (104). This is only one example of the ease with which model structures can be adjusted if required by further examination of experimental data. The methodology proposed to find optimal parameter sets in VOR and NI models is quite general.

Implications for clinical testing of the VOR - Future work

For the first time, there are validated tools to test whether a particular VOR data set is best represented by Linear, Hammerstein (NL gain, Linear dynamics) or truly NL dynamics. The identification algorithms allow for initial conditions in the sequence of slow phase segments and hence are more sensitive to imbedded dynamics despite multiple switching over short intervals. In contrast, traditional approaches based on reconstructed slow-phase velocity across fast-phase gaps will provide biased estimates that vary with the fast phase patterns. Thus the identification methods provided here are expected to provide more sensitive detection of anomalies in the ocular reflexes of patients even after long-term compensation. The preliminary tests on 4 normal subjects already imply that non-linear behavior can be present even in symptom-free subjects, but a larger pool of normal subjects and patients is now being studied to evaluate trends in

the two populations. This will determine if the form of the proposed models is adequate in a larger data set and or require modifications to the proposed nonlinear characteristics. Issues to be considered are what mathematical functions could be used to represent biases (non-zero response to zero input) and general right-left asymmetries in the VOR dynamics (Figure 14E is symmetric); whether the nonlinearity has a single peak; and whether there is a need to disassociate sensory non-linearities from NI nonlinearities (a hybrid of models Figure 14C&D). Only further analysis of VOR responses with optimally designed stimuli will resolve the minimal complexities required to represent human vestibular function.

Finally, it should now be clear that even the Neural Integrator in oculomotor reflexes should be treated as a complex potentially non-linear and context-dependent process. This theoretically could have beneficial impact on proper reflex function in a binocular system (Khojasteh and Galiana 2006), and we now have the tools to explore it systematically.

5.8 References

Abadie, J, and J Carpentier. "Generalization of the Wolfe Reduced Gradient Method to the case of Nonlinear Constraints." In *Optimization*, by R. Fletcher, 37-47. New York: Academic Press, 1969.

Angelaki, D E, A M Green, and J D Dickman. "Differential Sensorimotor Processing of Vestibulo-Ocular Signals during Rotation and Translation." *Journal of Neuroscience*, 2001: 3968-3985.

Cannon, S C, and D A Robinson. "Loss of the Neural Integrator of the Oculomotor System from Brain Stem Lesions in Monkey." *Journal of Neurophysiology*, 1987: 1383-1409.

Carlyle, W M, D C Montgomery, and G C Runger. "Optimization Problems and Methods in Quality Control and Improvement." *Journal of Quality Technology*, 2000: 1-17.

Chan, W., and H.L. Galiana. "Integrator Function in the Oculomotor System Is Dependent on Sensory Context." *Journal of Neurophysiology*, 2005: 3709-3717.

Collewijn, H, A J Martins, and R M Steinman. "Compensatory eye movements during active and passive headmovements: fast adaptation to changes in visual magnification." *Journal of Physiology*, 1983: 259-286.

Crane, B T, J Tian, and J L Demer. "Asymmetry of ocular motor and perceptual vestibular processing in humans with unilateral vestibular deafferentation." *Journal of Vestibular Research*, 2000: 259-269.

Drud, A. "CONOPT: A GRG Code for Large Sparse Dynamic Nonlinear Optimization Problems." *Mathematical Programming*, 1985: 153-191.

Galiana, H L. "A nystagmus strategy to linearize the vestibulo-ocular reflex." *IEEE Trans. Biomed. Eng.*, 1991: 532-543.

Galiana, H L, H Smith, and A Katsarkas. "Comparison of linear vs nonlinear methods for analyzing the VOR." *Acta Otolaryngol*, 1995: 585-596.

Gonzalez-Forero, D, R R de la Cruz, J M Delgado-Garcia, F J Alvarez, and A M Pastor. "Functional Alterations of Cat Abducens Neurons After Periphaeral Tetanus Neurotoxin Injection." *Journal of Neurophysiology*, 2003: 1878-1890.

Guitton, D, D P Munoz, and H L Galiana. "Gaze Control in the Cat: Studies and Modeling of the Coupling Between Orienting Eye and Head Movements in Different Behavioral Tasks." *Journal of Neurophysiology*, 1990: 509-531.

Idoux, E, et al. "Oscillatory and Intrinsic Membrane Properties of Guinea Pig Nucleus Prepositus Hypoglossi Neurons In Vitro." *Journal of Neurophysiology*, 2006: 175-196.

Jenkins, H A, H S Cohen, and K T Kimball. "Long-term Vestibulo-ocular Reflex Changes in Patients with Ablation." *Acta Otolaryngol*, 2000: 187-191.

Kaneko, C R S. "Eye Movement Deficits After Ibotenic Acid Lesions of the Nucleus Prepositus Hypoglossi in Monkeys. I. Saccades and Fixation." *Journal of Neurophysiology*, 1997: 1753-1768.

Khojasteh, E, and H L Galiana. "A non-linear model for context-dependent modulation of the binocular VOR." *IEEE Trans. Biomedical Engineering*, 2006: 986-995.

Kukreja, S L, R E Kearney, and H L Galiana. "A Least-Squares Parameter Estimation Algorithm for Switched Hammerstein Systems With Applications to the VOR." *IEEE Transactions On Biomedical Engineering*, 2005: 431-444.

Ljung, Lennart, and Torkel Glad. *Modeling of Dynamic Systems.* New Jersey: Prentice-Hall, 1994.

McConville, K M, R D Tomlinson, and E Q Na. "Behavior of eye-movement-related cells in the vestibular nuclei during combined rotational and translational stimuli." *Journal of Neurophysiology*, 1996: 3136-3148.

Mettens, P, E Godaux, G Cheron, and H L Galiana. "Effect of Muscimol Microinjections Into the Prepositus Hypoglossi and the Medial Vestibular Nuclei on Cat Eye Movements." *Journal of Neurophysiology*, 1994: 785-802.

Minor, L B, D M Lasker, D D Backous, and T E Hullar. "Horizontal vestibuloocular reflex evoked by high-acceleration rotations in the squirrel monkey. I. Normal responses." *Journal of Neurophysiology*, 1999: 1254-1270.

Pinter, J D. "Continuous global optimization software: A brief review." *Optima*, 1996: 1-8.

Robinson, D A. "Oculomotor control signals." In *Basic Mechanisms of Ocular Motility and Their Clinical Implications*, by G Lennerstrand and P Bach-y-Rita, 337-374. Oxford: Pergamon, 1975.

Robinson, D A. "The use of control systems analysis in the neurophysiology of eye movements." *Annual Review of Neuroscience*, 1981: 463-503.

Shikin, E V. *Handbook and Atlas of Curves.* Florida: CRC Press Inc., 1995.

Zhou, W, Y Xu, I Simpson, and Y Cai. "Multiplicative Computation in the Vestibulo-Ocular Reflex (VOR)." *Journal of Neurophysiology*, 2007: 2780-2789.

The previous paper presents the dynamic nonlinear Neural Integrator model that yields variable apparent VOR gain and NI time constant with different head velocity and eye position set-points. The next paper verifies the practical aspect of such a model by calculating estimates from real data collected from human subjects. It also compares the estimated parameters between different subject groups including patients.

6. A Nonlinear Model of the Neural Integrator Improves Detection of Deficits in the Human VOR

Wilbur W. P. Chan, Henrietta L. Galiana

This chapter was submitted to the **IEEE Transactions on Biomedical Engineering** on Oct. 6, 2008.

Abstract — A nonlinear model has been proposed to describe the setpoint-dependent characteristics of the Neural Integrator (NI) in the oculomotor system. It was shown to yield improved prediction of slow-phase eye position in the Vestibulo-Ocular Reflex (VOR) of normal subjects, when compared to the classical linear model of the NI. In this paper, we compare the parameters of this nonlinear NI model fitted to VOR data from 1) compensated subjects diagnosed with vestibular deficiencies such as Vestibular Neuronitis and Meniere's disease, and 2) normal (symptom-free) subjects. The identified models exhibit more severe nonlinearity in VOR patients than the normal controls. Several of the identified parameters in patients unmask asymmetries and more context-dependence in the NI and in the VOR gain that are consistent with the lesioned side and could serve to support detection of lesions even after compensation.

Keywords — Vestibulo-Ocular Reflex, Neural Integrator, Modeling, Lesion Detection

6.1 INTRODUCTION

Here the focus will be on the horizontal vestibulo-ocular reflex (VOR), involving the horizontal semicircular canals, the medial vestibular nuclei (VN) and an essential Neural Integration process (NI; Robinson 1989). The NI in the oculomotor system is widely distributed in the premotor circuits, including the Prepositus Hypoglossi [1]-[4], the Reticular Formation in the brainstem [5] and the cerebellum [6]. This process of integration is required to mathematically integrate velocity-modulated sensory signals into positional motor neuron signals (e.g. head velocity signals encoded by the semicircular canals and projecting via the vestibular nerve to premotor cells in the VN), and for the 'holding' of ocular deviations when stimuli are removed (gaze holding in the dark). In tasks such as gaze holding and head rotation in the dark, a subject's perception of orientation will be inaccurate if the NI is defective (leaky, small time constant). Generally, the NI is presumed well represented by a linear first order filter [4] with a large time constant (> 15s), according to decay patterns of fixation in the dark. However, we recently reported that the NI can have variable dynamics sensitive to protocol, head velocity and eye position set-points [7]. This was implied by prior experimental and theoretical work that reported NI changes with eye eccentricity, and their potential link to VOR modulation with target depth [8][9]. Thus, a dynamically nonlinear model was developed to imitate the set-point dependent dynamics of the NI and shown to yield an improved prediction of eye position during VOR nystagmus in controls [10]. A more accurate prediction implies a more robust and realistic model structure, so that estimated model parameters could have diagnostic relevance. In this paper, we present a systematic study of the dynamic linear or nonlinear model parameters estimated from the VOR of human subjects with different vestibular conditions: we report trends derived from the parameters and their global impact on VOR dynamics which could be used to detect anomalies even in the presence of long-term compensation.

6.2 Methodology

6.2.1 Recordings from Human Subjects

Angular VOR data are used to calculate and compare the NI parameters from different human subject groups: those who have compensated from vestibulopathy such as Vestibular Neuronitis and Meniere's disease, and a control group. A total of 18 trials were recorded from 7 patients (with 10 trials from 4 subjects showing dysfunction on the left side and 8 trials from 3 subjects with right side dysfunction) while 15 trials were taken from 7 normal subjects. A single recording session from patients took place varying from 1 to 10 months after occurrence of the first vestibular episode. Prognosis and time of recording session after first vestibular episode are tabulated on **Table 16**. The three subject groups will hereafter be referred to as Controls, Left patients or Right patients. All subjects signed a consent form outlining the protocol which was approved by the Institutional Review Board of McGill's Faculty of Medicine. Whole-body yaw rotation was achieved with either rotation at a single frequency (0.167Hz), or a sum of frequencies (0.03Hz, 0.1Hz and 0.17Hz,). The frequencies of the three sinusoids were selected such that none of them was a multiple of the others, so that harmonics in the reflex response could be assigned to a central non-linearity. It was demonstrated earlier that a more complex stimulus yields estimates that are more robust than those from a single sinusoid [11] for linear models. This should also be true for non-linear systems and will be addressed in the Results.

The VOR data were recorded with electrooculography (EOG) at 500Hz, well above the 50Hz upper limit of the ocular nystagmus bandwidth [12]. After retinal potential stabilization in the dark for at least 20 min, the subject was seated in a servo-driven chair with the head restrained by a fixation system. Pre- and post-rotation calibration allowed correction for any residual electrode drift. Each recording consists of duration of around 70s. A more detailed description of the experimental procedure can be found in Galiana et al [13].

6.2.2 Formulation of the NI model in the VOR system and Model Selection

As reported previously, a formulation for the NI can rely either on a low-pass filter with long memory (a separate block or process), or it can instead rely on placing a filter inside a feedback loop so that the global properties of the *loop* implement the desired filter characteristics [14], [15]. In the case of a linear process both approaches are equivalent. However, in the case of a context-dependent NI, changes in dynamics with operating point are easier to implement in the form of Figure 19, where a simple non-linearity in secondary vestibular neurons (function *f(i)*) will automatically cause the overall loop to behave in a context-dependent manner. The form of the nonlinearity, $f(i)$, can be represented by any nonlinear function which will characterize the behavior of the variable dynamics of the NI; for example, it is modeled by the 'Versiera' curve in our previous paper [10], [16] targeting controls with symmetric and unbiased VOR responses. To now accommodate for possible asymmetries in subjects, especially those with unilateral vestibular deficits, a third-order polynomial is now selected for the nonlinearity:

$$f(i) = a + i + ci^2 + di^3 \tag{116}$$

where i corresponds to the input, a is the offset in the nonlinearity, $\{c, d\}$ are the coefficients of the second and third order terms, respectively. The coefficient of the first order term is absorbed in the feedforward gain β. We search for the *shape* of the non-linearity, if applicable, not its particular functional definition.

The input $\dot{h}'$ is presumed to project from vestibular afferents, with the dynamics of a high-pass filter with respect to head velocity $\dot{H}$ [17]:

$$\dot{h}'(s) = \frac{T_{VS}\, s}{T_{VS}\, s + 1} \quad \dot{H}(s) \tag{117}$$

Where s is the Laplace variable, T_{VS} is the time constant of the processed vestibular signals (to be estimated) including potential velocity storage [18], [19], and the gain is presumed absorbed in the later projection gain β. On the other hand, the eye plant dynamics are represented by a low pass filter [18], [20] as:

$$\mathrm{D}(s) = \frac{1}{T_{EP}s + 1} \qquad with \qquad D^*(s) = \gamma D(s) \tag{118}$$

Where γ defines the ratio in sensitivity to eye position at the level of the internal model (neural), relative to the behavioral eye position (deg).

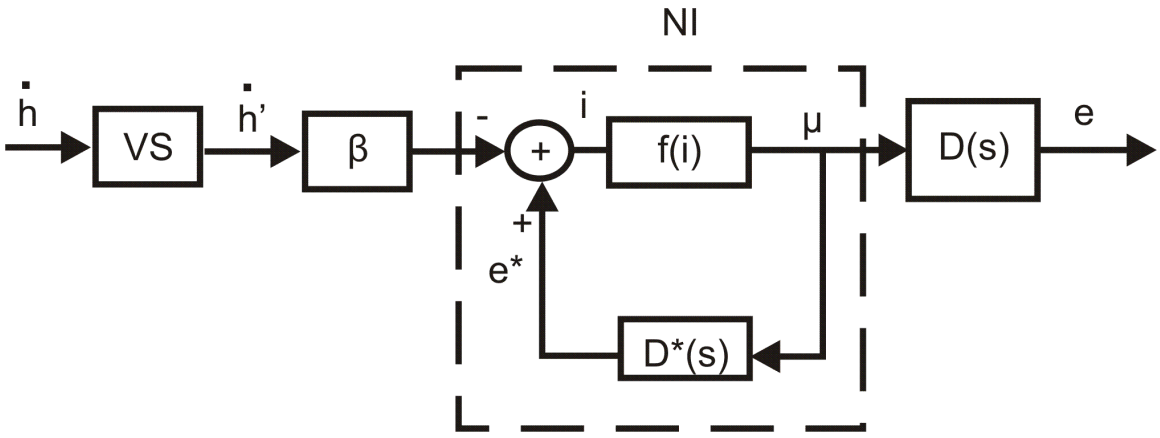

Figure 19: Block diagram of the nonlinear Neural Integrator model with preceding vestibular stage: $\dot{h}'$ corresponds to the head velocity signal projecting from the canal; VS is the vestibular stage; β is the gain of this projection to the NI; $f(.)$ is the static nonlinearity at the level of VN cells, modulated by head velocity and eye position context; i and μ are respectively the input and output of the nonlinearity; $D(s)$ and $D^*(s)$ are the eyeplant and internal model (eyeplant) dynamics presumed equal; e is the response as eye position; v is the measurement noise on the output; and e^m is the resulting *measured* eye position.

With these definitions, the ensemble of model equations can be grouped to relate sampled eye positions and head velocity during the protocol (see Appendix, and [10]).

$$e_n = \frac{2T_{EP} - \tau}{2T_{EP} + \tau} e_{n-1} + \frac{\tau}{2T_{EP} + \tau} \begin{bmatrix} 2a + \{\gamma(e_n + e_{n-1}) - \beta(\dot{h}'_n + \dot{h}'_{n-1})\} \\ + c\{(\gamma e_n - \beta \dot{h}'_n)^2 + (\gamma e_{n-1} - \beta \dot{h}'_{n-1})^2\} \\ + d\{(\gamma e_n - \beta \dot{h}'_n)^3 + (\gamma e_{n-1} - \beta \dot{h}'_{n-1})^3\} \end{bmatrix} \quad (119)$$

During parameter estimation and validation of proposed models, the data set is divided into two segments, with the first half used for the estimation process and the other for the model validation process. From the first half of the data set, the parameters that are to be identified are: $T_{EP}, \gamma, \beta, a, c$ and d . Since e_n is present on both sides of Eq. (119), and is expressed with its quadratic and cubic terms on the right hand side, the output cannot be expressed explicitly on one side of the equation as a function of the parameters and past sample values. Hence the Ordinary Least Square Method cannot be used on the ensemble of data. Instead, we rely on a non-linear optimization method to search for the optimal parameter set [21](GAMS software). For a more detailed description of the method, please refer to [10]. This requires an iterative approach, since the vestibular time constant is not expressed as a parameter in Eq.4. Thus, tentative profiles for $\dot{h}'$ are generated from the head velocity profile according to Eq. (117), for vestibular time constants ranging from 0.1s to 50s, in steps of 0.25s. For each possible T_{VS} , an optimal solution is found for the other model parameters. The parameter set and its associated T_{VS} yielding the lowest Mean Squared Error (MSE) for predictions in the second half of the data is deemed the best model, whether considering the linear or non-linear class. The MSE is defined as:

$$MSE = \frac{1}{N} \sum_{j=1}^{N} \left(e_j - \hat{e}_j \right)^2 \quad (120)$$

N denotes the number of data points, e_j denotes the j^{th} measured output eye position and $\hat{e}_j$ denotes the predicted j^{th} eye position from the estimated model. We also calculate the Akaike's Information Criteria (AIC) [22] which trades off increased model complexity with improved MSE, to compare the performance of linear (c=d=0) vs. non-linear (all parameters free) descriptions:

$$AIC = \left(1 + \frac{2q}{N}\right)\sum_{j=1}^{N}\left(e_j - \hat{e}_j\right)^2 \quad (121)$$

where q denotes the number of free parameters in the model used in the final tables. For example, with envelope fits during pure harmonic rotation, there are up to 3 parameters for linear fits and 5 parameters for non-linear fits, including the VS time constant (e.g. **Table 18Table 20**). The NL NI model for the VOR can have a maximum of 7 significant parameters (e.g. Table 12). Selecting between the linear or non-linear option in a given test relies on choosing the model type with the smallest MSE, provided the AIC is also lower.

6.2.3 Estimating VOR Gain and NI Time Constant in the Nonlinear VOR model

The parameter estimates for the optimal non-linear model in a test can be combined to extract the *apparent* dynamics of the Neural Integrator and VOR gain. The dynamics of the VOR are directly linked to the estimated optimal value of $\hat{T}_{vs}$ and to the shared NI integration process $\hat{T}_{NI}$. For the linear case, the classical form for the transfer function of the VOR in Figure 19 is:

$$\frac{\dot{E}(s)}{\dot{h}'(s)} = \frac{\hat{G}_{VOR}\hat{T}_{NI}s}{\hat{T}_{NI}s + 1} \quad (122)$$

which depends on all the NI parameters estimated (see below). Note that $\dot{h}'$ is the filtered head velocity from the velocity storage. If the best model is dynamically non-linear, the classical form is only valid for small changes about a given operating point (small-signal model). Here the non-linearity appears as a function varying with set-point 'i' which fixes the local value for *f(i)*. Hence for any given set-point, the local values of the VOR gain G_{VOR} at high frequencies (>0.01Hz) and the Neural Integrator Time Constant T_{NI} are given by [10]:

$$\hat{T}_{NI} = \frac{\hat{T}_{EP}}{1 - \hat{\gamma}\,\hat{f}\,'(i)} \tag{123}$$

$$\hat{G}_{VOR} = -\hat{\beta}\,\hat{f}\,'(i) / \hat{T}_{EP} \tag{124}$$

where the 'hat' symbol denotes estimated values from the fitting step. $\hat{f}\,'(i)$ is the derivative (slope) of the estimated non-linearity with respect to i (Eq. 1), at the same set-point,

$$\hat{f}\,'(i) = 1 + 2\hat{c}i + 3\hat{d}i^2 \tag{125}$$

Thus the non-linear NI representation will be associated with NI dynamics and VOR gain that change with sensorimotor context through the level of '*i*'. On the other hand, in the linear case $\hat{f}\,'(i)$ is 1 ($\hat{f}\,'(i) = 1$) and Eq. (123) & (124) produce constant dynamics independent of context.

6.2.4 Comparisons with Classical VOR Analysis

In classical VOR evaluation, the time constant of the NI is presumed large and invariant. Hence, vestibular time constants (or VOR phase) and the VOR gain are assumed fixed, and are unmasked by comparing eye velocity to head velocity during the slow phases of nystagmus (envelope analysis). During pure sinusoidal tests and assuming constant dynamics, the characteristics of the VOR can be deduced by using X-Y plots of data segments during slow phases: after shifting the head velocity trajectory to minimize the dispersion of data points around a line or curve, the VOR time constant can be calculated from the required time shift:

$$T_{VS} = \frac{1}{\omega \tan \theta} \tag{126}$$

where θ corresponds to the phase difference in the head and eye velocity (in radians) and ω corresponds to the frequency of the stimulus. $\Theta=2\pi\ \Delta T/P$, defines the proportion of the time shift (ΔT, in s) used in plots to the full period of the harmonic stimulus (P, in s).

The VOR gain (linear or non-linear) is approximated by the shape of the observed x-y curve relating slow-phase eye velocity segments to shifted head velocity (e.g. [13], [23]). This process was applied to the protocols consisting of pure sinusoidal head turns, to compare the results from alternative model fits that allow a context-dependent NI.

6.3 Results

The results are summarized below, referring to relevant figures. These are supported by annotated Tables of identification results, using both the standard envelope method for VOR analysis, versus fitting a context-dependent (non-linear) model for the VOR and NI (Table 10, Table 11 and Table 12).

6.3.1 Validation of the Nonlinear NI identification scheme

Validation of the algorithm for the identification of a Dynamic Nonlinear NI Model relied on its application to realistic, simulated, VOR data with known parameters. Two sets of simulated VOR data were defined with the sum-of-sines stimulus: one exhibits characteristics similar to normal subjects (nearly linear) and the other data set has characteristics similar to patients suffering from unilateral vestibular deficits. Both sets included the automatic generation of nystagmus, to provide realistic slow-phase segments (Please see [14] for further description of the process of nystagmus generation). The model parameters used in the simulations with the model structure in Figure 19 are given in Table 13, and noise was added to the resulting eye trajectories with a standard deviation of 1 deg (comparable to our EOG recordings). The two sets of simulated noisy data, with each lasting for 80s, were then analyzed to obtain model parameter estimates (Table 13) from the pooled slow phase data alone. Predicted eye trajectories and estimates of the internal non-linear curves could then be generated from the optimal parameter sets, using Eq. 1&4. They are provided for comparison in Figure 20, along

with the range of the input to their respective nonlinearities. Note that the polynomial curve of data set 1 resembles more a straight line, compared to that of data set 2, as expected from the parameter values. The predicted eye positions and eye velocities using the parameter estimates yield an extremely low MSE, and the 95% confidence intervals (2 standard deviations) on the estimated parameters include their true values (For a more thorough description of model validation, please refer to [10]). It is worth noting that the estimated polynomial curves have their largest errors at the extremes of the input domain as a consequence of first, lack of data beyond the edge due to switching, and second, because slow-phase segments tend to be shorter at high head speeds or large eye deviations (reproduced in the simulations).

6.3.2 Detection of lesions with Classical VOR analysis vs. the Dynamic Nonlinear Model

Here the estimated non-linear VOR characteristics are compared for the two methods described in Methods. The Dynamic Nonlinear NI model will be shown to be more effective in yielding estimates that correlate with the conditions of clinical subjects, when compared to the envelope method that is traditionally used in clinical diagnosis. Three representative examples are provided as X-Y plots of predicted eye velocity (Y-axis) versus appropriately time-shifted head velocity (X-axis) from VOR fits with both methods: a normal subject (jn08p5; Figure 21A), a subject suffering from left-side Meniere's Disease (ja67p4; Figure 21B) and a subject suffering from left side Vestibular Neuronitis (ap68p6; Figure 21C). The comparison here is restricted to the data collected during simple harmonic tests. Section 0 describes the required time shift for X-Y plots with the envelope method, while the phase expected from the estimated vestibular time constant defines the required time shift in the dynamic NL method (Eq. (126)). The plots superimpose the predictions from all models attempted. The optimal model from each method (linear or non-linear) is selected on the basis of achieved MSE and AIC.

Table 10: Envelope Estimates for Controls

	Linear Envelope		Nonlinear Envelope			
Subject Code	Linear	Bias	Cubic	Quadratic	Linear	Bias
jl61p5	-0.508	4.14	1.78E-06	2.63E-04	-0.545	1.89
jn08p6	-0.416	-0.281	-9.3E-06	-9.70E-04	-0.371	2.42
jn08p5	-0.423	-6.46	3.36E-06	-7.33E-04	-0.488	-2.85
mr81p5	-1.84	8.55	1.6E-06	-7.90E-04	-1.84	13.3
mr81p6	-0.918	2.01	-9.9E-06	3.19E-04	-0.749	1.018
mr82p5	-0.0809	-3.36	2.2E-05	3.13E-04	-0.540	-11.0
mr83p7	-0.776	10.2	9.58E-06	-1.45E-03	-1.03	14.9

Table 11: Envelope Estimate for Left Patients

	Linear Envelope		Nonlinear Envelope			
Subject Code	Linear	Bias	Cubic	Quadratic	Linear	Bias
nv10p3	-0.508	2.40	6.79E-06	1.83E-04	-0.547	1.71
nv10p5	-0.516	8.99	3.56E-06	4.82E-04	-0.577	5.62
ja67p4	-0.789	0.423	9.67E-07	-3.90E-04	-0.797	2.08
ja67p5	-0.689	-0.124	-7.3E-07	1.83E-05	-0.679	-0.163
ap68p6	-0.572	1.23	4.2E-06	1.43E-04	-0.735	2.12
jn30p6	-0.493	-7.96	4.65E-06	3.45E-04	-0.578	-11.0

Table 12: Envelope Estimates of Right Patients

	Linear Envelope		Nonlinear Envelope			
Subject Code	Linear	Bias	Cubic	Quadratic	Linear	Bias
oc26p5	-0.454	10.7	3.97E-06	-7.7E-06	-0.512	10.2
oc26p6	-0.457	14.6	4.03E-06	7.06E-04	-0.611	9.57
mr31p3	-0.738	4.18	1.06E-05	1.82E-04	-0.804	3.44
mr31p4	-0.709	8.18	1.05E-05	5.16E-05	-0.804	7.73
mr31p5	-0.616	12.4	3.04E-06	7.65E-04	-0.677	6.33
mr31p6	-0.403	11.2	3.04E-06	3.18E-04	-0.492	9.23
mr57p6	-0.996	-1.09	-4.1E-06	5.11E-05	-0.923	-0.921

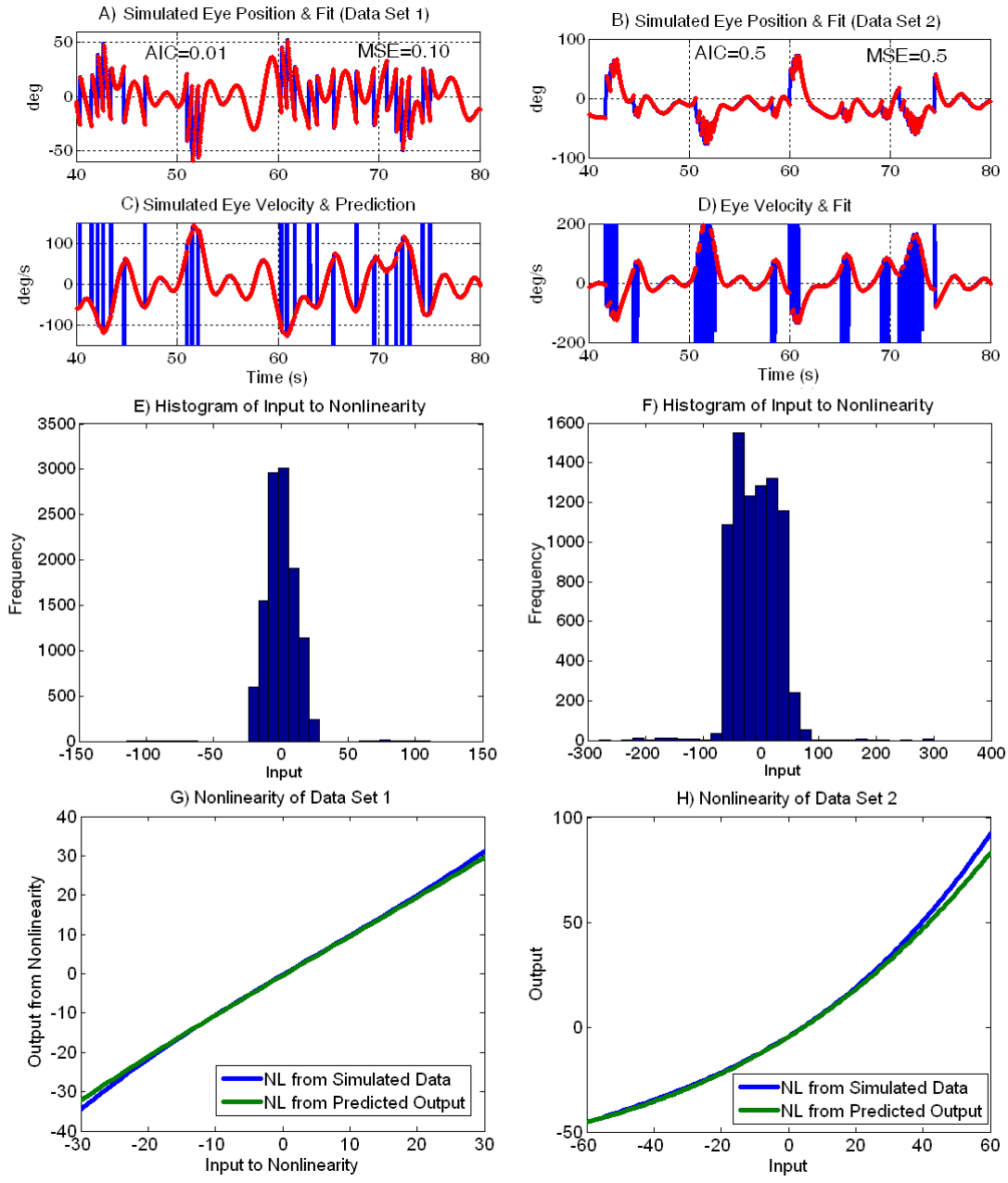

Figure 20: Validation with simulated data. A & B display the simulated and predicted eye position of data set 1 and 2, respectively; C &D display the simulated and predicted eye velocity of data set 1 and 2, respectively; E & F, the histograms of input range to their respective nonlinearities; G &H plot the estimated nonlinearities superimposed on the ones used in the simulations. Slow phase segments are shown in red in A&B. Note that the number of slow-phase segments is approximately the same for both trials (~8 in 10s), with data set 1 (normal) exhibiting a more uniform distribution of its fast phases throughout the data set.

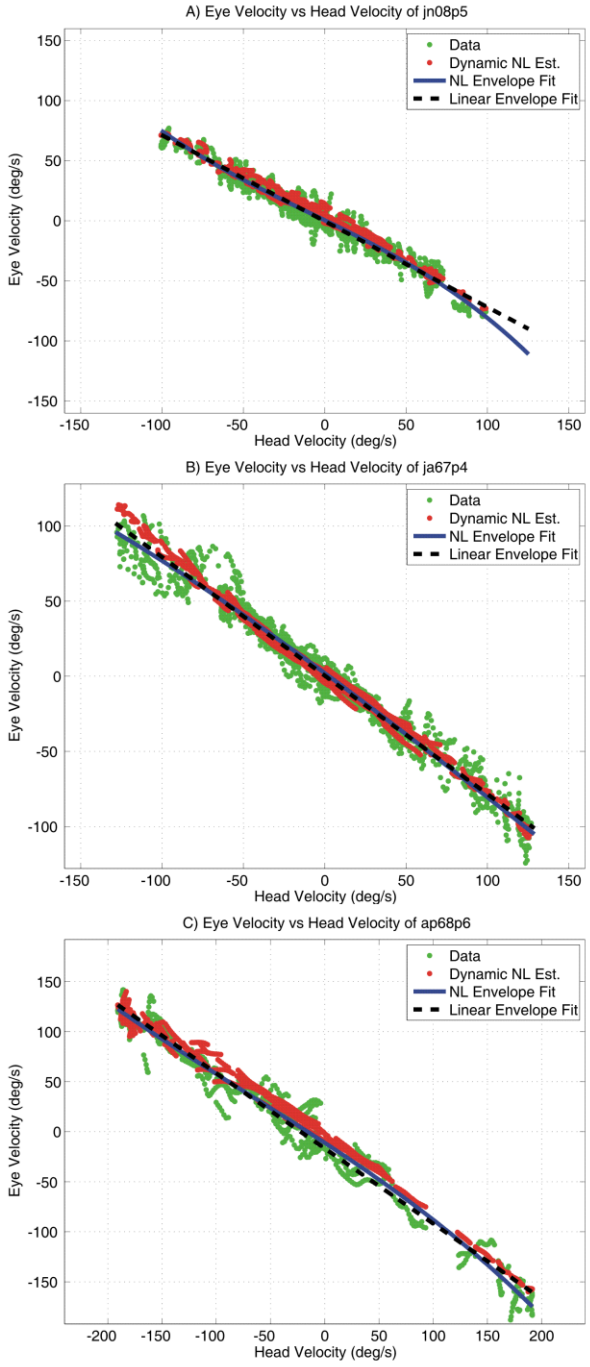

Figure 21: X-Y plots of eye velocity versus head velocity with simple harmonic rotation: control (A), patient suffering from Meniere's disease (B), and patient suffering from Vestibular Neuronitis (C). A linear model is selected by the envelope method for trials A & B, implying that both jn08p5 and ja67p4 might be from the normal group. The nonlinear (lesioned) property of ap68p6 (C) is detected by the envelope method on the basis of lower MSE and AIC (see methods). In all three cases, the dynamic NL model provides the best fits, even in the control group (compare MSE in Tables A.4-

A.6). To allow overlap, predictions from the dynamic NL model are plotted here with the same phase shift used in the envelope fit.

Table 13: True and Estimated Parameters in Simulation Validation of the NL-NI method

Parameters		β	γ	T_{EP}	a	b	c	d
Data Set 1	Simulated	0.191	0.940	0.284	-0.52	1	-11.8e-4	3.24e-5
	Estimated	0.213 (±0.053)	0.899 (±0.06)	0.293 (±0.031)	-0.57 (±0.013)	1.04 (±0.041)	-9.70e-4 (±5.6e-4)	3.42e-5 (±1.4e-5)
Data Set 2 (Patient)	Simulated	0.450	0.500	0.800	-3.82	0.86	8.03e-3	2.52e-5
	Estimated	0.487 (±0.072)	0.551 (±0.043)	0.799 (±0.063)	-3.58 (±0.38)	0.811 (±0.048)	7.40e-3 (±6.3e-4)	1.60e-5 (±8.1e-6)

For the first two trials **(Table 14)**, the *linear envelope* fit yields lower AIC and MSE than the third order polynomial *nonlinear envelope* fit ($AIC_{\text{linear envelope}} = 28244$ and $AIC_{\text{NL envelope}} = 29382$ for jn08p5; $AIC_{\text{linear envelope}} = 11782$ and $AIC_{\text{NL envelope}} = 18407$ for ja67p4). Hence the envelope method does not distinguish between a normal subject and the Meniere's patient.

Table 14: Estimates of Linear and Nonlinear Envelope Fits- 3 cases

		Linear Envelope Fit				Nonlinear Envelope Fit					
Trials	Tvs	Bias	Gain	MSE	AIC	Bias	Gain	Quadratic	Cubic	MSE	AIC
jn08p5	18s	-0.335	-0.715	13.0	28244	0.501	-0.659	-3.65e-4	-1.18e-5	13.3	29382
ja67p4	8s	0.423	-0.789	9.12	11782	2.08	-0.797	-3.95e-4	9.67e-7	14.2	18407
ap68p6	6s	-16.7	-0.751	22.5	19178	-11.1	-0.710	-4.02e-4	-1.84e-6	19.3	16353

In contrast, the *dynamic nonlinear* NI model provides a better fit in both these cases ($AIC_{Dyn\ NL}$=4383 for jn08p5 and $AIC_{Dyn\ NL}$=996 for ja67p4), with non-linear coefficients. In addition, the absolute value of the quadratic term in the Dynamic Nonlinear model (Table 15 & Table 16) is one order of magnitude larger for the Meniere's patient (Ja67p4) than for the normal subject (jn08p5) – compare $\hat{c}$ =-7.27e-4±5.8e-5 vs. $\hat{c}$ =-1.95e-5±1.5e-6. This implies not only that the dynamic NL NI model is a better choice, but that it is more sensitive to deficits than the envelope approach. Furthermore, the residuals between the measured data and predicted eye position from the dynamic nonlinear model from all trials appear to be random noise sequences. In terms of vestibular dynamics, the VOR time constants using the envelope method on the first two trials, jn08p5 and ja67p4, are close (19s and 21s, respectively); the corresponding fitting exercise with the dynamic NL model results in estimated vestibular time constants of 22.5s and 12.5s, respectively.

Table 15: NL-NI Model Estimates for Controls

Coefficient entries denoted by a dashed line indicate that they were not statistically different from zero at the 95% confidence level.

Subject Code	Tvs (s)	$\hat{\beta}$	std($\hat{\beta}$)	$\hat{a}$	std($\hat{a}$)	$\hat{c}$	std($\hat{c}$)	$\hat{d}$	std($\hat{d}$)	$\hat{\gamma}$	std($\hat{\gamma}$)	$\hat{T}_{EP}$	std($\hat{T}_{EP}$)	MSE
dc06s4	37.7	0.286	3.62E-03	-0.48	3.9E-02	3.21E-07	2.6E-06	-------	-------	0.890	3.9E-03	0.404	7.0E-02	2.51
dc06s6	37.3	0.207	4.23E-03	0.09	1.2E-02	-------	-------	-------	-------	0.311	4.7E-03	0.333	2.7E-02	6.23
jl61s5	32.5	0.101	1.66E-03	0.54	4.4E-02	-5.62E-05	4.5E-06	-3.23E-05	2.6E-06	0.941	1.6E-03	0.204	2.8E-02	15.2
jl61s7	32.5	0.096	2.68E-04	1.27	9.8E-02	-------	-------	-------	-------	0.913	5.6E-04	0.218	9.1E-03	4.61
jn08p6	22.5	0.097	1.23E-03	-0.59	4.5E-02	9.17E-05	7.1E-06	-------	-------	0.983	1.4E-03	0.195	1.3E-01	1.16
jn08p5	32.5	0.186	3.29E-03	-3.41	2.6E-01	-1.95E-05	1.5E-06	-2.62E-05	2.8E-06	0.517	3.5E-03	0.800	1.3E-02	2.82
jl61p5	22.5	0.433	7.01E-04	0.00	-------	2.46E-05	1.9E-06	-3.59E-05	2.0E-06	0.517	3.7E-03	0.800	1.3E-01	1.10
mr81p5	7.3	0.395	1.93E-02	5.95	8.0E-01	-------	-------	-------	-------	0.298	1.7E-02	0.475	7.7E-02	26.47
mr81p6	47.7	0.286	1.10E-02	0.07	9.5E-03	-------	-------	-------	-------	0.299	2.6E-02	0.800	3.3E-02	3.61
mr81s6	32.5	0.196	2.07E-03	0.53	6.3E-02	-------	-------	-------	-------	0.337	2.3E-03	0.214	1.0E-02	7.37
mr82p5	47.7	0.424	3.12E-02	6.07	8.0E-01	-1.93E-05	2.6E-06	-4.44E-05	5.9E-06	0.303	1.3E-02	0.438	2.2E-02	10.70
mr82s4	47.7	0.135	1.12E-02	5.92	2.4E-01	-4.46E-05	1.8E-06	-9.99E-05	4.0E-06	1.800	3.5E-03	0.400	9.4E-02	3.27
mr83s5	12.5	0.140	5.61E-03	1.42	1.2E-01	1.37E-05	1.2E-06	-2.23E-05	1.9E-06	0.833	1.5E-03	0.181	2.9E-03	1.47
my58z5	12.5	0.114	1.14E-04	-0.29	2.7E-02	5.59E-05	5.1E-06	-4.12E-05	3.8E-06	0.699	1.7E-04	0.186	2.0E-02	19.92
my58z6	34.5	0.101	1.04E-04	-0.44	3.6E-02	1.41E-04	1.1E-05	-2.04E-05	1.6E-06	0.941	9.4E-05	0.172	3.2E-02	4.92
MEAN	29.1	0.213	0.10	1.11	4.1	5.4E-06	3.1E-04	-7.81E-05	1.2E-04	0.705	0.21	0.388	0.26	4.45

Finally, for the subject recovered from Vestibular Neuronitis (ap68p6), where the recording was performed 5 months after the vestibular episode, the nonlinear envelope fit now yields a better fit than the linear envelope fit, but the Dynamic NL NI model continues to provide the best MSE and AIC (Table 19). The envelope method is able to detect an abnormality in a serious deficit, but not in more 'compensated' patients (e.g. previous paragraph). As we will see below, envelope results can also yield biases in estimated vestibular time constants and presumed integrator function.

Comparisons of the quality of fit with the two methods in all protocols using single harmonics are provided in Tables A.7& A.8. The optimal coefficients (linear or non-linear) obtained by the dynamic NL NI method and the envelope method are detailed in Table 15, Table 16 &Table 17; if a linear model is selected for a trial, then its corresponding quadratic and cubic terms are set to zero. The resulting non-linear coefficients from both methods (cubic vs. quadratic) are also provided as a scatter plot in Figure 22A&B. This highlights the fact that any VOR non-linearity is better segregated between the three subject categories when relying on the dynamic NL NI model (Figure 22B), rather than estimates from the envelope method (Figure 22A) which assumes a constant ideal NI. In Figure 22B, controls are clustered about the origin much more tightly than patients. We did not find any useful clustering in the bias and linear terms obtained from either method, probably because this can be sensitive to stimulus amplitude and nystagmus patterns (personal observations; see also [13]).

Table 16: NL-NI Model Estimates for Left Patients (MD: Meniere's disease, VN: Vestibular Neuronitis; #M indicates recording was performed # months after the first vestibular episode.)

Subject Code	Tvs (s)	$\hat{\beta}$	std(β)	$\hat{a}$	std($\hat{a}$)	$\hat{c}$	std($\hat{c}$)	$\hat{d}$	std($\hat{d}$)	$\hat{\gamma}$	std($\hat{\gamma}$)	$\hat{T}_{EP}$	std($\hat{T}_{EP}$)	MSE
nv10p3 (MD-10M)	12.5	0.33	1.8E-02	14.80	1.20	-1.56E-03	1.3E-04	-2.98E-05	2.4E-06	0.45	3.3E-02	0.276	1.2E-02	1.08
nv10p5 (MD-10M)	12.5	0.08	6.3E-03	3.19	0.28	-1.04E-03	8.3E-05	-1.34E-04	1.1E-05	0.78	1.8E-02	0.284	3.3E-03	1.64
ja67p4 (MD-2M)	12.5	0.09	3.1E-02	1.11	0.02	-7.27E-04	5.8E-05	-9.20E-05	7.4E-06	0.77	1.3E-06	0.150	1.7E-03	0.81
ja67p5 (MD-2M)	12.5	0.50	5.9E-04	-0.92	0.14	-3.12E-04	2.5E-05	-6.60E-05	5.3E-06	0.51	5.2E-03	0.684	2.9E-02	0.54
ap68p6 (VN-5M)	12.5	0.25	4.2E-02	-------	-------	-1.57E-03	1.3E-04	-6.88E-05	5.5E-06	0.25	2.2E-01	0.461	6.6E-03	3.82
ap68z4 (VN-5M)	12.5	0.38	2.1E-03	-3.77	0.06	-3.20E-03	2.6E-04	-2.32E-04	1.9E-05	0.59	6.4E-02	0.475	2.0E-03	1.33
ap68z5 (VN-5M)	22.5	0.12	2.8E-03	-1.30	0.08	-5.22E-03	4.2E-04	-8.88E-04	7.1E-05	0.84	1.3E-02	0.291	2.4E-03	2.07
jn30p6 (VN-1.5M)	12.5	0.18	1.2E-03	-1.15	0.04	-1.65E-02	1.3E-03	-1.49E-03	1.2E-04	0.83	8.5E-03	0.336	1.8E-02	2.38
jn30z5 (VN-1.5M)	12.5	0.71	2.1E-02	1.40	0.74	-1.96E-03	1.6E-04	2.09E-05	1.7E-06	0.36	3.9E-02	0.228	8.6E-03	1.52
jn30z6 (VN-1.5M)	12.5	0.22	6.4E-03	-4.81	0.13	-2.55E-02	2.0E-03	-6.45E-04	5.2E-05	0.55	2.0E-02	0.234	1.9E-03	3.72
MEAN	13.6	0.27	0.39	0.69	3.9	-5.37E-03	1.1E-02	-3.52E-04	7.2E-04	0.61	0.18	0.333	0.24	1.89

Figure 22: A & B) Nonlinear coefficients from (A) the envelope method and (B) the dynamic NL NI method for trials with single sinusoidal stimulus for Controls (N=7), Left patients (N=6) and Right patients (N=7). In A) coefficients are dispersed and overlap in the 3 groups. In B) with the dynamic NL NI coefficients, controls are clustered closer to the origin than patients; note the robust correlation between the sign of the quadratic term and the side of the lesion. C & D) Model coefficients for VOR Tests with pure harmonics C) There is no apparent segregation of the *envelope*

T_{VS} between the 3 groups; T_{VS} estimates from the *dynamic* NL approach, also appear mixed. D) On the other hand, taking full advantage of estimates for both velocity storage and NI time constants (maxima in Figure 25) in the NL NI model, there is a clear segregation of controls from all patients, mainly correlated with poor integrator function. E & F) Coefficients of *f(i)* in the NL NI Model for all subjects and protocols (Controls N=15, Left patients N=10, Right patients N=8). A) Grouped by protocol – showing that multi-harmonics distinguish patients from controls better than single sine rotation; B) Grouped by diagnosis- patients overlapping controls are mainly in the Meniere's pool and presumably compensated while vestibular neuronitis cases are clustered well away from controls especially with complex rotation protocols (compare A & B data points).

Table 17: NL-NI Model Estimates for Right Patients (MD: Meniere's disease, VN: Vestibular Neuronitis; #M indicates recording was performed # months after the first vestibular episode.)

Subject Code	Tvs (s)	β	std(β)	a	std(a)	c	std(c)	d	std(d)	γ	std(γ)	T_{EP}	std(T_{EP})	MSE
oc26p5 (VN-1M)	12.5	0.19	3.8E-04	-2.98	0.07	2.92E-03	2.3E-04	-1.29E-05	1.0E-06	0.45	2.4E-02	0.312	9.3E-04	1.83
oc26p6 (VN-1M)	47.7	0.28	7.1E-03	-1.50	0.60	6.95E-04	5.6E-05	-6.04E-05	4.8E-06	0.54	1.8E-01	0.273	1.8E-02	2.23
mr31p3 (VN-6M)	47.7	0.12	2.6E-04	0.75	0.10	5.59E-03	4.5E-04	-9.33E-05	7.5E-06	0.83	2.2E-02	0.119	3.8E-03	4.72
mr31p4 (VN-6M)	47.7	0.15	4.5E-04	1.74	0.52	5.91E-03	4.7E-04	-9.15E-05	7.3E-06	0.81	5.1E-02	0.170	1.1E-02	2.31
mr31p5 (VN-6M)	12.5	0.25	7.6E-03	4.83	0.35	2.09E-03	1.7E-04	-4.24E-05	3.4E-06	0.84	1.2E-01	0.353	1.5E-02	1.64
mr31p6 (VN-6M)	12.5	0.21	9.6E-04	1.58	0.04	6.20E-03	5.0E-04	-1.63E-04	1.3E-05	0.56	2.2E-03	0.388	5.5E-04	1.02
mr57p6 (VN-12M)	22.5	0.11	2.7E-04	-0.92	0.03	8.22E-03	6.6E-04	-3.36E-04	2.7E-05	0.90	1.3E-03	0.120	1.1E-04	2.14
mr57z5 (VN-12M)	34.5	0.19	3.0E-03	-0.66	0.06	3.01E-03	2.4E-04	-7.23E-05	5.8E-06	0.87	1.4E-02	0.254	2.0E-03	1.94
MEAN	28.2	0.19	0.17	0.36	2.6	4.33E-03	3.3E-03	-1.20E-04	1.1E-04	0.72	0.14	0.249	0.31	4.95

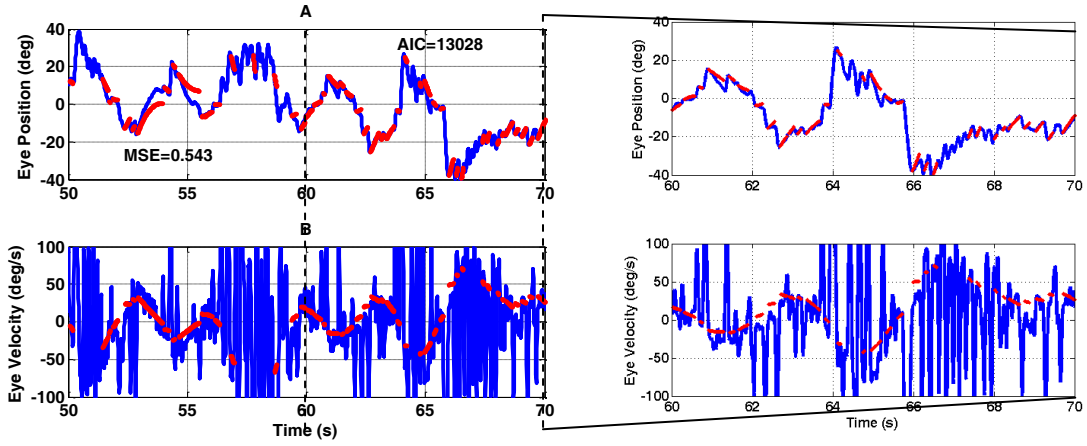

A & B: Linear Model Predictions MSE=0.543, AIC=13028

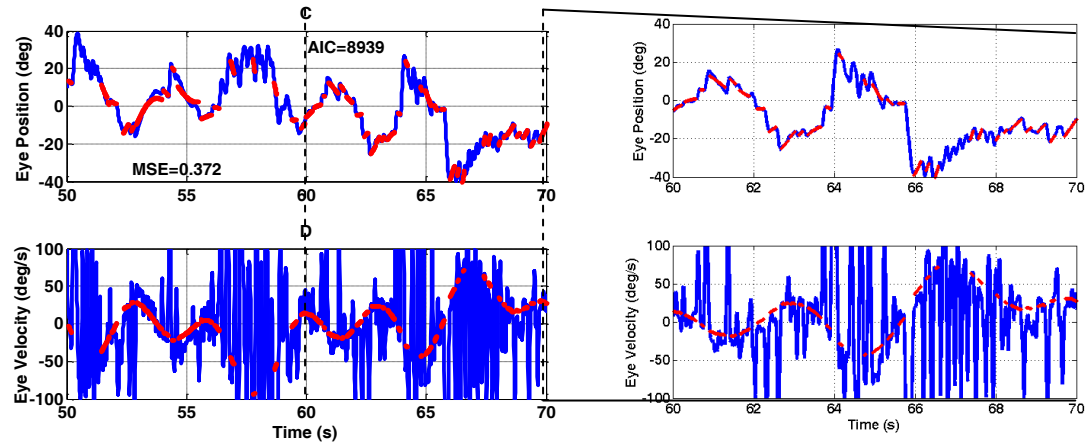

C & D: Nonlinear Model Prediction MSE=0.372, AIC=8939

Figure 23: Validation of identified linear (A: eye position & B: eye velocity) and non-linear (C: eye position & D: eye velocity) models for subject test jn30z6, multiple harmonic rotation: slow-phase predictions given in red, overlapping data in blue. From MSE and AIC criteria, the nonlinear model is justified, despite added complexity (figure zoomed in, but MSE/AIC computed over the whole validation data set, see Methods; N=1598 in validation).

We now turn to a comparison of *estimated dynamics* (VOR time constant (T_{vs}), and maximum NI time constant (T_{NI})). Only the NL NI method allows for the estimation of the NI time constant, and it will be context dependent (discussed below; see also peaks in Figure 25). Figure 22C&D provides the scatter plot for estimated vestibular time

constants with the two methods (Figure 22C): based on T_{vs} alone, there is no clear segregation by subject group and the correlation of estimates from the two groups is very poor. This is explained in part by the assumption of an ideal NI in the envelope method. Yet this assumption must be false in many cases, since the quality of fit is always better with the dynamic NL representation for the VOR. In all cases studied so far, the linear or non-linear options for the dynamic NI model fit produce lower MSEs and yield estimates that segregate more distinctly according to the subject types. Thus in Figure 22D, the NL NI model allows joint viewing of T_{VS} against T_{NI} and unmasks a deterioration of NI function that clearly segregates all patients from controls. Since the dynamic NL model provides the best predictions for the sinusoidal protocols, the assumptions in the envelope method must be faulty and are expected to produce biased and noisy estimates of little help in diagnosis.

6.3.3 Identifying & Selecting NL NI Models for Experimental VOR data

The dynamic NL NI model has the advantage that its application to segments of VOR slow phases can be used in any protocol. Hence, focusing on this method alone, estimates for VOR and NI dynamics are found and compared for the whole database, including both harmonic and mixed harmonic stimuli (see Methods). The intent was to potentially unmask parametric differences between the groups that might not be observable in conventional VOR analysis. All VOR tests were treated the same way: i) identification of the optimal parameter sets was performed assuming a linear model and a non-linear model, on half a data set, ii) by comparing the MSE and AIC for each alternative model in the second half of the dataset, the model with the lowest AIC was selected as the best description, provided that it had the lowest MSE. The optimal parameter estimates for all three subject groups are given in **Table 18** & Table 19 compare the quality of fit obtained from the optimal linear and non-linear model in each case, allowing selection of the best model type for each subject and test record. The analyses that follow are based on the parameters of the selected (optimal) model (Table 15 to Table 17). When a linear model was selected, unused parameters are entered as null (-----). Examples of predictions in one of the trials are shown in Figure 23A & B, for the optimal linear model (Figure 23A)

and dynamic nonlinear model (Figure 23B) of trial 'jn30z6', where the criteria (MSE, AIC) support selection of the non-linear model, though in this case the differences are small.

Table 18: Mean Square Error (MSE) and Akaike's Information Criteria (AIC) for Controls

Subject Code	Linear Envelope Fit		Nonlinear Envelope Fit		Linear Model		Dynamic NL Model	
	MSE	AIC	MSE	AIC	MSE	AIC	MSE	AIC
dc06s4	-----	-----	-----	-----	3.80	911.6	2.51	876
dc06s6	-----	-----	-----	-----	6.72	1014	6.23	1039
jl61s5	-----	-----	-----	-----	22.2	73106	15.2	60609
jl61s7	-----	-----	-----	-----	4.95	1299	4.61	1443
jl61p5	6.75	15614	6.22	14381	1.29	309	1.16	274
jn08p6	8.49	10532	7.86	9748	6.5	15052	2.82	11021
jn08p5	13.0	28244	13.3	29382	2.14	5129	1.10	4383
mr81p5	202	582427	200	575898	26.97	64720	26.47	68880
mr81p6	22.7	55500	16.7	40947	3.52	844	3.61	1022
mr81s6	-----	-----	-----	-----	6.11	1466	7.37	1825
mr82p5	121.6	253735	120.2	250845	13.19	9886	10.70	7078
mr82s4	-----	-----	-----	-----	5.78	2346	3.27	1762
mr83s5	-----	-----	-----	-----	1.76	4214	1.47	3052
my58z5	-----	-----	-----	-----	21.53	51666	19.92	45968
my58z6	-----	-----	-----	-----	5.07	2158	4.92	2374

Table 19: Mean Square Error (MSE) and Akaike's Information Criteria (AIC) for Patients

	Linear Envelope Fit		Nonlinear Envelope Fit		Linear Model		Dynamic NL Model	
Subject Code	MSE	AIC	MSE	AIC	MSE	AIC	MSE	AIC
nv10p3	4.99	7297	4.87	7127	1.86	2075	1.08	1178
nv10p5	8.78	11658	6.78	9004	2.93	7028	1.64	1625
ja67p4	9.12	23245	8.86	22586	1.30	3113	0.81	996
ja67p5	16.9	28295	16.9	28276	0.92	1724	0.54	413
ap68p6	14.3	19178	11.8	16353	9.14	12197	3.82	9193
ap68z4	-----	-----	-----	-----	1.57	3779	1.33	3218
ap68z5	-----	-----	-----	-----	2.54	6103	2.07	4964
jn30p6	43.6	77554	42.0	74726	2.49	5971	2.38	5713
jn30z5	-----	-----	-----	-----	4.41	10585	1.52	3412
jn30z6	-----	-----	-----	-----	5.43	13028	3.72	8939
oc26p5	34.0	63952	33.5	62894	2.15	5120	1.83	4923
oc26p6	49.2	107352	41.5	90486	5.29	12690	2.23	5353
mr31p3	4.82	9245	4.60	74727	82.9	198946	4.72	11320
mr31p4	6.70	9291	5.74	7959	3.62	8889	2.31	6732
mr31p5	9.36	13511	4.71	6798	1.89	4525	1.64	3945
mr31p6	6.10	7920	3.43	4456	1.34	3137	1.02	2904
mr57p6	30.3	73208	29.3	70834	7.08	16991	2.14	5131
mr57z5	-----	-----	-----	-----	3.56	8557	1.94	5127

To verify the convergence of the parameters to the same set of estimates from different initial starting points in the optimization algorithm, we randomly selected a normal trial (jl61s5) and performed the search for the optimal set of estimates from various initial values of the parameters within the constraints (**Table 17**). These constraints included known ranges in eye plant dynamics (T_{EP}) and limitations on loop gains in the system ($1 - \hat{\gamma}\hat{f}'(i) > 0$) to preserve stability in the NL NI responses (for a more detailed explanation on the constraints, please refer to [10]). From the ten different sets of initial values, the optimization process still converged to the same set of estimates. The convergence to the same optimal set from different initial parameters was also observed in the other trials. This implies that the optimization algorithm finds a global minimum, and provides robust repeatable estimates. The characteristics of optimal model descriptions (parameters) will now be examined in terms of the global VOR/NI properties associated with them.

6.3.4 Comparing central nonlinearities in the NI/VOR

The first step compares the estimated nonlinearity (or linearity) of the VN summing junction in the loop (*f(i)* in Eq. (125) and Figure 19) from all trials for the three subject groups (Figure 24). The input range to the nonlinearities was determined by the maximum and minimum values ('*i*' in Figure 19, Eq. (129)) of the input to the VN summing junction, derived from the data set and the estimated gains of the afferent and feedback paths:

$$i_n = \hat{\gamma} e_n - \hat{\beta}\dot{h}'_n \tag{127}$$

Estimated nonlinearities are only reliable over the range of data affecting the estimates, since polynomials are free to form any random shape beyond that range. Hence each individual trial has its own distinct span on the input range to its nonlinearity (or linearity).

Several conclusions can be drawn:

- Controls have symmetrical gains in the summing junction, representing VN premotor cells, and are dominated by linear characteristics (Figure 24A, Table 15);
- Left-patients have higher VN gains for negative inputs (Figure 24B), which corresponds to combinations of rightward head velocity and/or left eye position (Eq. (125)). They also tend to show a saturating behavior for positive inputs corresponding to head velocity towards the lesioned side.
- Right-patients have the opposite behavior from the left-sided patients (C).

Thus, the identified central gain inside the hypothesized NI loop has characteristics consistent with the laterality of the diagnosed vestibular condition. Controls are well represented in majority by a linear model, whereas the patients require the non-linear representation.

Table 20: Initial values for parameter search in the optimization process

	$\hat{\beta}$	$\hat{a}$	$\hat{c}$	$\hat{d}$	$\hat{\gamma}$	$\hat{T}_{EP}$
Initial Values	0.1	0	0	0	0.8	0.3
	0.2	1	0	0	0.8	0.3
	0.1	1	0.1	0	0.8	0.3
	0.15	-2	-0.1	0.1	0.8	0.3
	0.25	-1	-0.1	0.1	0.6	0.3
	0.15	2	0	-0.1	0.8	0.2
	0.05	1	-0.1	-0.1	0.6	0.15
	0.15	1	-0.5	0.1	0.9	0.35
	0.15	1	-0.1	-0.01	0.7	0.2
	0.10	0.5	0.02	0.01	0.8	0.3
Optimal Set	0.101	0.54	-5.62E-05	-3.23E-05	0.941	0.204

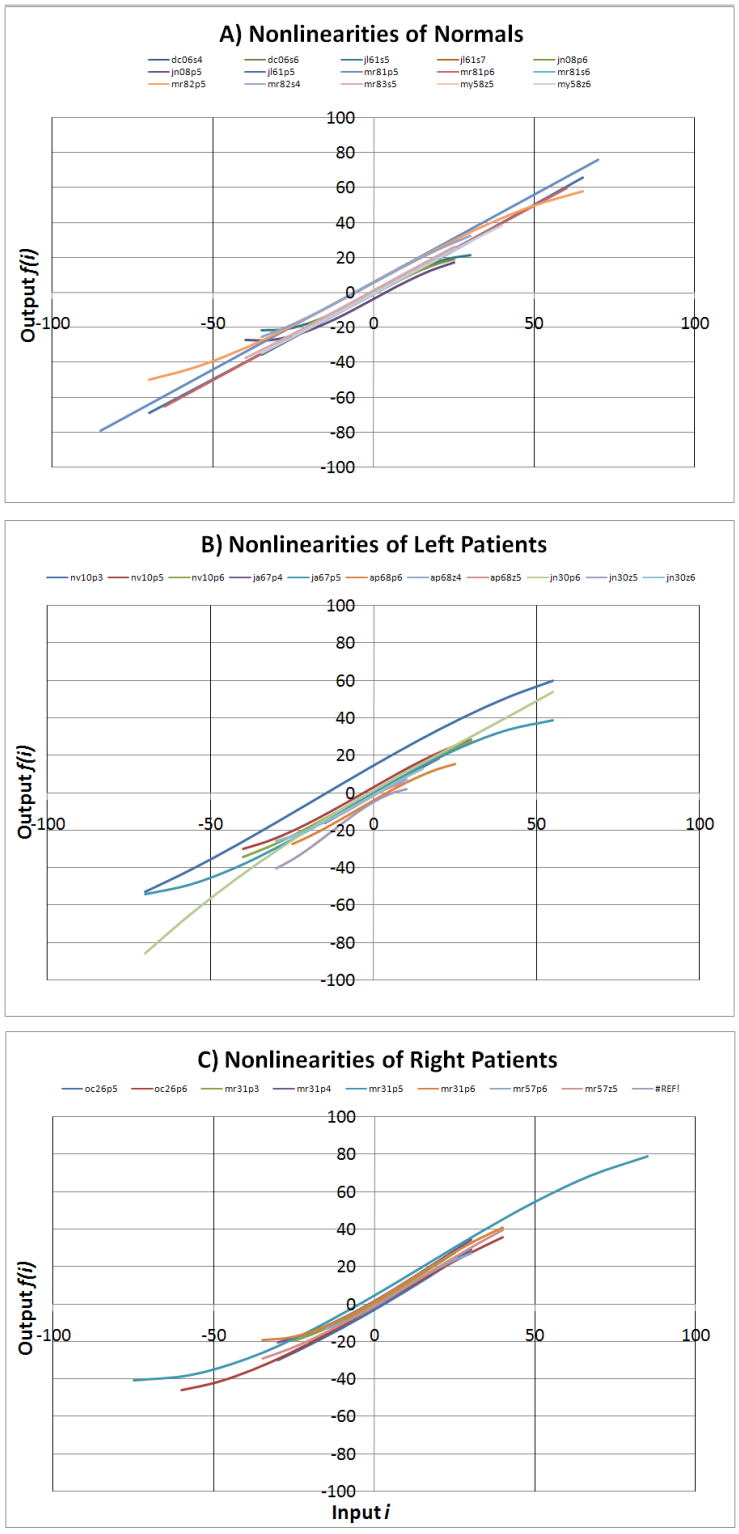

Figure 24: Estimated Nonlinear Gains f(i) (see Fig. 1) for controls and Left or Right Patients. See text for control/patient comparisons on the shifts in context and preferred gain zones.

6.3.5 Evaluating context-dependence of VOR gain and NI time constant:

For non-linear descriptions, the dynamics of the NI and VOR become dependent on the operating range of i, which itself varies with the range of head velocities and excursions in eye position during a given protocol (see Eq. (122)-(124)). The degree of this variability could be a significant factor in detecting lesions or anomalies.

Before examining estimated parameters individually, it is instructive to examine the VOR characteristics that are associated *globally* with the estimated VOR models as a function of the input 'i': the apparent NI time constant $\hat{T}_{NI}$ and VOR gain $\hat{G}_{VOR}$, as given respectively by Eq. (123) and Eq. (124). Again a clear pattern emerges in Figure 25:

- Most Controls have very stable $\hat{T}_{NI}$ and $\hat{G}_{VOR}$ even when their best model is non-linear. The range of large time constants (>2s) is quite broad in each case and clustered around i=0 (Figure 25 A&B); similarly, the VOR gain is either constant or with peaks near i=0 (mean gain=-0.60 ±0.21).
- Left patients have narrow ranges for effective $\hat{T}_{NI}$ with peaks shifted to the left (mean 1.18s ±0.69) – indicating a preference for right head turns and/or leftward deviations in eye position. (Figure 25 C&D). The high-frequency VOR gain, $\hat{G}_{VOR}$, tends to increase with rotation to the contralateral side (negative '*i*' in Eq. (125)). The dynamics of the NI and VOR in these subjects imply improved performance for contralateral head turns (to the right) and/or desirable ipsilateral biases in eye position (to the left).
- Right patients have a similar pattern with reversed directions. $\hat{T}_{NI}$ peaks (mean 1.72s ±0.90) are shifted toward leftward rotation and/or ipsilateral (right) eye deviation, and $\hat{G}_{VOR}$ increases its level for (contralateral) leftward rotation.

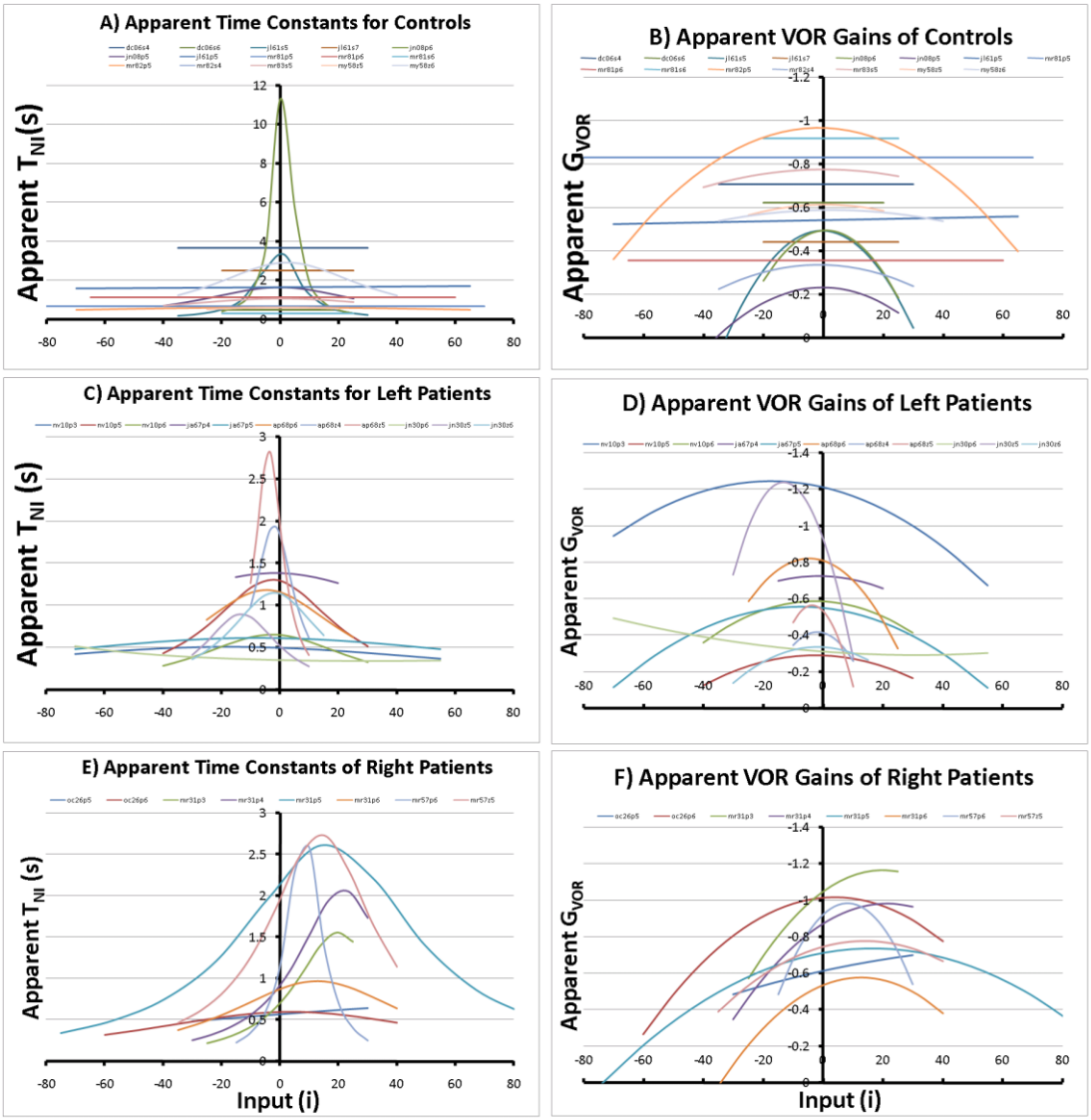

Figure 25: Estimated NI Time Constant and VOR gain as a function of the operating range of the input to the VN summing junction (i in Fig.1), while all protocols are included. A & B: Controls; C&D: Left patients; E&F: Right patients. Note different scales with lateral shift and broadening of NI curves in patients.

Furthermore, the operating ranges of the VN input i are different for the various subject groups: Left patients have their operating range centered towards the negative side of the i axis (with a mean center of the operating range at $i = -4.1 \pm 4$) while Right patients have their range centered towards the positive side on the i axis (with a mean

center of the operating range at $i = 1.9 \pm 5$). This suggests that the patients' operating range is part of the mechanism to compensate, or boost, responses during rotation towards the lesioned side, by shifting a non-linear curve so that its peak now coincides with the weaker sensory context.

The measured means in time constants and gains have a robust pattern across the 3 groups, but the standard deviations (quantitative estimates) can be quite large. This is likely due to the fact that all test patterns were grouped in this analysis: rotation with single harmonics and sum of sines. The next step explores the effects of protocols on the parameter estimates, and hence on the estimated VOR function.

6.3.6 Segregation of Data according to Stimulus Type

Artifacts in the nonlinear coefficient distribution could be introduced by the pooling of different protocols when collecting data from subjects. As mentioned in the Methods section, the VOR data were recorded from rotation either with a single sinusoid (0.167Hz) or a sum of multiple sinusoids (0.03Hz, 0.1Hz and 0.17Hz). The root mean squared values for the head velocity in two protocols were set to be the same to provide comparable power content in the two protocols. By re-categorizing the controls group and the patients group according to protocol, we obtain scatter plots for the following four categories: patients in a single sinusoid protocol, patients in a multiple sinusoids protocol, controls stimulated in a single sinusoid protocol, and controls in a sum of multiple sinusoids (Figure 22E). The nonlinear coefficients from both groups of patient data are further from the origin, and this aspect is emphasized for more complex inputs (1.04±0.25E-3 for the multiple sine rotation and 3.00±1.4E-4 for the single sine rotation); the control parameters acquired with both stimuli are much closer to the origin, with the mean distance from the origin of 1.2±0.8E-4 for the multi-sine protocol and 3.2±1.1E-4 for the single sine stimulus protocol. The plots confirm that complex stimuli enhance the detection of the side of a vestibular deficit.

6.3.7 Segregation of Data based on Diagnosis

Symptoms of vestibulopathy are intermittent for subjects with Meniere's disease (MD) [24], where some MD patients may not be exhibiting any vestibular abnormalities during the recording sessions. In order to discriminate between possibly transient deficits and more permanent ones, we segregate the patients' data into their respective categories (left and right Vestibular Neuronitis, left and right Meniere's disease and controls), and replot the nonlinear coefficients' distribution (Figure 22F). As before, the coefficients of the control group cluster around the origin, but it is now clear that it overlaps patient coefficients which belong to the Meniere's diagnosis. Patients with Vestibular Neuronitis have nonlinear coefficients that are much larger. The trials from patients suffering from Meniere's disease have their quadratic terms slightly deviating from the origin (with the mean for the quadratic terms of -1.04±0.5E-3 for patients with left sided Meniere's disease compared to -0.14±3.2E-5 for controls, $p<0.05$, t-distribution).

In Figure 22F, the coefficients of patients with Vestibular Neuronitis are located far from the origin when compared to the controls and patients with Meniere's disease. Furthermore, a number of coefficient sets from the Meniere's disease group appear indistinguishable from the controls coefficient sets. This may be due to the fact that some MD patients were not experiencing any vestibular malaise at the time of recording as mentioned earlier. On the other hand, the patients with prior Vestibular Neuronitis were recorded between 1 to 12 months from their primary episode.

6.4 Discussion

It has been demonstrated here that the function of gaze holding or oculomotor neural integration (NI) could vary with concurrent ocular context and VOR protocol [7]. This suggested that the dynamics of the NI are labile, varying with different eye position and head velocity set-points. Many previous models of the neural integrator in the oculomotor system rely on neural network formulations which are inherently non-linear in their elements, but are designed through large populations, to produce relatively linear behavior at the motor level [25]-[29]. A model is proposed here that *preserves* the

characteristics of local non-linearities at the global level, to replicate the experimentally derived properties. The model can describe context changes in NI values, and improved prediction of VOR data from normal subjects [10]. To accommodate for possible asymmetry in VOR patients, a third order polynomial was proposed here as the nonlinearity in this NI model (Eq. (116)). This model representation is first validated and then applied to VOR records from controls and vestibular patients.

Comparing the results from this model fitting exercise to traditional envelope analysis demonstrates that data fits and detection of deficits are improved with the non-linear NI model, and most robust with complex multi-frequency rotation profiles. The analysis approach allows the use of complex inputs, since it does not rely on steady-state envelopes to estimate the VOR phase, and it can probe the VOR over a broader frequency range. The number of patients here is relatively small, but the detected trends are very strong. They warrant a careful comparison of NI dynamics over a much larger pool of controls and patients, now underway.

6.4.1 Context Dependence of Neural Integrator and VOR Gain

The study here confirms that the classical gaze integrator or NI in oculomotor control is context dependent and often non-ideal (small time constant); it rarely achieves values over 15s, and this over narrow ranges of context; in patients the peak levels can be very small (< 3s) and are shifted to a context favoring contralateral head velocity and ipsilateral eye position with respect to the side of the deficit. Hence the hypothesis of non-ideal NI function is confirmed in patients and even some controls (Figure 25). The implication is that for most subjects, both the NI and the VOR dynamics will co-vary with the protocol type and with concurrent levels of eye position and head velocity. The more complex and intense the head rotation profile, the better controls can be segregated from patient responses. In contrast, envelope measures are not likely to take advantage of this, since estimated parameters are sensitive to both the nystagmus frequency and average eye deviations, creating noisy estimates.

The central nonlinearities from the different subject groups exhibited trends consistent with the subject groups: controls often had a linear NI representation or symmetric mild non-linearity about zero; nonlinearities of patients with left side vestibular deficiencies tend to have a higher gain for negative input to the nonlinearity, while the nonlinearities of patients with right side vestibular deficiencies have a higher gain for positive input to the nonlinearity (Figure 24). As a result, the maximal NI time constants and VOR gains will be shifted towards the same context, and decrease their performance with deviations from this optimal. Normal controls have a relatively broad operating range, but patients can have a very narrow range for adequate NI and VOR function (Figure 25). Optimal gaze holding performance (NI time constant) and VOR gain in patients are achieved during rotations contralateral to the lesion *combined with* eye deviations ipsilateral to the lesion. This could explain the tendency in compensated patients to produce nystagmus with a mean deviation towards the healthy side [14]. With the context-dependent NI model, the clearest indicator of VOR deficits is degradation (lower values) of the NI time contant, and highly tuned context-dependence.

6.4.2 Useful Trends in Model Coefficients from Patients and Controls

The section above addressed the results of model fitting on the *global* dynamic properties of the VOR and NI with context. Here we focus on the actual model coefficients estimated in the model identification step. We compare the estimates for subjects with vestibulopathy such as Meniere's disease and Vestibular Neuronitis against those from normal subjects. First at the sensory level, estimated time constants for the vestibular signal (T_{vs}) were always relatively large (>10s) using the NL NI model in the VOR, regardless of clinical status in this patient pool. Using the envelope approach, T_{vs} was very noisy (5-28s), with large overlap in the subject groups. Hence the estimate of vestibular sensory dynamics is not very useful on its own to detect anomalies. However, with the NL NI model, there is a significant trend for clustering of the combined estimates for the vestibular and NI time constants between controls and patients (Figure 22D). The other parameters of the VOR model are: the eye plant time constant (T_{EP}), the afferent vestibular gain (β) and the central feedback gain (γ), only

γ showed a noticeable trend between normal subjects and patients, with higher γ in normal subjects. Higher γ are associated with larger NI time constants (Eq. (123)), and this is already discussed above.

The remaining model coefficients involve the description of the internal non-linear gain f(i). The cubic and quadratic nonlinear coefficients(eq.(116)) were the most significant terms related to vestibular state, lying much further from the origin for vestibular patients than for controls (Figure 22F). The associated intensified context dependence of the VOR and NI can be considered a sign of clinical anomaly. It has long been assumed that deficits are localized in the vestibular primary afferents in patients with Vestibular Neuronitis [30] and Meniere's disease [31], but their long term effects on the entire vestibular network are yet to be studied. Our results suggest that at least the nonlinearity of the Neural Integrator behaves differently for subjects with long-term vestibulopathy, even if its origin is peripheral. Compensation for a peripheral deficit apparently requires central re-organization with negative side-effects on the oculomotor 'integrator'.

This paper presents a VOR model containing a single nonlinearity at the site of the Neural Integrator to mimic the 'set-point' dependent characteristic previously found even in gaze holding [7s]. Differences in the form of the non-linearity are evident when comparing the VOR of normal subjects to patients even after compensation A second nonlinearity would be required before the NI process to disassociate the variation of NI dynamics from potential set-point effects at the peripheral sensors/velocity storage stage. This approach might allow for a single set of model parameters in all protocols, instead of the current changes in estimated models with protocols in the same subject (Table 15, **Table 16 Table 17**). An alternative would also be to include data from all protocols in a given subject to find a single optimal model representation valid globally.

6.4.3 Comparing VOR dynamics obtained in different laboratories

We compared the estimated parameters from data acquired in different rotational profiles with two conclusions: first as expected from identification theory, a richer stimulus, such as one containing multiple sinusoidal profiles, allows a more accurate description of the VOR system dynamics compared to the single sinusoidal profile and most importantly, unmasks larger differences between controls and patients; second, with a context-dependent VOR-NI process, the selected protocol bandwidth and intensity can affect the values obtained for model coefficients by changing the sensory-motor context. As a result, it becomes impossible to directly compare the estimates of VOR function from other laboratories using different rotation trajectories, not to mention the unreliable envelope method for VOR analysis. Therefore, it is necessary to reach a consensus on clinical VOR protocols and analysis methods to allow comparisons. At the very least, data sets should now be coalesced and become available to multiple laboratories for testing of algorithms and for consistent comparison of results.

6.5 APPENDIX

6.5.1 Defining the optimization equations

In a previously published paper, we presented the Dynamic Nonlinear Model for the Neural Integrator (NI) which models the varying nature of the apparent dynamics of the NI [10]. It consists of a static nonlinearity within the feedback loop (Figure 19). The eye plant dynamics $D(s)$ are modeled by a first order low-pass filter with the form:

$$D(s) = \frac{1}{T_{EP}\, s + 1} \tag{128}$$

Since the parameter estimation process is carried out in the discrete domain, the eye plant dynamics are then converted into the discrete domain as:

$$D(z) = \frac{\tau(1 + z^{-1})}{2T_{EP} + \tau + (\tau - 2T_{EP})z^{-1}} \tag{129}$$

Where τ denotes the sampling interval of the data and z^{-1} is the delay operator. As a result of combining this with the equations in METHODOLOGY, the following summarizes the relationship between the variables in the Dynamic Nonlinear NI model:

$$i_n = e^*_n - \beta \dot{h}'_n \tag{130}$$

$$\mu_n = f(i_n) \tag{131}$$

$$e^*_n = \frac{2T_{EP} - \tau}{2T_{EP} + \tau} e^*_{n-1} + \frac{\gamma\tau}{2T_{EP} + \tau}(\mu_n + \mu_{n-1}) \tag{132}$$

$$e_n = \frac{2T_{EP} - \tau}{2T_{EP} + \tau} e_{n-1} + \frac{\tau}{2T_{EP} + \tau}(\mu_n + \mu_{n-1}) \tag{133}$$

Where the subscript n denotes a variable at sample time n ; i corresponds to the internal state i (Figure 19) merging head velocity and eye position states, e^*_n denotes the internal estimate of the eye position, β denotes the afferent gain of the system, $\dot{h}'$ is the input head velocity as detected by the semi-circular canal, μ corresponds to the output of the nonlinear function $f(i)$, T_{EP} is the eye plant time constant, γ corresponds to the feedback gain for the internal estimate of the eye position, and e is the output eye position of the system. For a further description of the model, please refer to Chan & Galiana 2008.

By incorporating the definition for the non-linearity (Eq. 1) into the set of equations above, the output of the system e_n becomes:

$$e_n = \frac{2T_{EP} - \tau}{2T_{EP} + \tau} e_{n-1} + \frac{\tau}{2T_{EP} + \tau} \begin{bmatrix} 2a + \{\gamma(e_n + e_{n-1}) - \beta(\dot{h}'_n + \dot{h}'_{n-1})\} \\ + c\{(\gamma e_n - \beta \dot{h}'_n)^2 + (\gamma e_{n-1} - \beta \dot{h}'_{n-1})^2\} \\ + d\{(\gamma e_n - \beta \dot{h}'_n)^3 + (\gamma e_{n-1} - \beta \dot{h}'_{n-1})^3\} \end{bmatrix} \quad (134)$$

This equation, together with the minimization criteria, is used to estimate the optimal model parameters to represent the slow phases of the VOR response over the whole recording interval (see Methods).

6.6 Acknowledgement

We thank Dr. A. Katsarkas from the Montreal Royal Victoria Hospital (Dept. Otolaryngology, Montreal QC, Canada) for providing the clinical background for subjects presented in this paper.

6.7 References

[1] Idoux, E, et al. "Oscillatory and Intrinsic Membrane Properties of Guinea Pig Nucleus Prepositus Hypoglossi Neurons In Vitro." *Journal of Neurophysiology*, 2006: 175-196.

[2] Mettens, P, E Godaux, G Cheron, and H L Galiana. "Effect of Muscimol Microinjections Into the Prepositus Hypoglossi and the Medial Vestibular Nuclei on Cat Eye Movements." *Journal of Neurophysiology*, 1994: 785-802.

[3] Navarro-Lopez, Juan de Bios, J C Alvarado, J Marquez-Ruiz, M Escudero, J M Delgado-Garcia, and J Yajeya. "A Cholinergic Synaptically Triggered Event Participates in the Generation of Persistent Activity Necessary for Eye Fixation." *The Journal of Neuroscience*, 2004: 5109-5118.

[4] Cannon, S C, and D A Robinson. "Loss of the Neural Integrator of the Oculomotor System from Brain Stem Lesions in Monkey." *Journal of Neurophysiology*, 1987: 1383-1409.

[5] Aksay, E, R Baker, H S Seung, and D W Tank. "Anatomy and discharge properties of pre-motor neurons in the goldfish medulla that have eye-position signals during fixations." *Journal of Neurophysiology*, 2000: 1035-1049.

[6] Ritchis, L. "Effects of Cerebellar Lesions on Saccadic Eye Movements." *Journal of Neurophysiology*, 1976: 1246-1256.

[7] Chan, W W P, and H L Galiana. "Integrator function in the oculomotor system is dependent on sensory context." *Journal of Neurophysiology*, 2005: 3709-3717.

[8] Crawford, J, and T Vilis. "Modularity and parallel processing in the oculomotor integrator." *Exp. Brain Res.*, 1993: 443-456.

[9] Khojasteh, E, and H L Galiana. "A non-linear model for context-dependent modulation of the binocular VOR." *IEEE Trans. Biomedical Engineering*, 2006: 986-995.

[10] Chan, Wilbur W P, and Henrietta L Galiana. "Modeling the Non-Linear Context Dependency of the Neural Integrator in the Vestibulo-Ocular Reflex." *IEEE Transactions on Biomedical Engineering* 55:1946-1955, 2008.

[11] Smith, H L, W W P Chan, and H L Galiana. "Optimizing Clinical Protocols to Test VOR Nystagmus." *Neural Control of Movement 15th Annual Meeting.* Key Biscayne: Neural Control of Movement, 2005. H5.

[12] Minor, L B, D M Lasker, D D Backous, and T E Hullar. "Horizontal vestibuloocular reflex evoked by high-acceleration rotations in the squirrel monkey. I. Normal responses." *Journal of Neurophysiology*, 1999: 1254-1270.

[13] Galiana, H L, H Smith, and A Katsarkas. "Comparison of linear vs nonlinear methods for analyzing the VOR." *Acta Otolaryngol*, 1995: 585-596.

[14] Galiana, H L. "A nystagmus strategy to linearize the vestibulo-ocular reflex." *IEEE Trans. Biomed. Eng.*, 1991: 532-543.

[15] Guitton, D, D P Munoz, and H L Galiana. "Gaze control in the cat: studies and modeling of the coupling between orienting eye and head movements in different behavioral tasks." *Journal of Neurophysiology*, 1990: 509-531.

[16] Shikin, E V. *Handbook and Atlas of Curves.* Florida: CRC Press Inc., 1995.

[17] Goldberg, J M, and C Fernandez. "Efferent vestibular system in the squirrel monkey: anatomical location and influence on afferent activity." *J. Neurophysiol.*, 1980: 986-1025.

[18] Robinson, D A. "The effect of cerebellectomy on the cat's vestibulo-ocular integrator." *Brain Research* 71 (1974): 195-207.

[19] Raphan, T, and B Cohen. "Brainstem mechanisms for rapid and slow eye movements." *Annu Rev Physiol.*, 1978: 527-552.

[20] Sylvestre, P, and K E Cullen. "Quantitative Analysis of Abducens Neuron Discharge Dynamics during Saccadic and Slow Eye Movements." *J. Neurophysiol.*, 1999: 2612-32.

[21] Abadie, J, and J Carpentier. "Generalization of the Wolfe Reduced Gradient Method to the case of Nonlinear Constraints." In *Optimization*, by R. Fletcher, 37-47. New York: Academic Press, 1969.

[22] Akaike, H. "A new look at the statistical model identification." *IEEE Trans. Automatic Control*, 1974: 716-723.

[23] Paige, G. "Nonlinearity and asymmetry in the human vestibulo-ocular reflex." *Acta Otolaryngol*, 1989: 1-8.

[24] Stapleton, E, and R Mills. "Clinical diagnosis off Meniere's disease: how useful are the American Academy of Otolaryngology Head and Nech Surgery Committee on Hearing and Equilibrium guidelines?" *The Journal of Laryngology & Otology*, 2007: 1-7.

[25] Mensh, B D, Aksay, E, Lee, D D, Seung, H S, Tank, D W. “Spontaneous eye movements in goldfish: oculomotor integrator performance, plasticity, and dependence in visual feedback.” *Vision Res* 44(7): 711-26, 2004.

[26] Cannon, S C, Robinson, D A, and Shamma S. “A Proposed Neural Network for the Integrator of the Oculomotor System.” *Biol Cybern* 49(2):127-36, 1983.

[27] Seung, H S, Lee, D D, Reis, B Y, Tank, D W. “Stability of the Memory of Eye Position in a Recurrent Network of Conductance-Based Model Neurons.” *Neuron* 26(1):259-71, 2000.

[28] Aksay, E, Olasagasti, I, Mensh, B D, Baker, R, Goldman, M S, and Tank, D W. “Functional dissection of circuitry in a neural integrator.” *Nat Neurosci* 10(4): 494-504, 2007.

[29] Galiana, H L, and Outerbridge, J S. “A bilateral model for central neural pathways in vestibuloocular reflex.” *J Neurophysiol* 51(2): 210-41, 1984.

[30] Goebel, J A, W O'Mara, and G Gianoli. "Anatomic Considerations in Vestibular Neuritis." *Otology & Neurotology*, 2001: 512-518.

[31] Sando, I, Y Orita, and B E Hirsch. "Pathology and pathophysiology of Meniere's disease." *Otolaryngologic clinics of North America*, 2002: 517-528.

7. Conclusion and Future Work

7.1 Conclusion

The analyses and experimental data appearing in this thesis were all aimed at testing the hypothesis that the classical Neural Integrator in the oculomotor system is not ideal, but in fact leaky and context dependent. This required

- Demonstrating the validity of the hypothesis in a simple protocol (Chapter 4)
- Developing new identification tools and models that could replicate such context-dependent behavior (Chapter 5)
- Fitting the new models and classical alternatives to clinical VOR data from controls and vestibular patients (Chapter 6)

The first two components of this work appear in published articles, and the third has been submitted to IEEE TBME. The following paragraphs summarize the results and their implications to oculomotor physiology, clinical diagnosis and perceptions of motor control.

A Leaky Neural and Labile Integrator

The observations from *Chapter 4* suggests that the Neural Integrator (NI) in the oculomotor system exhibits labile dynamics that depend on input and output oculomotor set-points, i.e. the current combination of sensory (head velocity) and motor levels (eye deviation). Two different experimental protocols were used to examine the possible context-dependent characteristics of the Neural Integrator. In one protocol, the Vestibulo-Ocular Reflex during horizontal rotational head profiles of either a single harmonic or sum of multiple harmonics were measured; in the other protocol, head fixed gaze shifts to various spatial targets were recorded and the trajectory of decaying gaze holding attempts in the dark were recorded. The NI characteristics from the two protocols differ

greatly : the NI time constant measured during decaying gaze shifts in the dark is much larger than that estimated during VOR reflexes. This suggests a labile NI mechanism. Furthermore, the NI dynamics also varied when binning the VOR data (from the first protocol) in a given protocol with respect to different ranges of input (head velocity) and output (eye position) levels. When modeling the NI as a first order low-pass filter, the apparent Neural Integrator time constant (T_{NI}) is observed to be at its maximum when both the conjugate eye position and the concurrent head velocity are close to zero; the T_{NI} decreases as the head velocity and/or the eye position deviate from the origin. These results pointed to the need to develop a new nonlinear formulation for the NI

A Model for the Labile Integrator –imbedding central cells that combine sensory and motor information

The above observation prompted us to modify existing, constant and ideal, models for the NI to accommodate for the variation in the apparent NI dynamics. In *Chapter 5*, a previous bilateral model of the VOR using positive feedback around models of the eye plants to achieve the function of 'integration' (large time constants) was presented. This feedback approach was modified to include a nonlinearity in the loop, representing non-linear premotor Position-Vestibular cells in the VN. As a result, the model characteristics allow for non-linear changes in the performance of the NI as observed experimentally. It yields apparent dynamics that are set-point dependent. The 'gain' of the nonlinearity, or the ratio between its input and output, affects the time constant and gain of the NI process: a lower nonlinear 'gain' yields a lower NI time constant and gain in the associated sensorimotor context. Thus, during the parameter estimation process, the apparent 'gain' of the nonlinearity is tuned to yield NI dynamics that correlate with those observed. Validation of the identification (parameter estimation) algorithms was provided with simulated VOR data and applied to data from normal subjects. This model is called a dynamic nonlinear formulation for the NI in VOR processes – hence the acronym NL NI in Chapter 5. In all normal cases tested so far, the NL NI formulation fit gaze holding trajectories and VOR responses in some cases as well as traditional models, but in most cases with much improved residuals in the range of the noise on the recordings.

In controls, the NL NI appears to reflect better the underlying dynamics in oculomotor circuits, during gaze holding and VOR. Since it is shared by all ocular reflexes including VOR, pursuit and OKN and saccades, it is logical to assume that a better model structure should have a more robust capacity to detect differences between normal subjects and patients. That is model identification could help in clinical diagnosis of deficits in oculomotor pathways.

Clinical Relevance of the NL NI Approach

A NL NI process was found to be a more accurate description of the function of the neural integrator during gaze holding even in normal subjects. This NI process supports the function of all ocular reflexes including the VOR. Hence a non-linear integrator of necessity would be expected to be associated with dynamic non-linear characteristics in VOR responses, and that this would be aggravated in patients. In *Chapter 6*, a pilot study to test these hypotheses was performed on patients with peripheral vestibular deficits during and after long-term compensation. The expectation was that trends in the nature of the non-linearity in a postulated NL NI process could be consistent with the state of a patient and/or the side of the peripheral deficit. In many long-term compensated cases, classical analysis of the VOR often reported return to normal in VOR tests, and so often fail to detect a long-term compensated sensory deficit.

The Dynamic NL NI formulation was used to calculate NI parameters and VOR dynamics in a database of human VOR recordings from normal subjects and patients suffering from VOR dysfunctions. In most instances (60% of controls and 100% of patients), the dynamic NL NI model following a sensory VOR process yields superior prediction of the recorded data compared to the traditional VOR representations assuming linearity and a perfect NI. The variation of the NI dynamics projected from the model estimates differ greatly between different subject groups, allowing for robust detection of patients versus controls and the side of the sensory deficits. This was true even in patients whose VOR behavior is indistinguishable from that of the control when studied using the other classical VOR analysis techniques. Hence the Dynamic NL NI

model could be used to effectively segregate VOR patients from normal subjects in diagnostic tests of vestibular function both at the acute and the compensated stages.

7.2 Original Contributions

The following original contributions/discoveries are claimed as part of the thesis:

- First demonstration that head-fixed gaze shifts in the dark are followed by decay rates sensitive to the initial orbital eye deviation – the so-called oculomotor neural integrator depends on sensory-motor context.

- Demonstration that the NI context dependence extends to concurrent sensory-motor context in the VOR (head-fixed vs passive head-turns)

- Development of a NL NI model that replicates observed behavioural changes with combined sensory-motor context

- Development and validation of identification techniques that can optimally fit the NL NI model in any ocular reflex containing nystagmus

- Development of a tool to determine the precision of the parameter estimates in the non-linear model fitting process, and thereby allow model 'pruning'. Based on the mean squared error formulation for the cost function in the process of optimization, we were able to derive the Taylor Series based estimates on the standard deviation of the parameters.

- Demonstration that both controls and unilateral vestibular patients can have significant central non-linearities. Despite apparent global symmetries using traditional VOR analysis in controls and many compensated patients, the non-linearity from the NL NI representation is more symmetric in controls while it is asymmetric and shifted towards the side of the lesion in patients, regardless of compensation state.

- Demonstration that the degree of nonlinearity (amplitude of higher order coefficients in model) is much higher in patients than controls, allowing detection of the side of a deficit even after long-term compensation.

- Demonstration that the working range of the NL NI and VOR in controls is broad while that in patients is narrow, of much smaller amplitude and shifted towards the side of the lesion.

7.3 Future Work

The contributions above indicate that the NI and VOR can no longer be presumed to be well represented by constant dynamics, with or without static non-linearities. Dynamic non-linearities are present in the ocular reflexes considered and this, together with the presence of nystagmus, requires models and analyses that allow for such characteristics. This thesis relied on models with non-linearities imbedded in a loop, thereby causing responses to be highly context-dependent (hence dynamic nonlinearity) and protocol dependent. For further applications in general studies of central neural processes participating in the control of eye movements, several directions for further work can be suggested.

Extending or Refining the NL Sites in the Proposed Models

As presented, the structure of the NL NI model can represent behavioural non-linearities relying on local non-linear premotor centres in the VN, and/or in the eye plants. These two sites are not distinguishable in the current model, since it places a model of the eye plant inside the feedback loop that creates the function of 'integration'. Hence if the eye plant is non-linear it is expected that this non-linearity would be included in the loop model, creating the same form assumed here, merging a premotor non-linearity with a motor-model non-linearity. The behavioural effect would be the same, resulting in context-dependence of the NI performance. However it should be possible to at least evaluate the site and weight of a NL contribution from VN versus eye plant sites (if any). One approach for neurophysiologists would be to identify any non-linear component in

the dynamics of relationships between measured VN responses and eye responses, between VN responses and motoneural responses and finally between motoneural responses and eye responses in matched protocols.

The Dynamic NL NI model currently consists of a single nonlinearity within a feedback loop, and allows description of the context-dependent dynamics of the so-called neural integrator. In effect it is forced to merge the NI non-linearity with potential sensory non-linearities that occur before projecting onto the NI. A second nonlinearity can be included before the feedback loop to dissociate the variability of the VOR gain caused by the sensor stage from those caused by the NL NI time constant. The site of abnormalities in a VOR patient may be better pinpointed with such model. Also, it would allow discriminating the source of the nonlinearity in controls (normal subjects with apparently no vestibular deficits) – it could be due in part to symmetric but limited (saturating) responses in bilateral sensors. Protocols for the identification of these more complex models would have to be designed carefully to ensure sufficiently 'rich' inputs for robust estimates. Testing with simulated data would help in the design process.

The VOR model in the thesis combines a postulated NL NI circuit cascaded with a vestibular sensory process. This passive VOR model should be extended to include visual feedback with the addition of a visual pathway involving say the Superior Colliculus (Guitton 1991), and the coordination of eyes and head in head-free gaze control. This would allow analytical exploration of the behavioural effect of non-linearities in visual vs dark protocols, head-fixed vs head-free, etc.

Applications in the Clinic and Basic Research

A limited number of experimental trials were used in the thesis to compare the difference between the apparent NI dynamics of normal subjects and VOR patients, and to demonstrate feasibility and consistency of deficit detection. With the addition of a second sensory nonlinearity, a more systematic study can be carried out in a larger number of patients to map out the different model parameters with respect to VOR abnormalities.

Clustering of identified coefficients would offer the possibility of quantitatively-guided diagnosis and distinction between peripheral and central deficits. Studies so far focused on the passive rotational VOR acquired in the dark, and associated *conjugate* eye movements. Concurrent studies on the VOR and its modulation with target depth suggest that the VOR is likely to have both vergence and conjugate components in the dark (Khojasteh & Galiana 2006). Hence all VOR tests should include *binocular* recordings and explore the dynamics of crosstalk between version and vergence.

Since the NI apparently has significant non-linearities, and is imbedded in reflexes such as pursuit and the VOR, the results here imply that all reflexes are likely to be significantly context-dependent. This has not been considered previously. In fact the formulations above would imply that context-dependence could depend on both fusion of sensory modalities (retinal, vestibular, etc) and on available motor platforms to achieve a goal (eyes, head, body…)

All the questions above can also be posed in the analysis of central cell activities in animal experiments (cat or monkey) to determine if the context-dependence appears at the expected pre-motor levels and on which type of cells. This would have significant impact on our understanding of how the brain tunes motor behavior with the task at hand, without necessarily switching between separate task-dependent controllers.

Bibliography

Abadie, J, and J Carpentier. "Generalization of the Wolfe Reduced Gradient Method to the case of Nonlinear Constraints." In *Optimization*, by R. Fletcher, 37-47. New York: Academic Press, 1969.

Akaike, H. "A new look at the statistical model identification." *IEEE Trans. Automatic Control*, 1974: 716-723.

Aksay, E, R Baker, H S Seung, and D W Tank. "Anatomy and discharge properties of pre-motor neurons in the goldfish medulla that have eye-position signals during fixations." *Journal of Neurophysiology*, 2000: 1035-1049.

Aksay, E, Olasagasti, I, Mensh, B D, Baker, R, Goldman, M S, and Tank, D W. "Functional dissection of circuitry in a neural integrator." *Nat Neurosci* 10(4): 494-504, 2007.

Alkhamis, T M, and M A Ahmed. "A modified Hooke and Jeeves algorithm with likelihood ratio performance extrapolation for simulation optimization." *European Journal of Operational Research*, 2006: 1802-1815.

Angelaki, D E, A M Green, and J D Dickman. "Differential Sensorimotor Processing of Vestibulo-Ocular Signals during Rotation and Translation." *Journal of Neuroscience*, 2001: 3968-3985.

Atkinson, M. "Meniere's original papers reprinted with an English translation together with commentaries and biographical sketch." *Acta Otolaryngol. Suppl.*, 1961: 1-78.

Baker, R, M Gresty, and A Berthoz. "Neuronal activity in the prepositus nuclei correlated with vertical and horizontal eye movement in the cat." *Brain Res.*, 1975: 366-371.

Balaban, C D, R J Schuerger, and J D Porter. "Zonal organization of flocculo-vestibular connections in rats." *Neuroscience*, 2000: 669-682.

Barnes, G R. "Head-eye coordination in normals and in patients with vestibular disorders." *Adv Otorhinolaryngol.*, 1979: 197-201.

Basser, L. "Benign paroxysmal vertigo of childhood: a variety of vestibular neuritis." *Brain*, 1964: 141-152.

Becker W., Klein H. M., Accuracy of saccadic eye movements and maintenance of eccentric eye positions in the dark. *Vision Res.* 13: 1021-1034, 1973.

Buttner, U, and J A Buttner-Ennever. "Present concepts of oculomotor organization." *Progress in Brain Research*, 2006: 1-42.

Buttner, U, J A Buttner-Ennever, and V Henn. "Vertical eye movement related activity in the rostral mesencephalic reticular formation of the alert monkey." *Brain Research*, 1977: 239-252.

Cannon, S C, and D A Robinson. "Loss of the Neural Integrator of the Oculomotor System from Brain Stem Lesions in Monkey." *Journal of Neurophysiology*, 1987: 1383-1409.

Cannon, S C, Robinson, D A, and Shamma S. “A Proposed Neural Network for the Integrator of the Oculomotor System.” *Biol Cybern* 49(2):127-36, 1983.

Carlyle, W M, D C Montgomery, and G C Runger. "Optimization Problems and Methods in Quality Control and Improvement." *Journal of Quality Technology*, 2000: 1-17.

Ceuflhard, P. "Newton Methods for Nonlinear Problems. Affine Invariance and Adaptive Algorithms." *Springer Series in Computational Mathematics*, 2004.

Chan, W W P, and H L Galiana. "Integrator function in the oculomotor system is dependent on sensory context." *Journal of Neurophysiology*, 2005: 3709-3717.

Chan, Wilbur W P, and Henrietta L Galiana. "Modeling the Non-Linear Context Dependency of the Neural Integrator in the Vestibulo-Ocular Reflex." *IEEE Transactions on Biomedical Engineering*, 2008.

Chan W.W.P. , H.L.H. Smith and H.L. Galiana, Gaze holding and implications for the evaluation of VOR dynamics, *14th Annual Meeting on Neural Control of Movement*, Sitges, Spain, March 28-April3, 2004.

Cheron, G. "Effect of incisions in the brainstem commissural network on the short-term vestibulo-ocular adaptation of the cat." *J Vestib Res.*, 1990-1991: 223-39.

Cheron, G, E Godaux, J M Laune, and B Vanderkelen. "Lesions in the cat prepositus complex: Effects on the vestibulo-ocular reflex and saccades." *J Physiol.*, 1986: 75-94.

Cohen, B. "The vestibulo-ocular reflex." In *Handbook of Sensory Physiology. Vestibular System Part I: Basic Mechanisms*, by H H Kornhuber, 477-540. New York: Springer, 1974.

Collewijn, H, A J Martins, and R M Steinman. "Compensatory eye movements during active and passive headmovements: fast adaptation to changes in visual magnification." *Journal of Physiology*, 1983: 259-286.

Crane, B T, J Tian, and J L Demer. "Asymmetry of ocular motor and perceptual vestibular processing in humans with unilateral vestibular deafferentation." *Journal of Vestibular Research*, 2000: 259-269.

Crawford, J D, and T Vilis. "Symmetry of oculomotor burst neuron coordinates about listing's plane." *Journal of Neurophysiology*, 1992: 432-448.

Crawford, J, and T Vilis. "Modularity and parallel processing in the oculomotor integrator." *Exp. Brain Res.*, 1993: 443-456.

Cureoglu, S, P A Schachern, S Paul, M M Paparella, and R K Singh. "Cellular changes of Reissner's membrane in Meniere's disease: human temperal bone study." *Otolaryngol Head Neck Surg*, 2004: 113-119.

Dai, M, A Klein, B Cohen, and T Raphan. "Model-based study of the human cupular time constant." *Journal of Vestibular Research*, 1999: 293-301.

Demer, J L, and D A Robinson. "Effects of reversible lesions and stimulation of olivocerebellar system on vestibuloocular reflex plasticity." *Journal of Neurophysiology*, 1982: 1084-1107.

Dener, J L, and D A Robinson. "Effects of reversible lesions and stimulation of olivocerebellar system on vestibuloocular reflex plasticity." *Journal of Neurophysiology*, 1982: 1084-1107.

Drud, A. "CONOPT: A GRG Code for Large Sparse Dynamic Nonlinear Optimization Problems." *Mathematical Programming*, 1985: 153-191.

Fernandez, C, and J M Goldberg. "Physiology of peripheral neurons innervating semicircular canals of the squirrel monkey. II. Response to sinusoidal stimulation and dynamics of peripheral vestibular system." *Journal of Neurophysiology*, 1971: 661-675.

Freund, J E, and R E Walpole. *Mathematical Statistics.* New Jersey: Prentice-Hall, 1987.

Galiana, H L. "A nystagmus strategy to linearize the vestibulo-ocular reflex." *IEEE Trans. Biomed. Eng.*, 1991: 532-543.

Galiana, H L, Outerbridge J S. “A bilateral model for central neural pathways in vestibuloocular reflex.” *J Neurophysiol.*, 51(2): 210-41, 1984.

Galiana, H L, H Smith, and A Katsarkas. "Comparison of linear vs nonlinear methods for analyzing the VOR." *Acta Otolaryngol*, 1995: 585-596.

Gill, P, and W Murray. "Algorithms for the solution of the nonlinear least-squares problem." *SIAM Journal on Numerical Analysis*, 1978: 977-992.

Gizzi, M S, and H W Harper. "Suppression of the human vestibulo-ocular reflex by visual fixation or forced convergence in the dark, with a model interpretation." *Current Eye Research*, 2003: 281-290.

Goebel, J A, W O'Mara, and G Gianoli. "Anatomic Considerations in Vestibular Neuritis." *Otology & Neurotology*, 2001: 512-518.

Goldberg, J M, and C Fernandez. "Efferent vestibular system in the squirrel monkey: anatomical location and influence on afferent activity." *J. Neurophysiol.*, 1980: 986-1025.

Goldman M. S., Kaneko C. R. S., Major G., Aksay E., Tank D. W., Seung H. S. Linear Regression of Eye Velocity on Eye Position and Head Velocity Suggests a Common Oculomotor Neural Integrator. *J Neurophysiol.* 88: 659-665, 2002.

Gonzalez-Forero, D, R R de la Cruz, J M Delgado-Garcia, F J Alvarez, and A M Pastor. "Functional Alterations of Cat Abducens Neurons After Periphaeral Tetanus Neurotoxin Injection." *Journal of Neurophysiology*, 2003: 1878-1890.

Grantyn, A, and R Grantyn. "Axonal patterns and sites of ternimation of cat superior colliculus neurons projecting in the tecto-bulbo-spinal tract." *Experimental Brain Research*, 1982: 243-256.

Green A., Galiana H.L. Hypothesis for Shared Central Processing of Canal and Otolith Signals. *J Neurophysiol.* Rapid Communication, 2222-2228, 1998.

Guitton, D. "Control of Saccadic Eye and Gaze Movements by the Superior Colliculus and Basal Ganglia." In *Eye Movements*, by R H S Carpenter, 244-276. Boca Raton: CRC Press Inc., 1991.

Guitton, D, D P Munoz, and H L Galiana. "Gaze control in the cat: studies and modeling of the coupling between orienting eye and head movements in different behavioral tasks." *Journal of Neurophysiology*, 1990: 509-531.

Han, Lixing, and Neumann Michael. "Effect of dimensionality on the Nelder-Mead simplex method." *Optimization Methods and Software*, 2006: 1-16.

Heardman, S J, P Blatt, M C Schubert, and R J Tusa. "Falls in patients with vestibular deficits." *Am. J. Otol.*, 2000: 847-851.

Henn, V, B Cohen, and L R Young. "Neurosciences Research Program." *Visual-Vestibular Interaction in Motion Perception and the Generation of Nystagmus.* Cambridge: MIT Press Journals, 1980.

Hestenes, M R, and E Stiefel. "Methods of Conjugate Gradients for Solving Linear Systems." *Journal of Research of the National Bureau of Standards*, 1952: 409-436.

Hooke, R, and T Jeeves. "Direct search solutions of numerical and statistical problems." *Journal of the Assiciation for Computing Machinery*, 1961: 212-229.

Horn, A K E. "The reticular formation." *Progress in Brain Research*, 2006: 127155.

Idoux, E, et al. "Oscillatory and Intrinsic Membrane Properties of Guinea Pig Nucleus Prepositus Hypoglossi Neurons In Vitro." *Journal of Neurophysiology*, 2006: 175-196.

Jackler, R K, and Kaplain M J. "Ear, Nose & Throat." In *Current Medical Diagnosis and Treatment*, by McPhee S. Stanford: Appleton & Lange, 1997.

Jenkins, H A, H S Cohen, and K T Kimball. "Long-term Vestibulo-ocular Reflex Changes in Patients with Ablation." *Acta Otolaryngol*, 2000: 187-191.

Kaneko, C R S. "Eye Movement Deficits After Ibotenic Acid Lesions of the Nucleus Prepositus Hypoglossi in Monkeys. I. Saccades and Fixation." *Journal of Neurophysiology*, 1997: 1753-1768.

Kariya, S, et al. "Histopathologic changes of contralateral human temporal bone in unilateral Ménière's disease." *Otology & Neurotology*, 2007: 1063-1068.

Khojasteh E., Modeling Fixation-Distance-Related Modulations in the Vestibulo-Ocular Reflex (VOR), Master Thesis, McGill University, 2003a.

Khojasteh, E, and H L Galiana. "A non-linear model for context-dependent modulation of the binocular VOR." *IEEE Trans. Biomedical Engineering*, 2006: 986-995.

Kuhn, H W, and A W Tucker. "Nonlinear Programming." *Proceedings of 2nd Berkeley Symposium.* University of California Press, 1951. 481-492.

Kukreja, S L, R E Kearney, and H L Galiana. "A Least-Squares Parameter Estimation Algorithm for Switched Hammerstein Systems With Applications to the VOR." *IEEE Transactions On Biomedical Engineering*, 2005: 431-444.

Langer, T P, C R Kaneko, C A Scudder, and A F Fuchs. "Afferents to the abducens nucleus in the monkey and cat." *Journal of Comparative Neurology*, 1986: 379-400.

Lazarini, P R, and A C Camargo. "Idiopathic sudden sensorineural Hearing loss: etiopathogenic aspects." *Rev. Bras. Otorrinolaringol. (Engl. Ed.)*, 2006: 554-561.

Ljung, Lennart, and Torkel Glad. *Modeling of Dynamic Systems.* New Jersey: Prentice-Hall, 1994.

McConville, K M, R D Tomlinson, and E Q Na. "Behavior of eye-movement-related cells in the vestibular nuclei during combined rotational and translational stimuli." *Journal of Neurophysiology*, 1996: 3136-3148.

McCrea, R A, and A K E Horn. "Nucleus prepositus." *Progress in Brain Research*, 2006: 205-230.

McCrea, R, A Strassman, E May, and S Highstein. "Anatomical and physiological characteristics of vestibular neurons mediating the horizontal vestibulo-ocular reflex of the squirrel monkey." *J. Comp. Neurol.*, 1987: 547-570.

Mensh, B D, Aksay, E, Lee, D D, Seung, H S, Tank, D W. “Spontaneous eye movements in goldfish: oculomotor integrator performance, plasticity, and dependence in visual feedback.” *Vision Res* 44(7): 711-26, 2004.

Mettens, P, E Godaux, G Cheron, and H L Galiana. "Effect of Muscimol Microinjections Into the Prepositus Hypoglossi and the Medial Vestibular Nuclei on Cat Eye Movements." *Journal of Neurophysiology*, 1994: 785-802.

Mills, E S. "Clinical diagnosis of Meniere's disease: how useful are the American Academy of Otolaryngology Head and Nech Surgery Committee on Hearing and Equilibrium guidelines?" *Journal of Laryngology & Otology*, 2007: 1-7.

Minor, L B, D M Lasker, D D Backous, and T E Hullar. "Horizontal vestibuloocular reflex evoked by high-acceleration rotations in the squirrel monkey. I. Normal responses." *Journal of Neurophysiology*, 1999: 1254-1270.

Moschovakis, A K, and S M Highstein. "The anatomy and physiology of primate neurons that control rapid eye movements." *Annual Review of Neuroscience*, 1994: 465-488.

Munoz, D P, and D Guitton. "Control of orienting gaze shifts by the tectoreticulospinal system in the head-free cat. II. Sustained discharges during motor preparation and fixation." *Journal of Neurophysiology*, 1991: 1624-1641.

Munoz, D P, and R H Wurtz. "Fixation Cells in Monkey Superior Colliculus I. Characteristics of Cell Discharge." *Journal of Neurophysiology*, 1993: 559-575.

Nakashima, T, et al. "Visualization of endolymphatic hydrops in patients with Meniere's disease." *The Laryngoscope*, 2007: 415-420.

Narozny, W, J Kuczkowski, J Kot, C Stankiewicz, Z Sicko, and B Mikaszewski. "Prognostic factors in sudden sensorineural hearing loss: our experience and a review of the literature." *Ann. Otol. Rhinol. Laryngol.*, 2006: 553-558.

National Institutes of Health. "Cerebellar Degeneration Information Page." *National Institute of Neurological Disorders and Strke.* February 12, 2007. http://www.ninds.nih.gov/disorders/cerebellar_degeneration/cerebellar_degeneration.htm (accessed January 18, 2008).

Navarro-Lopez, Juan de Bios, J C Alvarado, J Marquez-Ruiz, M Escudero, J M Delgado-Garcia, and J Yajeya. "A Cholinergic Synaptically Triggered Event Participates in the Generation of Persistent Activity Necessary for Eye Fixation." *The Journal of Neuroscience*, 2004: 5109-5118.

Nelder, J A, and R Mead. "A Simplex Method for Function Minimization." *Computing Journal*, 1965: 308-313.

Nocedal, J, and S J Wright. *Numerical Optimization.* New York: Springer Science+Business Media, LLC., 2006.

Paige, G. "Nonlinearity and asymmetry in the human vestibulo-ocular reflex." *Acta Otolaryngol*, 1989: 1-8.

Paige G. D., Telford L., Seidman S. H., Barnes G. R. Human Vestibuloocular Reflex and Its Interactions With Vision and Fixation Distance During Linear and Angular Head Movement. *J Neurophysiol.* 80: 2391-2404, 1998.

Pelletier, K R. "The Best Alternative Medicine, Part II." In *CAM Therapies for Specific Conditions: Meniere's Disease*. New York: Simon & Schuster, 2002.

Pinter, J D. "Continuous global optimization software: A brief review." *Optima*, 1996: 1-8.

Powell, M J D. "Direct Search Algorithms for Optimization Calculations." *Acta Numerica*, 1998: 287-336.

Radinsky I., Galiana H.L. Improved algorithm for classification of ocular nystagmus, *Proc. 26th Annual International Conference of the IEEE EMBS,* San Francisco USA, Sept. 1-4, 2004.

Raphan, T, and B Cohen. "Brainstem mechanisms for rapid and slow eye movements." *Annu Rev Physiol.*, 1978: 527-552.

Raphan T., Cohen B. Velocity storage and the ocular response to multidimensional vestibular stimuli, in Adaptive Mechanisms in Gaze Control – Fasts and Theories, eds. Berthoz and Melvill Jones, Elsevier/New York, 123-143, 1985.

Rasekh, C H, and L A Harker. "The prevalence of migraine in Meniere disease." *Laryngoscope*, 1992: 135-138.

Rey C.G., Galiana H.L. Transient analysis of vestibular nystagmus. *Biol Cybern* 69: 395-405, 1993.

Ritchis, L. "Effects of Cerebellar Lesions on Saccadic Eye Movements." *Journal of Neurophysiology*, 1976: 1246-1256.

Robinson D.A. Eye movement control in primates. *Science* 161: 1219-1224, 1968.

Robinson, D A. "Eye movements evoked by collicular stimulation in the alert monkey." *Vision Research*, 1972: 1795-1808.

Robinson, D A. "Integrating with Neurons." *Ann Rev. Neurosci.*, 1989: 33-45.

Robinson, D A. "Oculomotor control signals." In *Basic Mechanisms of Ocular Motility and Their Clinical Implications*, by G Lennerstrand and P Bach-y-Rita, 337-374. Oxford: Pergamon, 1975.

Robinson, D A. "The effect of cerebellectomy on the cat's vestibulo-ocular integrator." *Brain Research* 71 (1974): 195-207.

Robinson, D A. "The use of control systems analysis in the neurophysiology of eye movements." *Ann. Rev. Neurosci.*, 1981: 463-503.

Sando, I, Y Orita, and B E Hirsch. "Pathology and pathophysiology of Meniere's disease." *Otolaryngologic clinics of North America*, 2002: 517-528.

Schiller, P H, J H Sandell, and J H R Maunsell. "The effect of frontal eye field and superior colliculus lesions on saccadic latencies in the rhesus monkey." *J. Neurophysiol.*, 1987: 1033-1049.

Schneider E., Glasauer S., Dieterich M. Central processing of human ocular torsion analyzed by galvanic vestibular stimulation. *Neuroreport* 11: 1559-1563, 2000.

Scudder, C A, A F Fuchs, and T P Langer. "Characteristics and functional identification of saccadic inhibitory burst neurons in the alert monkey." *Journal of Neurophysiology*, 1988: 1430-1454.

Scudder, C S. "A new local feedback model of the saccadic burst generator." *J. Neurophysiol.*, 1988: 1455-1475.

Seung, H S, Lee, D D, Reis, B Y, Tank, D W. "Stability of the Memory of Eye Position in a Recurrent Network of Conductance-Based Model Neurons." *Neuron* 26(1):259-71, 2000.

Shelhamer M., Robinson D. A., Tan H. S. Context-specific adaptation of the gain of the vestibulo-ocular reflex in humans. *J Vestibular Research* 2: 89-96, 1992.

Shikin, E V. *Handbook and Atlas of Curves.* Florida: CRC Press Inc., 1995.

Skavenski, A A, and D A Robinson. "Role of Abducens motorneurons in the vestibulo-ocular reflex." *J Neurophysiol.*, 1973: 724-738.

Smith H. L. H., Chan W. W. P., Galiana H. L. Transient Analysis of Non-Linear VOR Nystagmus – Clinical Implications. *Proc. 24th Annual International Conference of the IEEE EMBS*, Houston Texas, 2002, Vol. 3, pp. 2137-2138.

Smith, H L, W W P Chan, and H L Galiana. "Optimizing Clinical Protocols to Test VOR Nystagmus." *Neural Control of Movement 15th Annual Meeting.* Key Biscayne: Neural Control of Movement, 2005. H5.

Stahle, J, U Friberg, and A Svedberg. "Long-term progression of Meniere's disease." *Acta Otolaryngol*, 1991: 75-83.

Stapleton, E, and R Mills. "Clinical diagnosis off Meniere's disease: how useful are the American Academy of Otolaryngology Head and Nech Surgery Committee on Hearing and Equilibrium guidelines?" *The Journal of Laryngology & Otology*, 2007: 1-7.

Strassman, A, S M Highstein, and R A McCrea. "Anatomy and physiology of saccadic burst neurons in the alert squirrel monkey II. Inhibitory burst neurons." *Journal of Comparative Neurology*, 1986: 358-380.

Sylvestre, P, and K E Cullen. "Quantitative Analysis of Abducens Neuron Discharge Dynamics during Saccadic and Slow Eye Movements." *J. Neurophysiol.*, 1999: 2612-32.

Uemura, T, and B Cohen. "Effects of vestibular nuclei lesions on vestibulo-ocular reflexes and posture in monkeys." *Acta Otolaryngol. Suppl.*, 1973: 1-71.

Wilson, V J, and G Melvill Jones. *Mammalian vestibular physiology.* New York: Plenum Press, 1979.

Zhou, W, Y Xu, I Simpson, and Y Cai. "Multiplicative Computation in the Vestibulo-Ocular Reflex (VOR)." *Journal of Neurophysiology*, 2007: 2780-2789.